TECHNISCHE UNIVERSITÄT MÜNCHEN

Fakultät für Medizin

Klinik und Poliklinik für Plastische Chirurgie und Handchirurgie

Towards Autotrophic Tissue Engineering: Photosynthetic Gene Therapy for Dermal Regeneration

Myra Noemi Chávez Rosas

Vollständiger Abdruck der von der Fakultät für Medizin der Technischen Universität München zur Erlangung des akademischen Grades eines

Doctor of Philosophy (Ph.D.)

genehmigten Dissertation.

Vorsitzender: Univ.-Prof. Dr. Jürgen Ruland

Betreuer: Univ.-Prof. Dr. Hans-Günther Machens

Prüfer der Dissertation:

1. apl. Prof. Dr. Yves Harder (schriftliche Beurteilung)
   Priv.-Doz. Dr. Jan Thorsten Schantz (mündliche Prüfung)
2. Univ.-Prof. Jörg Nickelsen, Ludwig-Maximilians-Universität München

Die Dissertation wurde am 25. März 2015 bei der Fakultät für Medizin der Technischen Universität München eingereicht und durch die Fakultät für Medizin am 6. Juli 2015 angenommen.

„Eine wirklich gute Idee erkennt man daran, dass ihre Verwirklichung von vornherein ausgeschlossen erschien."

Albert Einstein

Abstract

The regenerative potential of artificial tissues is limited due to hypoxia. As a strategy to overcome this drawback, it has been previously suggested that photosynthesis could be used as an alternative source of oxygen supply to blood vessel-perfusion. In that approach, it was demonstrated that photosynthetic biomaterials can be created by incorporating the unicellular algae *Chlamydomonas reinhardtii* (*C. reinhardtii*) into tissue engineered constructs. Further it was shown that photosynthetic oxygen is able to substitute the metabolic oxygen requirements of animal cells under conditions of hypoxia.

In this work, *C. reinhardtii* algae were encapsulated in a fibrin hydrogel to produce oxygen-releasing scaffolds for dermal regeneration. The microalgae were able to live and proliferate inside the collagen matrices. Moreover, the oxygen produced and released by the photosynthetic scaffolds was proportional to the density of the algae and dependent on light exposure. The inflammatory response towards photosynthetic algae was evaluated in a zebrafish model and in a full-skin defect model using athymic and wild type mice. The results showed no signs of systemic inflammation and demonstrated the biocompatibility of the microalgae with other organisms.

Taking this evidence and the availability of genetic tools to generate transgenic *C. reinhardtii*, the possibility of engineering scaffolds that, in addition to oxygen, provide other key molecules that contribute to wound regeneration was explored. As a proof of concept, two genetically modified *C. reinhardtii* strains capable to constantly secrete the pro-angiogenic human vascular endothelial growth factor (hVEGF-165) and human platelet-derived growth factor B (hPDGF-B) in relevant amounts were generated. The functionality of the recombinant proteins was evaluated *in vitro* by their ability to bind and induce auto-phosphorylation of their respective receptors. Furthermore, scaffolds seeded with transgenic algae showed a sustained release of both, oxygen and growth factors. As for *in vivo* models, the injection of the transgenic microalgae into the yolksack of zebrafish larvae induced the ingrowth of the developing vasculature. In the full-skin defect model, the recombinant human growth factors were found present in the lysates obtained from scaffolds explanted after seven and fourteen days.

This work provides scientific basis for the use of genetically modified microalgae as an alternative gene therapy to supply wounds with pro-regenerative biomolecules. The incorporation of gene-modified algae into autotrophic tissues, which shall be able to survive from photosynthetic oxygen and will be therefore autonomous from a growing vascularization, will promote the survival of artificial grafts after implantation in a host and be advantageous for the treatment of several pathophysiological conditions related to tissue hypoxia.

Zusammenfassung

Das regenerative Potenzial künstlicher Gewebe ist durch Hypoxie begrenzt. Als Strategie, diesen Nachteil zu beseitigen, wurde die Sauerstoffzufuhr über Photosynthese als Alternative zur Sauerstoffzufuhr über Durchblutung eines Gefäßnetzwerks vorgeschlagen. Bei diesem Ansatz wurde gezeigt, dass durch das Einsähen von einzelligen Algen der Art *Chlamydomonas reinhardtii* (*C. reinhardtii*) in künstliche Matrices, photosynthetisch aktive Scaffolds erzeugt werden können. Ferner wurde gezeigt, dass photosynthetischer Sauerstoff in der Lage ist, den metabolischen Sauerstoffbedarf von Tierzellen unter hypoxischen Bedingungen zu bedienen.

In dieser Arbeit wurde *C. reinhardtii* in einem Fibrinhydrogel verkapselt um Sauerstoff freisetzende Scaffolds für die dermale Hautregeneration herzustellen. Die Mikroalgen waren in der Lage in den Kollagen-Matrices zu überleben und sich zu vermehren. Außerdem wurde weiterhin Sauerstoff von den Algen synthetisiert und aus den photosynthetischen Scaffolds freigesetzt. Die entzündliche Reaktion auf die photosynthetischen Algen wurde mit einem Zebrafisch Modell und einem Vollhautdefekt Regenerationsmodell mit athymischen und immunkompetenten Mäusen ausgewertet. Es zeigten sich keine Anzeichen einer systemischen Entzündung, weshalb auf eine Biokompatibilität der Mikroalgen mit anderen Organismen geschlossen wurde. Angesichts dieser Erkenntnisse und der Verfügbarkeit von gentechnischen Werkzeugen, die die Erzeugung von transgenen *C. reinhardtii* erlauben, wurde nun die Möglichkeit erkundet, artifizielle Geweben zu erzeugen, die neben Sauerstoff auch weitere wichtige Regeneration fördernde Moleküle freisetzen sollen. Um das Konzept zu beweisen wurden zwei gentechnisch veränderte *C. reinhardtii* Stämme erzeugt, die in der Lage waren, die pro-angiogenen Wachstumsfaktoren hVEGF-165 und hPDGF-B zu synthetisieren und auszuschütten. Die Funktionalität der rekombinanten Proteine wurde durch ihre Fähigkeit zur Phosphorylierung ihrer jeweiligen Rezeptoren *in vitro* bewertet. Die mit transgenen Algen besiedelten Scaffolds zeigten eine konstante Freisetzung von Sauerstoff und Wachstumsfaktoren über eine Woche. In einem Zebrafisch Modell konnte durch Einspritzung von transgenen Mikroalgen in den embryonalen Dottersack Gefäßwachstum induziert werden. In einem Vollhautdefektmodell konnten die, von den eingesäten transgenen Algen produzierten, humanen Wachstumsfaktoren, in den nach sieben und vierzehn Tagen explantierten Scaffolds nachgewiesen werden.

Diese Arbeit liefert die wissenschaftliche Grundlage für die Verwendung von genetisch veränderten Mikroalgen als eine alternative Gentherapie, um Wunden mit pro-regenerativen Molekülen zu versorgen. Die Verwendung von Algen zur Erzeugung von autotrophen Geweben, die durch den photosynthetischen Sauerstoff überleben können und daher autonom von Vaskularisation sein können, wird das Überleben von künstlichen Transplantaten nach Implantation erhöhen und sich bei der Behandlung von pathophysiologischen Bedingungen, die in Verbindung zur Gewebehypoxie stehen, wirksam zeigen.

Contents

I. Introduction

Humans rely on external supply of oxygen due to the lack of tissues that can produce or store it inside our body. In a normal situation, the cardiopulmonary system gives cells access to nutrients and oxygen through blood perfusion. However, in different scenarios, where tissue perfusion has been compromised or is non-existent, this dependence becomes pathological, in particular, during the process of wound healing, where it is absolutely critical that the site of injury receives the required amounts of metabolites. That is the case of chronic wounds, massive burns, or defect-treatments based on non-vascularized biomaterials.

The main idea behind this doctoral thesis is that the local induction of photosynthesis, the source of all the oxygen being metabolized by living organisms, could function as an alternative source of oxygen supply to blood vessel perfusion.

In the first stage of this work, photosynthetic biomaterials were created by incorporating the unicellular photosynthetic microalgae *Chlamydomonas reinhardtii* (*C. reinhardtii*) into scaffolds for dermal regeneration and characterized both in *in vitro* and *in vivo* models. In the second stage, making use of the tools available for genetic manipulation, *C. reinhardtii* were genetically modified to be able to release pro-angiogenic growth factors, which will help to promote revascularization in the wounded tissue and restore blood perfusion more rapidly during the course of regeneration.

Considering that tissue engineering is defined as an emerging interdisciplinary field that applies the principles of biology and engineering to the development of viable substitutes that restore, maintain, or improve the function of human tissues (Langer *et al.*, 1993), this work pursues to create autotrophic engineered tissues to improve regeneration and proposes the use of photosynthetic gene therapy in a broad range of clinical conditions.

1.1 Skin

Skin is the outermost organ of the body and together with the hair, nails and the subcutaneous tissue, it forms the integumentary system. This system is the largest organ of the body and creates a barrier between the organism and the environment, therefore preventing pathogen invasion and protecting it from chemical and physical assaults. Additionally, it regulates the body's temperature and controls the loss of water and solutes. Other functions of the skin also include sensation, vitamin synthesis, respiration and transpiration (Tortora *et al.*, 2012).

The skin is divided into two layers of ectodermal origin; the epidermis and the dermis (Fig. 1). The main function of the epidermis is to produce the protective, semi-permeable stratum corneum formed by tightly connected cornocytes and patterned extracellular lipids, which serves as a barrier to water loss (Madison *et al.*, 2003). In addition, it provides the antimicrobial barrier with humoral and cellular constituents of the immune system. The main cell constituents of the nucleated epidermis are keratinocytes of different differentiation stages, melanocytes, Langerhans cells and Merkel cells (Tortora *et al.*, 2012). The epidermis contains no blood vessels, therefore cells depend on oxygen diffusion from the dermal blood capillaries and cutaneous uptake of atmospheric oxygen (Stücker *et al.*, 2002).

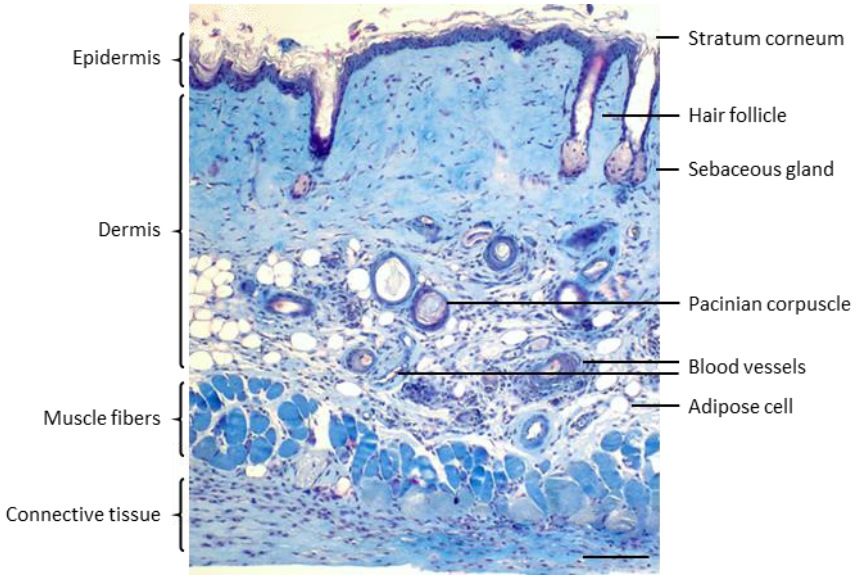

Figure 1: Structure of the skin of a hairless Skh1 mouse. Masson's trichrome staining of a histological section of the skin of the back of a mouse. Major structures within the integumentary system are labelled. Scale bar represents 100 µm.

The dermis is composed of a layer of collagen, elastic fibers and glycosaminoglycans that cushion the body from stress and strain, and provide tensile strength and elasticity to the skin. It is divided into two layers; the superficial papillary region connected to the epidermis through the basement membrane and a deep thicker reticular region. The dermal vasculature is arranged parallel to the skin surface with perpendicularly oriented capillaries looping upwards into the papillae. The dermis encloses primary nerves such as mechanoreceptors, which provide the sense of touch and heat, sweat and sebaceous glands, apocrine glands, lymphatic vessels, and hair follicles (Tortora *et al.*, 2012). Besides being the base for hair restoration, hair follicles are also a source of epidermal stem cells, also known as bulge cells, which are being currently characterized in their role in epidermis and hair follicle regeneration (Mokos *et al.*, 2014). The major cell types of the dermis are fibroblasts, macrophages, and adipocytes.

The skin, as the most external layer in the body and its largest organ, is an excellent model to study the mechanisms involved in tissue regeneration. Given its accessibility for manipulation, large surface, transparency, and anatomic homogeneity, processes like tissue survival and inflammation can be studied easily in skin as compared to other tissues. Furthermore, the repair of skin defects bid an ideal regeneration model to study angiogenesis, due to its easy accessibility that permits the observation and manipulation of the process (Eming *et al.*, 2007). Furthermore, skin injuries are highly relevant in clinical practice and in several cases represent an unmet clinical need (Eming *et al.*, 2014).

1.2 Dermal regeneration

1.2.1 Skin injuries and the wound healing process

Skin injuries result in a break in the epithelial integrity and may be accompanied by disruption of the underlying tissue. According to its severity, different wound healing mechanisms are induced to achieve wound closure (Enoch *et al.*, 2005). Unlike fish and amphibians, the process of wound healing in humans does not result in complete tissue regeneration and often cannot return the skin to its original functionality. This is especially true in the case of large, deep or physiologically compromised injuries (Egaña, 2009).

Wound healing involves a complex, dynamic, well-orchestrated series of events that require the interactions of extracellular matrix (ECM) molecules, soluble mediators, various resident cells, and infiltrating leukocytes. The healing process can be divided into four phases that overlap in time and space: hemostasis, inflammation, proliferative tissue formation and tissue remodeling (Fig. 2). Its main objectives are to re-establish homeostasis, prevent infection and minimize fluid loss (Greaves *et al.*, 2013).

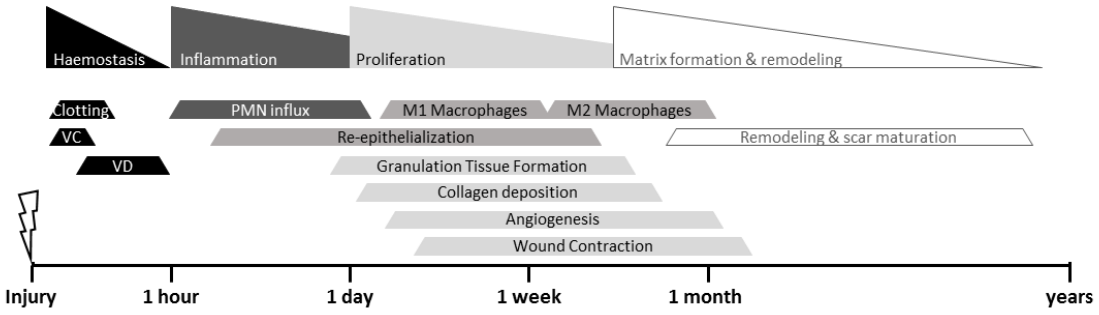

Figure 2: Overview of acute wound healing. Hemostasis: After cutaneous injury, vasoconstriction (VC), clotting cascades and platelets act together to prevent further blood loss. Once the fibrin clot is formed, vasodilation (VD) enables polymorphonuclear cells (PMN) extravasation to the wound site. Inflammation: Influx of macrophages, which have an early inflammatory (M1) and later reparative (M2) phenotype. There is phagocytosis of bacteria and wound debris, plus simultaneous secretion of multiple growth factors, chemokines and cytokines, which drive fibroblast and endothelial cell recruitment to the wound bed. Re-epithelialization begins within hours of injury and continues until restoration of epithelial continuity is complete. Proliferation: Endothelial cells and fibroblasts migrate and proliferate promoting collagen deposition, angiogenesis and granulation tissue formation. Remodeling: the provisional fibrin-collagen scaffold is degraded and rebuild by a variety of enzymes throughout wound maturation. The granulation tissue evolves into a predominantly collagenous structure with myofibroblasts triggering wound contraction and gradually reducing cellularity with eventual scar formation. Modified from Greaves *et al.*, 2013.

Hemostasis is the immediate process that follows injury. Disruption of the microvasculature and extravasation of blood into the wound initiate the coagulation cascade that results in clot formation and platelet aggregation. Platelet-degranulation then releases several growth factors, including platelet-derived growth factor (PDGF), insulin-like growth factor-1 (IGF-1), epidermal growth factor (EGF), transforming growth factor-β (TGF-β), and platelet factor-IV (PF4), to attract and activate fibroblasts, endothelial cells and innate immune cells. The clot also provides the provisional matrix for the migration of these cells (Enoch *et al.*, 2005).

Inflammation begins with the activation of the classical and alternative pathways of the complement cascade. Two to three days after wounding, polymorphonuclear leukocytes are attracted to the wound site and once in the wound environment, they phagocytize and kill foreign microorganisms by releasing degrading enzymes and reactive oxygen species (ROS). Infiltrated monocytes, which undergo a phenotypic change to become phagocytic tissue macrophages, release growth factors that trigger the proliferation of fibroblasts, endothelial cells, and smooth muscle cells, and synthesize proteolytic enzymes to complete the debridement of the wound (Greaves *et al.*, 2013).

The proliferative phase starts right after the inflammation phase and lasts two to four weeks after wounding. It is characterized by fibroblast migration, fibrocyte differentiation, ECM-deposition and formation of granulation tissue which replaces the provisional fibrin-matrix (Enoch *et al.*, 2005). The granulation tissue is characterized by a dense population of proliferating fibroblasts and macrophages found within in a loose ECM composed of collagen type I and III, fibronectin and hyaluronic acid (Greaves *et al.*, 2013).

Wound contraction is initiated with myofibroblast differentiation about ten to fourteen days after injury and is regulated by a number of cytokines including TGF-β, PDGF, and basic fibroblast growth factor (bFGF), in addition to cell-matrix interactions (Mutsaers *et al.*, 1997). Wound edges are pulled together by the interaction of the myofibroblasts with the ECM, consequently reducing the size of the wound (Enoch *et al.*, 2005).

Wound revascularization takes also place during this phase and is essential to replace damaged capillaries and restore the supply of oxygen, blood cells and nutrients to wounded tissue, and thus reset normoxic conditions in the tissue (Eming *et al.*, 2007).

Epithelialization of the wound represents the final stage of the proliferative phase. It involves the migration of epithelial cells from the wound edges to first cover the exposed area, followed by their proliferation and further migration across the provisional matrix. Once contact inhibition stops their mobilization, the basement membrane is regenerated and keratinocyte differentiation promotes the reestablishment of the epidermis. Epithelialization requires a moist environment, adequate nutrition and bacteriological control, and is modulated by several growth factors, including keratinocyte growth factor (KGF), EGF, and bFGF (Enoch *et al.*, 2005).

The remodeling of the ECM involves the continuous synthesis and breakdown of collagen, by matrix metalloproteases and reaches a steady-state 21 days after wounding. Then, the granulation tissue is replaced by an avascular scar with disperse inactive fibroblasts, dense collagen fibers, and fragments of elastic tissue over a thin underlying contractile connective tissue. As the scar matures, collagen bundles increase in diameter conferring the wound an increase in tensile strength, which is still lesser than the original strength of unwounded skin.

In a chronic wound the normal process of healing is disrupted. Systemic conditions such as vascular insufficiency, nutritional deficiencies, neuropathy and ischemia, or local abnormalities like excessive presence of inflammatory cells, lower secretion of growth factors and cytokines, and unbalanced activity of proteases may lead to non-healing wounds. Opposite to this, hypertrophic scars and keloids are forms of excessive healing resulting from overproduction of all the cellular and molecular elements involved. Hence, molecular and cellular mechanisms involved in wound healing must be tightly regulated in order to lead to successful healing (Enoch *et al.*, 2005).

1.2.2 Skin vascular regeneration

Functional tissue homeostasis requires an adequate supply of oxygen and nutrients delivered through blood vessels. The formation of new blood vessels is normally suppressed in most adult tissues. However, tissue injury induces various cellular and molecular processes that are responsible for restoring the vascular network and preventing a sustained deprivation of oxygen supply, which is defined as tissue hypoxia. This is done by two main processes: angiogenesis and vasculogenesis (Eming *et al.*, 2007).

Angiogenesis is the physiological process through which new blood vessels form based on preexisting vascular structures. It is orchestrated by the tight interaction between endothelial cells, soluble angiogenic growth factors and extracellular molecules. The process is divided into four main steps: endothelial cell sprouting, lumen formation, tubulogenesis and maturation of the newly formed vessels. Vessel tip cells sprout out of existing vessels, invade the fibrin clot and grow along the growth factor gradient, which is built upon the activation of the innate immune response as a consequence of cell disruption and changes in oxygen levels (Tonnesen *et al.*, 2000). Endothelial cells then assemble as cords, which subsequently acquire a lumen and increase vessel length. Vessel outgrowth is accompanied by the degradation of the surrounding ECM by proteases, the recruitment of vascular support cells, including pericytes and smooth muscle cells, and the formation of the basement membrane (Krock *et al.*, 2011). Capillary sprouts eventually branch and anastomose to form capillary arcades through which blood flow begins (Tonnesen *et al.*, 2000).

The primary angiogenesis-related gene activation mechanisms occur via the hypoxia-inducible factor-1 (HIF-1). The HIF-1α subunit, which is rapidly degraded under normoxic and hyperoxic conditions, but upregulated in response to hypoxia, binds as a transcription factor to hypoxia response elements within the promotor region of different genes thereby starting their transcription. HIF-1α controls the expression of numerous angiogenic, metabolic, and cell cycle genes, including the vascular endothelial growth factor (VEGF) and the matrix metalloproteinase-2 (MMP-2) which play a key role during vessel sprouting (Krock *et al.*, 2011).

The angiogenic processes during the initial granulation phase of cutaneous wound repair is mediated mainly by the VEGF, bFGF, PDGF and angiopoietins. TGF-β also induces endothelial cells to produce a provisional vessel matrix as well as assume the correct phenotype for capillary tube formation. Moreover, ECM-proteins including collagen, laminin, vitronectin and fibronectin promote endothelial cell proliferation, survival and migration.

Vasculogenesis, is defined as the *de novo* formation of vessels by mobilization and differentiation of bone marrow-derived endothelial progenitor cells (EPC's) and it has been extensively described in the context of vascular system development and tumor vascularization. Research on neovascularization involved in adult vascular repair parted from the discovery of circulating mononuclear cells in peripheral blood that were shown to incorporate into sites of physiological and pathological neovascularization and to differentiate into mature endothelial cells (Asahara *et al.*, 1997). The homing of EPCs is believed to be primarily mediated by the binding of the chemokine stromal cell-derived factor-1 (SDF-1 or CXCL12), which is released by the injured tissues, to the C-X-C chemokine receptor 4 (CXCR4) on circulating EPC's (Ceradini *et al.*, 2004). The potential use of EPCs in vascular regenerative medicine has been studied ever since and they have been effectively used to stimulate angiogenesis in several experimental settings. However, the definition and a detailed functional characterization of these cells is still debated (Fadini *et al.*, 2011). Interestingly, recent evidence suggests that circulating EPC's secrete paracrine growth factors to enhance vascular regeneration, rather than becoming part of the newly formed vasculature (reviewed by Zhang *et al.*, 2014).

Impaired vascular regeneration is often age-related and frequent in patients suffering from *diabetes mellitus*. Some factors contributing to a delayed vascular repair are the reduced expression of angiogenic growth factors, compromised endothelial progenitor cell recruitment and homing, vascular dysfunction, chronic hyperglycemia and reduced neuropeptide signaling (Baltzis *et al.*, 2014).

1.2.3 Scaffolds for dermal regeneration

Full-thickness wounds with extensive loss of soft tissue of both epidermal and dermal layers, as seen in major trauma or severe burns, are not able to close by simple epithelial cell regeneration and may lead to contractures and functional restrictions. In this case, autologous transplantation remains the gold standard of treatment. However, this is not an option when it comes to large tissue defects or in patients with impaired healing capacity. It also has many disadvantages in regards to pain, scarring, infection, and delayed healing in the tissue donor site (Lalan *et al.*, 2001). In order to avoid such transplantation procedures, the development of scaffolds for tissue regeneration has been a long pursued goal in the field of tissue engineering and biomaterials. Such scaffolds are three-dimensional structures that can be placed over the wound bed and serve as a backbone for cell infiltration (Fig. 3).

Scaffolds should be able to meet the physiological needs of the regenerating tissue. They should mimic the native extracellular matrix, and should possess mechanical properties matching those of the tissue at implantation site. Further, they should support cell adhesion by facilitating cell-to-cell contact and promote cell proliferation and migration through an adequate matrix porosity and cell-matrix interaction sites. They must be biocompatible and biodegradable so that they can be replaced by the growing tissue in a determined time-period. Scaffolds may be used to deliver proteins, such as growth factors, to enhance their regenerative potential. For this, they should have a high and homogeneous loading capacity for the drug, stably maintain the biological activity of the drug and release it in a controlled fashion (Sokolsky-Papkov *et al.*, 2007).

Tissue-engineered skin replacements are broadly of two types: artificial scaffolds, which are produced from isolated animal proteins, such as collagen and glycosaminoglycans, to create porous matrices; and biological scaffolds, which are matrices made from tissues that have been treated to remove the cells, but preserve their structure and biochemical composition (Shahrokhi *et al.*, 2013).

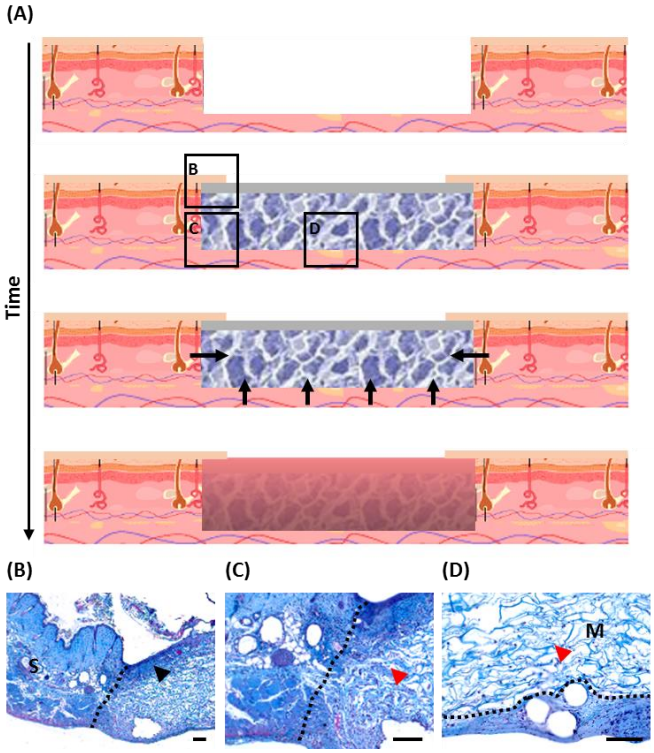

Figure 3: Illustration of the use of collagen-based dermal scaffolds. Biodegradable porous matrices are used to cover full-thickness skin defects (A). Histological sections show how artificial constructs are cellularized by host-cells (red arrow-heads) through their migration and proliferation (A, arrows) from the wound edges (B, C dotted line) and the wound bed (D, dotted line). Epidermal-extension (black arrow-head) connects the artificial tissue (M) to the skin (S) during the process of scaffold-based wound regeneration. Scale bar represents 100 µm. Modified from Egaña, 2009.

Although the use of scaffolds is a promising approach, clinical results have been so far disappointing. To date there is no bioengineered scaffold that replaces the skin, both functionally and morphologically in its entirety. Particularly, the absence of built-in vascular components in scaffolds and their consequent dependence on host neovascularization, is one of main challenges to overcome (Debels *et al.*, 2015).

Due to lack of vascularization, scaffolds are poorly perfused with oxygen, nutrients and immune cells and therefore often lead to low regeneration and high infection rates (Shahrokhi *et al.*, 2013). Alternative strategies to ensure the nourishment of implanted scaffolds are essential to improve the therapeutic potential of skin substitutes.

1.3 Oxygen

1.3.1 Oxygen in wound healing and regeneration

Oxygen is an essential molecule for cell metabolism and energy production. However, during wound healing, oxygen takes part in additional reparative processes, therefore increasing its importance and demand. Oxygen is a key factor in four main healing mechanisms: oxidant production for bacterial killing, collagen synthesis, angiogenesis, and epithelialization (Tandara *et al.*, 2004). In native tissues, oxygen distribution is provided by the circulatory system and the oxygen-carrier hemoglobin (Hb). Oxygen tension values found in tissues are commonly expressed in terms of oxygen partial pressure (pO_2), and normally fall within the range of 20 to 50 mmHg. In contrast, oxygen tension in tissue injuries drops beyond 10 mmHg due to damage in the microvasculature, diffusion restrictions and peripheral vasoconstriction (Bland *et al.*, 2013; Colom *et al.*, 2013).

Tissue oxygenation is crucial to support ECM-formation. Collagen is a component of the ECM and can be exported from fibroblasts only when it is in a triple helical structure. The formation of these triple helices is regulated by the activity of prolyl- and lysyl-hydroxylases, which in turn is proportional to the tissue oxygen tension. Hence, the pO_2 in the tissues controls collagen synthesis by fibroblasts. Collagen deposition results in the gain of tissue tensile strength, and when impaired the likelihood of scar tissue formation is greater. Furthermore, vessels require a sheath of ECM, mainly collagen and proteoglycans, to guide tube formation and resist the pressures of blood flow (Sen, 2009).

Oxygen also plays a key role in the prevention of infections. Reactive oxygen species are the major components of the bactericidal defense against wound pathogens. They are produced by nicotinamide adenine dinucleotide phosphate (NADPH) -linked oxygenases by consuming high amounts of oxygen (Tandara *et al.*, 2004). Similarly superoxide, besides being bactericidal, is a signaling molecule that leads to enhancement of the bacterial killing capacity by granulocytes (Hopf *et al.*, 2007). Hence, activated inflammatory cells rely on an increased oxygen demand.

The function of several pro-angiogenic growth factors and numerous mechanisms, like leukocyte recruitment, cell motility and integrin function ultimately rely on redox signaling, which depends to great extent on tissue oxygenation. In addition to this, oxygen is required to sustain the elevated consumption by cells that migrated into the wound site and are involved in the process of epithelialization and tissue remodeling, and are therefore metabolically more active and in a proliferative state (Tandara *et al.*, 2004).

Hypoxia is a hallmark of all ischemic diseases. It is described as a lower tissue pO_2 as compared to the one present in the specific tissue under healthy conditions. Hypoxia results from a reduction in oxygen delivery below tissue demand. Cells exposed to hypoxia either induce an adaptive metabolic response that includes increasing the rates of glycolysis and conservation of energy, or undergo cell death (Sen, 2009).

Acute, severe and chronic hypoxia have different impacts on wound healing. For example, energy conservation mechanisms, such as an overall down-regulation of protein synthesis, promote survival under low oxygen conditions, yet they are not compatible with the formation of new tissue (Sen, 2009). Endothelial cells have been shown to initiate angiogenesis at around 5% pO_2, but at extreme hypoxia, they initiate apoptosis (Fong, 2009). The anaerobic production of lactate promotes macrophage activation and granulation, however levels in excess of 15 mM are usually associated with excess inflammation or infection. Lactate, hypoxia, and the by them induced growth factors promote collagen mRNA synthesis and procollagen production. However, collagen deposition, hydroxylation and polymerization are only possible in the presence of molecular oxygen (Hopf *et al.*, 2007).

From a diagnostic point of view, measurements of wound oxygenation are commonly used to guide treatment planning, such as the decision of amputation. The transcutaneous oxygen tension ($TcPO_2$) measurement is an accurate, non-invasive, and good predictor of ischemic ulcer healing. Chronic foot ulcers have been reported to have a low probability of ulcer healing if they showed a $TcPO_2$ of less than 20 mmHg (Ruangsetakit *et al.*, 2010). Also, $TcPO_2$ values between

10 mmHg and 20 mmHg are related to an increased risk of amputation in patients with skin lesions and arterial disease (Carter *et al.*, 2006).

Hyperbaric oxygen (HBO) and topical oxygen therapies have been found to benefit the healing of chronic wounds. HBO is a treatment modality in which a person breathes 100% oxygen, while exposed to two to three atmospheres of pressure. During treatment, the arterial oxygen tension often exceeds 2000 mmHg and levels of 200 to 400 mmHg are reached in tissues (Thom, 2011). HBO is known to increase tissue oxygen in ischemic tissue and increase angiogenesis in hypoxic or injured tissue. In order to apply oxygen topically, a clinical device that isolates the wounded area is connected to an oxygen gas cylinder. This method has showed to elevate the wound bed pO_2 and promote closure in superficial wounds (Fries *et al.*, 2005).

The decision over the implementation of one therapy or the other, means a compromise between the net tissue pO_2 increase required and the risks of exposing oxidative-stress pre-disposed patients to oxygen toxicity, unfavorable systemic effects caused by the approach, and the risk of tissue damage from excessive oxygen. Still, none of these therapies provides a constant supply of oxygen to the tissue (Sen, 2009).

Although both therapies merely aim to increase the pO_2 in wounded tissues and by these means rescue the injured tissue from pathologic hypoxic conditions, oxygen-mediated mechanisms appear to synergistically co-activate the signaling of growth factors such as bFGF, TGF-β, PDGF-B, nitric oxide (NO), and VEGF, and decrease excessive inflammatory cells infiltration. This evidence sustains that oxygen also functions as an intracellular signal transducer, and therefore as a regulator of gene expression and immune response (Sen, 2009, Tandara *et al.*, 2004).

Hypoxia is an early and important event in the initiation of the healing process. However, near-anoxic hypoxia, is not compatible with life or tissue repair (Krock *et al.*, 2011). Complications such as failure to heal, infection, and excessive scarring are to great extent related to insufficient regenerative tissue oxygenation. To avoid infection of the wounds, ensure rapid tissue synthesis, and optimize the immune response, adequate wound-tissue oxygen levels have to be provided (Hopf *et al.*, 2007).

1.3.2 Oxygen in tissue engineering approaches

Hypoxia is broadly recognized as a critical factor limiting the progress of tissue engineering. Cells within a bioengineered tissue will not survive if they are located more than a few hundred micrometers away from a blood vessel due to oxygen and nutrient deprivation. Thus, the risk of necrosis due to diffusion restrictions hinders the development of functional artificial tissues greater than 1 mm^3 (Kim *et al.*, 2014).

Some attempts to increase oxygen transport and transfer within biomaterials considered the use of artificial oxygen carriers, like perfluorocarbon or modified hemoglobin (Centis *et al.*, 2009). The former is characterized by a high gas dissolving capacity and a remarkable chemical and biological inertness. Though, the efficiency of oxygen transport by fluorocarbon has been demonstrated, due to its linear relationship between pO_2 and oxygen content, high arterial pO_2 is necessary to maximize its transport capacity. Moreover, the toxic build-up of its compounds due to failure of metabolic removal, allergies related to the fluorocarbon emulsifiers, and the unknown metabolism of fluorocarbon in humans, are possible risks of their implementation (Spahn, 2000).

The human Hb molecule has been modified, in order to avoid both immunogenic issues and the rapid breakdown of Hb outside of the red blood cell. Modified Hb is similar to native Hb in its profile for loading and unloading of oxygen, but is designed to show a decreased oxygen affinity. This allows an efficient gas transport and facilitates its transfer into the tissue (Chang, 2004). Although, the modified Hb seems to be very promising in improving tissue oxygenation, its use is associated with side effects such as vasoconstriction, resulting in an increase in systemic and pulmonary artery pressures (Bland *et al.*, 2013).

Another interesting approach has been the development of oxygen generating biomaterials by incorporation of solid sodium percarbonate particles that release oxygen upon their chemical decomposition once they come in contact with water. A sustained release of a small but statistically significant increase in the dissolved oxygen concentration has been shown for ten

days leading to an extended cell viability under hypoxic conditions (Oh *et al.*, 2009). Yet these materials raise concerns about the intermediate hydrogen peroxide generation, and residuals, which would require the further incorporation of anti-oxidants into the biomaterial. Further, the factors that control the rate of oxygen generated from scaffolds are not entirely understood (Oh *et al.*, 2009; Harrison *et al.*, 2007).

A novel approach previously presented by our group, has shown that photosynthetic algae can be compatibly incorporated to artificial collagen scaffolds for dermal replacement to create photosynthetic biomaterials (Hopfner *et al.*, 2014). Proliferation and oxygen production were sustained upon seeding, the last showing to be light and cell-density dependent. Their compatibility with animal cells *in vitro* was tested in both two- and three-dimensional co-cultures using murine fibroblasts and algae, and in both cases, cells proliferated under conditions formerly optimized for the co-culture. Furthermore, the oxygen released by the algae, sustained the requirements of the fibroblasts under hypoxic conditions. The authors concluded that the combined use of biomaterials with photosynthetic cells generates scaffolds that create normoxic microenvironments in response to light, which meant the first scientific evidence supporting that photosynthesis can overcome the need of oxygenation in tissue engineering approaches.

1.4 Gene therapy to improve vascularization in tissue engineering

1.4.1 State of the art

As introduced in section 1.2.3, strategies to enhance vascularization are crucial for the success of tissue engineering approaches. In order to overcome this issue, scaffold activation with growth factors has been intensively investigated to induce angiogenesis in the engineered tissues (reviewed by Lee *et al.*, 2011 and Reed *et al.*, 2014)

Growth factors are soluble-secreted signaling polypeptides, which influence the biological activities of responsive cells in both, an autocrine and a paracrine fashion (Riedel *et al.*, 2006). Two main strategies are being followed for their use in therapeutic angiogenesis: the use of recombinant growth factor proteins and gene therapy.

The direct administration of recombinant growth factors has major limitations related to the short biological half-life of the molecules, and therefore, consequent necessity for repeated administration of large doses, in addition to their cost-intensive production (Hirsch *et al.*, 2007). To overcome this issue, immobilization and physical encapsulation of growth factors in either natural or artificial polymers have been suggested to regulate their delivery (Lee *et al.*, 2011). Also, smart delivery systems are being developed to ensure a constant supply of the factors into the wounds, based on their controlled release from the scaffold (Richardson, *et al.*, 2001; Jin *et al.*, 2008; Reckhenrich *et al.*, 2011).

Gene therapy is defined as the insertion and expression of a foreign gene in cells of a host organism with the aim of synthesizing therapeutic active proteins directly at a desired location in the patient, thus warranting their sustained expression. Target genes are delivered by either viral, chemical or mechanical methods into the patient's cells. The method of delivery is often a compromise between stability of expression, which depends on the transfection efficiency, titer and half-life of the vector; and safety, concerning potential oncogenicity, risk of insertional mutagenesis and vector-related immune reactions.

Furthermore, gene regulation tools are required to control the expression of the foreign gene once it has been introduced into the host tissue, especially if, as in wound healing, only time limited expression is desired (Hirsch *et al.*, 2007).

Some of the growth factors which have shown to be promising in the induction of angiogenesis are VEGF-165, PDGF-B, bFGF, KGF, TGF-β, hepatocyte growth factor (HGF), and the granulocyte-macrophage colony-stimulating factor (GM-CSF). From these, only the recombinant human variant of PDGF-B has successfully completed randomized clinical trials and is approved by the Food and Drug Administration (Barrientos *et al.*, 2008).

The contradiction between the published success of growth factor-based therapies in preclinical models and their rather disappointing clinical results, has led some authors to conclude, that combinations of growth factors rather than the overexpression of a single one, is required (Castellon *et al.*, 2002; Liu *et al.*, 2005). The combined stimulation with VEGF-A, PDGF-B, and bFGF has emerged as a potent strategy for therapeutic angiogenesis (Kano *et al.*, 2005). Further, sequential delivery of VEGF, PDGF-B, and TGF-β from alginate scaffolds has shown superior vascularization to bFGF alone (Freemann *et al.*, 2009). Similarly, the temporally coordinated expression of VEGF-A and PDGF-B led to an increase in functional blood vessels (Banfi *et al.*, 2011). Unfortunately, the joint delivery of growth factors increases the complexity of the approach and might not be possible for some vector systems, and therefore alternative paths for gene delivery in therapeutic angiogenesis are still required.

1.4.2 Vascular Endothelial Growth Factor

The VEGF-family and their receptors are key mediators in embryonic vascular development and angiogenesis in the adult. The VEGF-ligands consist of seven members, VEGF-A - VEGF-F, and placenta growth factor (PlGF). They share a common structure, known as the cystine knot motif, consisting of eight invariant cysteine residues involved in inter- and intramolecular disulfide bonds (Hoeben *et al.*, 2004). Besides VEGF-A, only VEGF-E and PlGF seem to be involved in wound repair and have been studied as targets for therapeutic angiogenesis (Ferrara, 2001).

VEGF-A is a 34- to 42-kDa dimeric, disulfide-bound glycoprotein of singular importance in vascular biology. By differential messenger RNA (mRNA) splicing, the VEGF-A gene gives rise to eight isoforms that differ in their ability to bind to cell surfaces and ECM-components, like fibrin. The 165-amino-acid isoform is the major gene product found in human tissues, it has a medium heparin binding affinity and is the only one able to bind to all VEGF tyrosine kinase receptors: VEGFR-1 - VEGFR-3 and neuropilin-1 (NRP-1).

VEGFR-2 is the most important receptor in VEGF-induced mitogenesis and is predominantly expressed by endothelial cells. Binding of VEGF to VEGFR-2 induces the receptor autophosphorylation and the activation of diverse kinase cascades that lead to proliferation of pre-existing endothelial cells, migration and recruitment of marrow-derived endothelial progenitor cells, endothelial cell survival and increase in vascular permeability (Hoeben *et al.*, 2004). Also, VEGF-A mediates the influx of inflammatory cells into the site of injury and upregulates the synthesis of other angiogenic growth factors, such as PDGF-B (Kano *et al.*, 2005).

Mechanical injury, hypoxia, and hypoglycemia induce VEGF-A expression in skin. Similarly, pro-inflammatory cytokines (IL-1α, IL-1β, IL-6), growth factors, such as TGF-β, EGF and PDGF-BB, and estrogens, stimulate VEGF-A gene transcription. VEGF-A is predominantly released by keratinocytes, but also secreted from intracellular pools within platelets, neutrophils and infiltrating macrophages (Hoeben *et al.*, 2004).

1.4.3 Platelet-derived Growth Factor

The PDGF-family consists of five disulfide-bonded dimeric molecules, which assemble as homodimers (PDGF-AA, PDGF-BB, PDGF-CC and PDGF-DD) or heterodimers (PDGF-AB). PDGF isoforms bind with different specificities to two receptor subunits that are homo- or heterodimerized to form three functional tyrosine kinase receptors: PDGFR-α, PDGFR-αβ, and PDGFR-β. Only the 28 kDa glycosylated dimer PDGF-BB is capable of binding to all three receptors (Tallquist *et al.*, 2004).

PDGF is known to be produced by a number of cell types such as platelets, macrophages, monocytes, smooth muscle cells, fibroblasts and keratinocytes. It has also been found to be a mitogen for almost all mesenchymal-derived cells (Barrientos *et al.*, 2008). The patterns of ligand and receptor expression suggest a paracrine mechanism of action, since PDGF is predominantly expressed in the epidermis, whereas the PDGF-receptors are found in the dermis and the granulation tissue (Werner *et al.*, 2003). Upon ligand binding, the PDGF-receptors dimerize and autophosphorylate on tyrosine residues, which are used as anchor sites for various SH2 domain-containing signaling enzymes and adaptor molecules, leading to the activation of diverse kinases triggering signaling pathways for cell survival and directed cell migration (Tallquist *et al.*, 2004).

PDGF is involved in each stage of wound healing. Upon injury, PDGF released from degranulating platelets stimulates fibroblast proliferation and chemotaxis of neutrophils and macrophages to the wound site. It also stimulates the secretion of growth factors such as TGF-β, IGF-1, and thrombospondin-1, which are involved in wound re-epithelialization. During the proliferative phase, PDGF promotes collagen synthesis in fibroblasts, whereas in the later remodeling phase it induces myofibroblast differentiation. In regard to angiogenesis, PDGF-BB seems to modulate endothelial proliferation and angiogenesis via PDGF-β receptors. Also, PDGF-BB works synergistically with hypoxia to increase the expression of VEGF-A (Barrientos *et al.*, 2008). Although, PDGF is not essential for initial blood vessel formation, it is particularly important in blood vessel maturation, since it increases pericyte and smooth muscle cells recruitment, leading to an increased integrity of the capillaries (Raica *et al.*, 2010).

1.5 *Chlamydomonas reinhardtii*

1.5.1 General considerations about *C. reinhardtii*

The taxonomic classification of the unicellular eukaryotic green algae of the genus *Chlamydomonas* assigns them to the family of the *Chlamydomonadaceae* within the order of the *Volvocales* of the class of *Chlorophyceae*. The wild-type *C. reinhardtii* (Fig. 4) is usually found in soil and fresh water. It has an oval shape of about 5-10 micrometers in diameter and is enclosed by a multilayered cell wall made of hydroxyproline-rich glycoproteins and non-cellulosic polysaccharides. *C. reinhardtii* has a prominent cell nucleus with nucleolus, both surrounded by a membrane that is continuous with the endoplasmic reticulum and Golgi bodies. Characteristic organelles of the alga include two anterior inserted whiplash flagella of 10 -12 micrometers in length; contractile vacuoles located just below; a single large cup-shaped chloroplast that occupies two thirds of the cell and partially surrounds the nucleus; cytosol dispersed mitochondria; a large pyrenoid, which is the site of carbon dioxide (CO_2) fixation; and an eyespot of highly condensed carotenoid pigments that work as a directional antenna for the phototactic response (Harris, 2009).

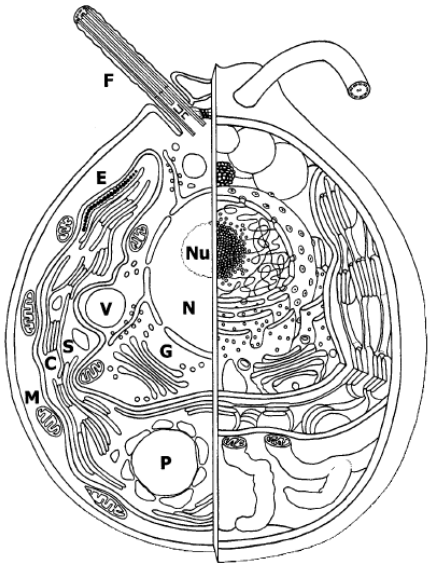

Figure 4: Cell structure of *C. reinhardtii*. The two and three-dimensional view of the cells shows the nucleus (N) with the nucleolus (Nu), the two isoform flagella (F), the cup-shaped chloroplast (C), the eyespot (E) and the starch-containing pyrenoid (P) and the mitochondria (M). In addition, one may distinguish the Golgi vesicle (G), starch grains (S) and vacuoles (V). Taken from Nickelsen & Kück, 2000.

The principal laboratory *C. reinhardtii* strains are thought to derive from isolates made near Amherst, Massachusetts, in 1945 by Gilbert M. Smith. Under a vegetative stadium, *C. reinhardtii* cells are haploid with a nuclear genome of about 120 Mb, organized in seventeen chromosomes; a 15.8 kb mitochondrial genome; and 50-80 identical copies of a 195 kb chloroplast circular genome. All three of them have been fully sequenced (Merchant *et al.*, 2007). *C. reinhardtii* algae can reproduce both sexually and asexually depending on the conditions they are grown.

C. reinhardtii is one of the best studied algae and has been long used as a model organism in biology to study a wide range of questions in areas such as flagellar function, photobiology, photosynthesis, and protein synthesis (Pröschold *et al.*, 2005). In the laboratory, *C. reinhardtii* cells grow at an optimal temperature between 20-25°C in defined salt based liquid or agar media at neutral pH. They can be grown under three different conditions: with light and CO_2 as the sole carbon source (phototrophic growth), in acetate-containing medium with light (mixotrophic growth) or without light (heterotrophic growth). However, growth in light either with or without acetate is faster than dark growth. They show a generation time of 6-8 h, when cultured with adequate illumination (200–400 μEinsteins $\cdot m^{-2} \cdot sec^{-1}$ photosynthetically active radiation; Harris, 2001).

C. reinhardtii cells are enclosed by a multilayered cell wall, which consists of an insoluble hydroxyproline-rich glycoprotein innermost layer and three layers of chaotrope-soluble glycoproteins forming the so called central triplet, which is itself covered by a an amorphous outer layer of branching glycoprotein fibers. Back in the seventies, *C. reinhardtii* cell-wall deficient mutants were isolated and classified into three morphological groups, class A-C, according to the amount of cell wall material and its attachment to the plasma membrane as compared to wild-type cells. The widely used *cw15* wall-less laboratory strain belongs to class C. This mutant has a rudimentary cell wall with reduced amounts of cell wall components, because it fails to assemble the layers of the central triplet. Instead it creates a structure of branched cell-wall fibers that resemble the outer layer of the wild-type wall (Harris, 2009).

Wall-deficient mutants have found widespread use as recipients of exogenous deoxyribonucleic acid (DNA), as their transformation appears to be convenient and successful. They do not require a prior enzymatic removal of the cell wall and show efficient protein secretion into the culture medium. Also, cell wall-deficient *C. reinhardtii* strains are unwieldy to cross, because they often have only short flagella and are thus practically immotile (Neupert *et al.*, 2009).

In an attempt to overcome the poor expression of transgenes from the alga's nuclear genome and the difficulty to identify clones that express foreign genes of interest efficiently, Neupert *et al.* developed a genetic screen to isolate algal strains that significantly increased the synthesis of recombinant proteins expressed from nuclear transgenes. The screening strategy included first, a co-transformation selection procedure using a cell wall-deficient flagella-less arginine-auxotrophic *C. reinhardtii* strain (*cw15 arg*$^-$) for restoration of arginine prototrophy and later for gaining of tolerance to the translational inhibitor emetine. Then, those strains showing poor transgene expression were subjected to UV light-induced mutagenesis, with the purpose of inactivating the transgene suppression mechanism. The obtained strains were next tested for their potential to express other transgenes to high levels. Finally, the strain named UVM4, was identified for having a significantly higher transformation efficiency. It accumulated foreign protein to a level of 0.2% of the total soluble protein, gave rise to much higher numbers of transformant colonies and had a one-hundred success rate of transgene expression. The authors believed these strains could help to overcome the serious limitation of transgene expression in basic and applied research with *C. reinhardtii* (Neupert *et al.*, 2009).

1.5.2 *C. reinhardtii* as a model organism to study photosynthesis

In 1772, Joseph Priestley, demonstrated the dependency of animal survival on photosynthesis (Priestley, 1772). He showed that a mouse died if it was placed in a closed compartment, but it survived if a plant was introduced as well. Priestley concluded that plants restore whatever breathing animals remove from the air[1]. Later, it was established that oxygen (O_2) was the molecule released by plants that was required by animals.

Oxygenic photosynthesis is an energy-transducing process through which photosynthetic organisms are able to transform light energy into biochemical energy. This process involves a series of electron transfer reactions from water (H_2O) molecules to the electron acceptor $NADP^+$, known as light-reactions, which are coupled to adenosine triphosphate (ATP) synthesis and the byproduct release of O_2. In a second step, the fixation of CO_2 and the biosynthesis of carbohydrates takes place, during the so-called dark-reactions (Singhal *et al.*, 1999).

C. reinhardtii has been used as a model organism in photosynthesis research for over fifty years. Its photosynthetic apparatus is closely related to that of vascular plants, and its photosynthesis genes are too encoded by both the nuclear and chloroplast genomes (Dent *et al.*, 2001).

The primary light-reactions occur in a complex protein system in the thylakoid membrane within the chloroplast (Fig. 5). This system is composed by the peripheral antenna system bound to a light-harvesting complex (LHCII); the photosystem II (PSII), which mediates the electron transfer to plastoquinone (PQ) through photolysis of H_2O; the cytochrome b_6f complex (cyt b_6f); the photosystem I (PSI), which is a light-driven oxidoreductase that transfers electrons from cytochrome b_6f, in the thylakoid lumen, to ferredoxin (Fd) in the stroma, in turn generating NADPH; and a proton-ATP synthase (Eberhard *et al.*, 2008).

[1] "This observation led me to conclude, that plants instead of affecting the air in the same manner with animal respiration, reverse the effects of breathing, and tend to keep the atmosphere sweet and wholesome, when it is become noxious, in consequence of animals living and breathing, or dying and putrefying in it". (Priestley, 1781)

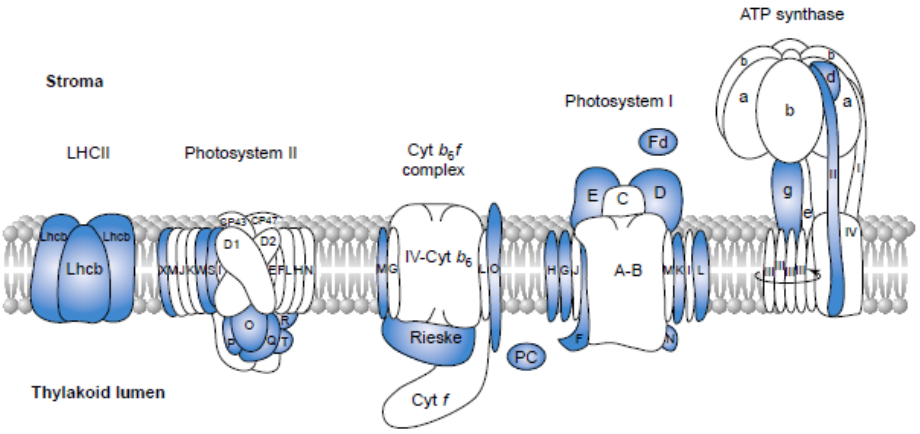

Figure 5: Photosynthetic complexes of the thylakoid membrane in *C. reinhardtii*. The composition of the complexes is drawn according to the structural data available, but position of subunits within the complexes is arbitrary. Nucleus-encoded subunits are shaded blue, chloroplasts-encoded subunits are white. Taken from Dent et al., 2001.

First, visible light is absorbed by pigment molecules of antenna system, such as chlorophyll a and b, and carotenoids. The absorption of a photon causes the transition of an electron from the electronic ground state to an excited state. The LHCII transfers the excited electron to the reaction center of the PSII. This starts a series of energetically downhill electron transfer steps from a donor to an acceptor electron carrier molecule, which are driven by the proximity of the electron carriers and their electronic environment.

The PSII uses light energy to drive two chemical reactions, the oxidation of H_2O and the reduction of PQ. Five redox components are involved in transferring electrons from H_2O to the PQ pool: the H_2O oxidizing manganese cluster, the amino acid tyrosine, the reaction center chlorophyll (P680), pheophytin, and the PQ molecules, QA and QB. PSII is the only known protein complex that can oxidize H_2O, resulting in the release of O_2 into the atmosphere. This reaction is driven by the oxidized reaction center, P680+, and involves four sequential turnovers of the reaction center, requires two molecules of H_2O and results in the release of one O_2. The reduced PQ molecule is released from PSII and diffuses in the photosynthetic membrane until it encounters a specific binding site on the cyt b_6f complex.

The cyt b_6f complex is a membrane bound protein complex that contains four electron carriers, three cytochromes and a FeS-cluster. It removes the electrons from reduced PQ and transfers them to the PSI by small copper-containing protein, plastocyanin (PC).

The PSI complex catalyzes the oxidation of PC, and the reduction of Fd, a small FeS-protein. The electron transfer with the activation of a primary donor, P700, which is a chlorophyll dimer, and a chlorophyll monomer Ao in the PSI reaction center. Electron transfer from PSI to $NADP^+$ requires Fd, and the ferredoxin-NADP oxidoreductase (FNR), a peripheral flavoprotein that operates on the outer surface of the photosynthetic membrane. The FNR catalyzes the final electron transfer from PSI to $NADP^+$, producing the reduced form, NADPH.

An electrochemical gradient of protons across the photosynthetic membrane is created in the course of the photosynthetic process. The energy stored in the proton electrochemical potential is used by a membrane bound ATP-Synthase to covalently attach a phosphate group to adenosine diphosphate (ADP), forming ATP. The energy stored in ATP can be transferred to another molecule by transferring the phosphate group. The NADPH and ATP formed by the light reactions provide the energy for the dark reactions of photosynthesis (Singhal *et al.*, 1999).

Like plants, *C. reinhardtii* algae have the ability to adapt and to modulate the operation of the photosynthetic apparatus in response to changes in light quality and quantity, as well as to tune their photosynthetic activity to their environmental nutrient status (Rochaix, 2001). This photosynthetic acclimation encompasses changes in light harvesting capacity, stoichiometry between antenna protein system and reaction centers, and in the relative stoichiometry between the two photosystems (Eberhard *et al.*, 2008). *C. reinhardtii* has a maximal photosynthetic activity of 7.584 ± 0.416 μg O_2 (237 ± 13 nmol O_2) per 10^6 cells in one hour under continuous illumination (Jansen *et. al.*, 2000).

1.5.3 Expression of recombinant proteins in *C. reinhardtii*

1988 was the first demonstration of a stable chloroplast transformation. Three years later, the first recombinant protein was synthesized in *C. reinhardtii* (Leon *et al.*, 2008). Today the list of recombinant proteins successfully expressed by the so called "green yeast" include stable active monoclonal antibodies, antigenic proteins for oral vaccines, and human growth factors (Tab. 1; Rasala *et al.*, 2014).

Table 1. Summary of recombinant proteins manufactured in *C. reinhardtii* (adapted from Rasala *et al.*, 2014)

Protein	Function	Genome	Notable results	References
Proteins in therapeutics				
Metallothione-2	Anti-radiation	Chloroplast	Increased resistance to UV-B	Zhang *et al.*, 2006.
TRAIL	Anti-cancer	Chloroplast	Protein accumulated to 0.43–0.67 % TSP	Yang *et al.*, 2006.
Allophycocyanin	Anti-cancer	Chloroplast	Expression of two genes from a polycistronic vector Protein accumulated to 2–3 % of TSP	Su *et al.*, 2005.
VEGF	Stimulates vasculogenesis and angiogenesis	Chloroplast	Protein accumulated to 2 % of TSP Bioactivity demonstrated through a receptor-binding assay	Rasala *et al.*, 2010.
HMGB1	Wound repair	Chloroplast	Protein accumulated to 2.5 % of TSP Algal-HMGB1 induced chemotaxis of mouse and pig fibroblasts, demonstrating bioactivity	Rasala *et al.*, 2010.
14FN3	Antibody mimic	Chloroplast	Protein accumulated to 3 % of TSP	Rasala *et al.*, 2010.
SAA-10FN3	Antibody mimic	Chloroplast	Fusion of a protein that did not express alone to a well expressed protein enabled significant fusion protein accumulation	Rasala *et al.*, 2010.
Erythropoietin	Treatment for anemia	Nuclear	EPO was secreted and accumulated to 100 lg/L	Eichler-Stahlberg *et al.*, 2009.
MAA	Prophylaxis for enteric bacterial infections	Chloroplast	Protein accumulated to above 5 % of total soluble protein Purified algal-MAA induced mucin secretion, demonstrating bioactivity	Manuell *et al.*, 2007.

Table 1: Summary of recombinant proteins manufactured in *C. reinhardtii* (continued).

Protein	Function	Genome	Notable results	References
Subunit vaccines				
VP1-CTB	Protection against FMDV	Chloroplast	Protein accumulated to 3 % of TSP	Sun *et al.*, 2003.
E2	Protection against CSFV	Chloroplast	Protein accumulated to 1.5-2 % of TSP Subcutaneous injections elicited an immune response in mice	He *et al.*, 2007.
V28	Vaccine against white spot syndrome virus	Chloroplast	Protein accumulated to up to 21 % of total protein	Surzycki *et al.*, 2009.
GAD65	Treatment to prevent onset of type 1 diabetes	Chloroplast	Protein accumulated to 0.3 % of TSP Algal-GAD65 stimulated the proliferation of spleen lymphocytes from NOD mice	Wang *et al.*, 2008.
D2-CTB	Protection against S. aureus	Chloroplast	Protein accumulated to up to 0.7 % of TSP Oral vaccination of mice offered protection against a lethal dose of S. aureus	Dreesen *et al.*, 2010.
E7 of HPV-16	Cancer vaccine against HPV-16	Chloroplast	Protein accumulated to up to 0.12 % of TSP Subcutaneous injections of algal lysates and purified protein elicited specific IgG responses Tumor protection was demonstrated following tumor cell line challenge	Demurtas *et al.*, 2013.
GBSS-AMA1	Malaria vaccine	Nuclear	Immunization with transgenic starch particles led to reduced parasitemia with extended life spans upon challenge	Dauville´e *et al.*, 2010.
GBSS-MSP1	Malaria vaccine	Nuclear	Immunization with transgenic starch particles led to reduced parasitemia with extended life spans upon challenge	Dauvillée *et al.*, 2010.
Pfs25	Malaria transmission blocking vaccine	Chloroplast	Coluble and folded correctly	Gregory *et al.*, 2012.
Pfs28	Malaria transmission blocking vaccine	Chloroplast	Soluble and folded correctly	Gregory *et al.*, 2012.
Pfs48/45	Malaria transmission blocking vaccine	Chloroplast	Soluble and folded correctly	Jones *et al.*, 2013.
Pfs25-CTB	Malaria transmission blocking oral vaccine	Chloroplast	Oral administration of mice elicited an IgA mucosal response to Pfs25 and CTB	Gregory *et al.*, 2013.

Table 1: Summary of recombinant proteins manufactured in *C. reinhardtii* (continued).

Protein	Function	Genome	Notable results	References
Antibodies and immunotoxins				
Anti-HSV glycoprotein D lsc	Antibody against herpes simplex virus	Chloroplast	Soluble protein expression Dimerization with disulfide bond formation Bound HSV protein	Mayfield et al. (2003)
Anti-PA 83 anthrax IgG1	Antibody against antrax	Chloroplast	Expression of full-length IgG Correct assembly of light and heavy chains with disulfide bond formation	Tran et al. (2009)
Anti-CD22-ETA sc	Immunotoxin against B-cell lymphoma	Chloroplast	Soluble protein expression Bound and killed CD22-positive Burkitt's lymphoma cells Inhibited tumor growth in animal models	Tran et al. (2013b)
Anti-CD22-gelonin sc	Immunotoxin against B-cell lymphoma	Chloroplast	Soluble protein expression, 0.1–0.3 % TSP Bound and killed CD22-positive B-cell lymphoma cells	Tran et al. (2013a)
Industrial enzymes and enhanced animal feeds				
Phytase (AppA)	Increase phytate phosphorus utilization.	Chloroplast	Oral delivery of AppA-algae to broiler chicks led to a decrease in phytate content in manure	Yoon et al., 2011.
Xylanase, a-galactosidase, phytase	Feed additives	Chloroplast	All three classes of enzymes were shown to be bioactive	Georgianna et al., 2013.
b-1,4-Endoxylanase	Feed additives, food manufacturing, paper bleaching	Nuclear	Demonstrated secretion of bioactive enzyme Developed an improved method for nuclear transformation that led to increased recombinant protein accumulation	Rasala et al., 2012.
Nutritional supplements				
Sep15	Selenium supplement	Nuclear	Human selenoprotein accumulated to detectible levels	Hou et al., 2013.

Electroporation, vortexing, and microparticle bombardment are some of the methods to generate genetically modified (GM) microalgae. All of them are based on causing a temporal permeabilization of the cell membrane and so enable DNA molecules to enter the cell while preserving their viability. Agitation in the presence of glass beads, is a simple technique to achieve nuclear transformation. It works efficiently with cell-wall deficient mutants or wild-type algae following enzymatic degradation of the cell wall (León-Bañares *et al.*, 2004).

Transgene expression from the nuclear genome of *C. reinhardtii* bids to direct proteins to organelles of the secretory pathway, thus enabling posttranslational modification and their targeting for excretion. Nuclear transformation of the algae occurs through non-homologous recombination. The transforming DNA integrates at random locations of the nuclear genome, often causing deletions (5-20 kb) of the host DNA or rearrangements at the integration site. As a result, levels of transgene expression depend greatly on the chromosomal position of transgene insertion. The integration of multiple copies of the transgene is possible, their number being proportional to the initial foreign-DNA concentration and they are often found as concatamers inside the genome (Leon *et al.*, 2008).

To ensure transcription and achieve a stable expression of the protein, strong constitutive homogenic promoters should be selected. Fischer and Rochaix showed that the flanking regions of PsaD drive efficient nuclear gene expression of endogenous and exogenous genes. The PsaD-gene is present in a single copy in the genome of *C. reinhardtii*. It encodes a 20 kDa subunit of the PSI located on the stromal side of the thylakoids. It does not contain introns, which means that all the regulatory sequences required for its high-level expression lie in the flanking promoter and untranslated regions downstream. Thus, the insertion of introns to mimic the composition of the wild-type gene and so create a favorable pattern to enhance transgene expression is not required (Fisher *et al.*, 2001).

Since *C. reinhardtii* is haploid, the expression of the mutant phenotype is immediate once the gene was integrated correctly. However, genes in *C. reinhardtii* have a higher GC-content (61%) than other organisms. Hence, the expression of foreign genes in the microalgae requires their adaptation to the codon usage bias of the algae. Otherwise, the transgenes might be susceptible to silencing effects and translational stalling, premature translation termination, translation frame shifting or amino acid misincorporation due to insufficient transfer RNA (tRNA) pools.

Resistance selection, for instance against the antibiotic paromomycin, is one of the most prevalent strategies to identify the transformants. The selection gene is usually cotransformed in the same construction as the target gene to achieve a high frequency of expression of both genes.

Moreover, transgenic algal clones have to be maintained under selection conditions, otherwise expression of the exogenous gene might be suppressed. The mechanism seems to occur both transcriptionally or post-transcriptionally, and involves epigenetic changes in gene expression and processes to promote the foreign gene-transcript degradation that are not well understood. Nevertheless, algae can be frozen in liquid nitrogen to maintain transgenic cell lines (Leon *et al.*, 2008).

C. reinhardtii combines the fast and easy growth of unicellular microorganisms with the advantages from eukaryotic protein expression hosts. They are able to efficiently produce properly folded full-length proteins and perform post-translational modifications, like O- and N-glycosylation and the correct formation of disulfide bonds (Eichler-Stahlberg *et al.*, 2009). The microalgae are industrially attractive for recombinant protein expression because of their well-known genomics with three genomes amenable to genetic manipulation; the simple and well-established transformation techniques that allow the fast generation of transformant lines within 4-6 weeks; and a high scalability due to the eight-hours generation time, which significantly shortens the time required from initial transformation to protein production in liters.

Furthermore, photosynthetic algae are less expensive, since they utilize sunlight as their energy source and extract CO_2 from the air as their carbon source, unlike mammalian or yeast cells that have high media costs and require complex cultivation systems. They pose little risk of viral, prion or bacterial endotoxin contamination in the protein extract, and unlike earth plants, they pose no threat to the environment, since gene flow to surrounding food crops is not possible. Moreover, because green algae are not traditional foods, there is low danger of food supply becoming contaminated with therapeutic proteins (Rosales-Mendoza *et al.*, 2012, Rasala *et al.*, 2014). Finally, since the algae do not harbor any known pathogenic viruses or other harmful molecules, it is a generally recognized as safe (GRAS) organism by the Food and Drug Administration (FDA) from the United States of America (Almaraz *et al.*, 2014).

1.6 Motivation: life complementarity and symbiosis

Symbiogenesis is the evolutionary theory which explains the origin of eukaryotic cells from prokaryotes. It states that the incorporation of organisms such as proteobacteria and cyanobacteria by a larger free living cell once lead to the formation of eukaryotic organelles like mitochondria and chloroplasts, respectively. These series of endosymbiotic events 1.5 billion years ago provided host cells with new capabilities, which allowed them to live under different environmental conditions (McFadden, 2001).

On a major scale, some organisms have known to profit from symbiotic relationships and turned them into a strategy of survival. For example, the green hydra, *Hydra viridissima* (Dunn, 1987) and the sea slug, *Elysia chlorotica* (Rumpho *et al.*, 2011), have established forms of endosymbiosis with photosynthetic organisms such as *Chlorella* and *Vaucheria litorea*, respectively, which allow them to live through periods of starvation, turn them to some degree into photoautotrophs and could even be considered an advantageous camouflage tactic in their aquatic environment.

The limited diffusion of oxygen through tissues gave rise to highly developed pulmonary, hematopoietic, and vascular systems to ensure that each of the approximately 10^{14} cells in the adult human body are provided with oxygen (Hoeben *et al.*, 2004). While animal evolution gave rise to erythrocytes, *i.e.* cells transporting oxygen, plant evolution has carried microalgae, which are cells capable to synthesize it. Hereafter, the insinuation that symbiosis might be key to overcome tissue hypoxia is strikingly intriguing.

II. Hypothesis and aims of the project

This work aims to explore the potential of locally induced photosynthesis to fulfill the oxygen requirements of non-vascularized tissues and hence be used as a treatment for wound regeneration. It is hypothesized, that by incorporating the unicellular algae *C. reinhardtii* into biocompatible scaffolds, a tissue with the intrinsic potential to produce and release oxygen can be developed, which will be able to decrease local hypoxia. This tissue should be implantable, should maintain its viability until complete tissue restoration is achieved and should not induce any major inflammatory reaction. The specific objectives defined to evaluate the approach are:

- Evaluate a method of hydrogel cell-encapsulation to deliver *C. reinhardtii* into biomaterials.
- Examine the feasibility of implanting photosynthetic biomaterials in mice models.
- Assess the distribution and survival of the algae in implanted photosynthetic biomaterials.
- Estimate the local and systemic inflammatory response towards photosynthetic biomaterials.
- Study the interaction between the algae and the host immune system in a zebrafish model.

Further, the development and incorporation of a complementary gene therapy to promote angiogenesis within the photosynthetic approach shall be studied. It is proposed, that genetically modified algae can be engineered so that they are able to synthetize and secrete the recombinant human vascular endothelial growth factor (hVEGF-165) and human platelet-derived growth factor B (hPDGF-B), as well as oxygen, when seeded in scaffolds. Here the specific aims are:

- Transform *C. reinhardtii* algae to express and release human angiogenic growth factors.
- Estimate the rate of expression of the recombinant growth factors in this organism.
- Validate the functionality of the growth factors, in both *in vitro* and *in vivo* models of study.
- Prove the sustained release of both oxygen and growth factors by genetically modified algae seeded in dermal scaffolds *in vitro*.
- Evaluate the feasibility of photosynthetic gene therapy in tissue engineering *in vivo*.

III. General experimental approach

A schematic view of the general experimental approach of this work, and the proposed application of the photosynthetic gene therapy developed in this doctoral thesis project is shown (Fig. 6). Photosynthetic dermal scaffolds will be created by seeding *C. reinhardtii* microalgae into collagen scaffolds. These scaffolds will be able to locally produce and release oxygen when exposed to light. By the incorporation of genetically modified algae into the photosynthetic scaffolds, it is intended that the biomaterial will supply the injured tissue with both, therapeutic-active molecules and oxygen. As a proof of concept, the use of scaffolds seeded with genetically modified microalgae releasing recombinant pro-angiogenic growth factors will be evaluated.

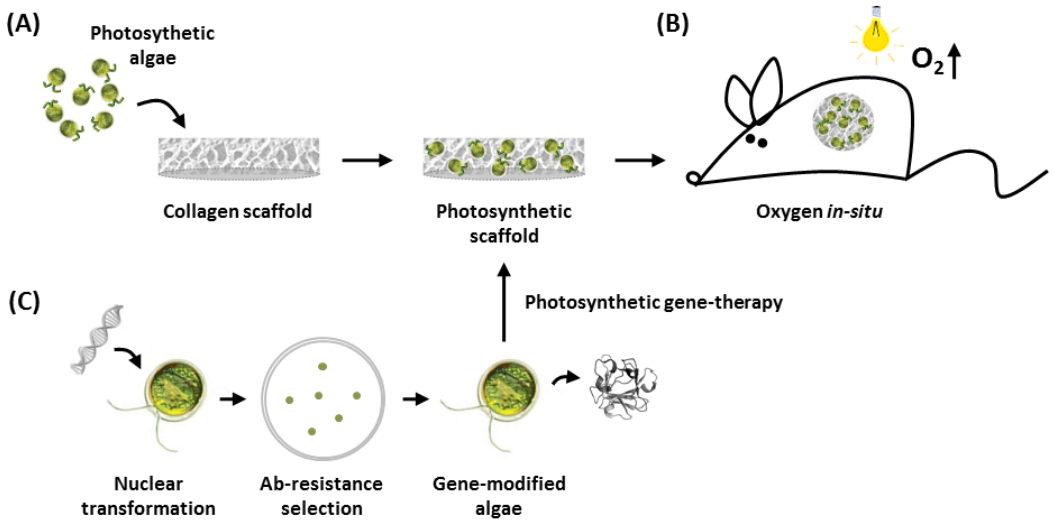

Figure 6: General experimental approach. Photosynthetic dermal scaffolds will be created by seeding unicellular microalgae into artificial collagen-based scaffolds (A). Following implantation, scaffolds exposed to light will supply oxygen to the tissue defect (B). By introducing human genes encoding therapeutic-active molecules into the algal genome, GM-algae seeded in the scaffold will synthesize and secrete recombinant proteins that will assist the wound healing process (C).

IV. Material and methods

4.1 Cell culture of *C. reinhardtii*

Cell-wall deficient, arginine phototrophic, cw15-30-derived UVM4 *C. reinhardtii* strains (Neupert *et al.*, 2009) were grown photomixotrophically at 20°C in either solid Tris Acetate Phosphate (TAP) medium or liquid TAPS-medium supplemented with 1% (w/v) sorbitol (Harris, 2009).

For light stimulation, a lamp with the full spectrum of white light (Nano Light, 11 Watt, Dennerle, Vinningen, Germany) was used to provide constant illumination (2500 lux, eq. 72.5 µE $\cdot m^{-2} \cdot s^{-1}$). Cell concentration in the culture was determined using a Casy Counter TT (Roche Diagnostics, Mannheim, Germany).

4.2 Cell seeding in the scaffolds

For *in vitro* experiments, if not stated otherwise, Integra® matrix single layer (IM, Integra Life Science Corporation, Plainsboro, NJ, USA) was used as a scaffold. For seeding, a *C. reinhardtii*, suspension was mixed with fibrinogen (Tissucol-Kit 2.0 Immuno, Baxter GmbH, Unterschleißheim, Germany) in a 1:1 ratio to the respective final concentration. Pieces of IM (ø 12 mm) were cut using a biopsy punch and dried with sterile gauze. 50 µl thrombin-solution (Tissucol-Kit 2.0 Immuno, Baxter GmbH, Unterschleißheim, Germany) followed by 100 µl of the algae-fibrinogen solution were pipetted over each scaffold. Control scaffolds were prepared by adding 50 µl thrombin and 100 µl TAPS-fibrinogen 1:1 solution.

After 1 h, the scaffolds were covered with TAPS-buffer and incubated over the desired period of time at room temperature and constant illumination. Pictures of the scaffolds were taken with a stereomicroscope (Stereomicroscope Stemi 2000-C, Carl Zeiss AG, Oberkochen, Germany).

4.3 Scanning electron microscopy

Scaffolds were seeded with $1 \cdot 10^4$ *C. reinhardtii* cells as described in section 4.2 and incubated for four days at room temperature under constant white light exposition. After fixation in 3% glutaraldehyde and dehydration with graded ethanol, samples were air-dried and sputtered with 20 nm gold (Baltec, SCD 005; Leica Microsystems, Wetzlar, Germany). 5 kV were used for the scanning electron microscope analysis (Hitachi, S-3500-N, Tokyo, Japan).

4.4 Chlorophyll measurements

Scaffolds were seeded with $3 \cdot 10^5$ *C. reinhardtii* cells as described in section 4.2. At different times in culture (day 1 and 7) the scaffolds were placed in 500 µl dimethyl sulfoxide (DMSO, Sigma-Aldrich, MO, USA) and shock frozen in liquid nitrogen. Afterwards samples were defrosted and additional 500 µl DMSO were added to each sample. Next, scaffolds were mechanically disrupted with a pestle and the optical density was measured at 435 nm, which is where the chlorophyll a absorption peak lies (Nanodrop, Thermo Fischer Scientific, Waltham, MA, USA).

4.5 Oxygen release measurements

Scaffolds were seeded at a final concentration of $2.5 \cdot 10^6$ cells per scaffold and incubated for three or five days at room temperature, followed by a 16 hours dark time incubation period, prior to the start of the measurement. Afterwards, samples were placed under hypoxic conditions (1% pO_2) and oxygen concentrations *in vitro* were constantly measured by the SensorDish® Reader (PreSens GmbH, Regensburg, Germany) in Oxodish® well-plates according to the manufacturer's instructions.

The principle of measurement is based on the effect of dynamic luminescence quenching by molecular oxygen. The well-plates are equipped with a sensor dye at the bottom of each well. Upon excitation with blue light, the sensor dye emits a fluorescent signal. Dissolved oxygen acts as a quencher by colliding with the luminophore in its excited state and absorbing the excess of energy through a radiationless energy transfer process. As a result, the indicator molecule does

not emit luminescence and the measurable luminescence signal decreases. The degree of quenching correlates with the pO_2. The decay time measurement is internally referenced and converted to oxygen values by a software program.

For light stimulation, a lamp (Nano Light, 11 Watt, Dennerle, Vinningen, Germany) was placed at 40 cm distance over the sample. Oxygen concentration was recorded and measurements stopped once saturation of the system (≥ 50% pO_2) was maintained for one hour or after 24 hours.

4.6 Full-skin defect model

For *in vivo* experiments, scaffolds were prepared as for the oxygen release measurements, but in this case a double layered scaffold was used. This collagen scaffold is covered with a silicon layer on top, which acts as a temporary epidermis (Integra® dermal regeneration template, Integra Life Science Corporation, Plainsboro, NJ, USA). Before implantation, control and microalgae-seeded scaffolds were incubated in TAPS medium for three or five days at room temperature and exposed to continuous white light.

All procedures on laboratory animals were approved by the District Government of Upper Bavaria (Regierung von Oberbayern) and performed according to the current German animal welfare act (TierSchG). Experiments were performed on female Nu/Nu nude mice (Crl:NU-*Foxn1*^{nu}, Charles River, Sulzfeld, Germany) or Skh1 hairless mice (Crl:SKH1-*Hr*^{hr}, Charles River, Sulzfeld, Germany) of 6-8 weeks age and body weight of 20-25 g. Under inhalative anesthesia (Isoflurane, Baxter Germany, Unterschleissheim, Germany) a bilateral 10 mm full skin defect was created on the back of the mice by first using a 10 mm biopsy punch to delineate the excision areas, and then, fine surgical scissors to remove the skin. Next, a round piece of titanized mesh (ø 13 mm) was placed over the wound bed and under the wound edges. Control and microalgae-seeded scaffolds were placed over the mesh and then sutured to the adjacent wound edges with 6 to 8 single knots, leaving the edges slightly over the scaffold. The wound are was covered with a transparent dressing (V.A.C. ® Drape, KCI Medical Products, Wimborne Dorset, UK), which

was also sutured to the skin. In order to trigger the oxygen production, cages were equipped with a flexible LED module (20V, 14.4W, WW, 2700K, Ledxon, Landshut, Germany) to stimulate the photosynthetic scaffolds with additional 3500 Lux during daytime. According to the TierSchG, animals must be subjected to circadian cycles of 12/12 hours light/darkness. Thus, photosynthetic implants could not be exposed for more than 12 hours to light stimulation per day. Control animals were kept under the same light stimulation conditions.

At the end of the experimental times, animals were sacrificed via isofluorane overdose and the skin from the back including the scaffolds was excised for further analysis. To evaluate the systemic effects of implanting photosynthetic biomaterial, weight loss at the end of the experimental time was recorded. Further, the immune organs, thymus, spleen, mesenteric lymph nodes (MLN), and iliac lymph (LN), were removed and their size and weight were measured and related to their final body weight. Whole blood was collected directly from the heart and allowed to clot by leaving it undisturbed on ice for 1h. The clot was removed by centrifugation at 2000 g for 10 minutes at 4°C. Serum was transferred into a clean test tube and stored at -80°C for further analysis. Three to six animals per group were used in this study.

4.7 Visualization and quantification of the vascular network

In order to quantify the rate of vascularization over the wound, tissue transillumination and digital segmentation was performed as described before (Egaña *et al.*, 2009). Briefly, the skin from the back of the animals was removed and stretched out on a petri dish over a transilluminator device. Then, pictures of the growing vascular network over the wound bed were taken using a stereomicroscope (Stereomicroscope Stemi 2000-C, Carl Zeiss AG, Oberkochen, Germany). A mask of the growing network under each scaffold and the vasculature of the uninjured skin was drawn and then processed by the VesSeg-Tool analysis software. For the analysis, vascular length was evaluated. Therefore, prior to the estimation of the area covered by the microvasculature, all vessels were thinned to a width of one pixel. Results were expressed as percentage of vascularized area compared to normal skin.

4.8 Viability of the algae *in vivo*

In order to evaluate the metabolic activity of the algae after transplantation, reverse transcription-PCR (RT-PCR) analysis was performed to determine the presence of the psbD mRNA encoding the PSII reaction center protein D2. Three and five days post implantation scaffolds were removed and stored at -80°C in RNAlater (Qiagen, Hilden, Germany). After homogenization with a pestle, total ribonucleic acid (RNA) isolation was performed using the high pure RNA isolation kit (Roche Applied Science GmbH, Mannheim, Germany). To determine the expression of the algal psbD gene, the Transcriptor One Step RT-PCR Kit (Roche Applied Science GmbH, Mannheim, Germany) was used.

4.9 Viability of the algae *ex vivo*

Biopsies of the explanted scaffold of approximately 12 mm x 1 mm were taken, and incubated for 24 h in liquid TAPS medium supplemented with 10 $\mu g \cdot ml^{-1}$ paromomycin (Sigma-Aldrich, MO, USA). Next, samples were centrifuged (290 g, 5 min) and cultured for two weeks in TAPS-agar plates containing the same concentration of antibiotics.

4.10 Cytokine protein array profile

A mouse cytokine panel-A protein assay was performed using both, the scaffold lysates and serum, following the manufacturer's instructions (R&D Systems, MN, USA). In this assay, an array of selected capture antibodies (Tab. 2), spotted on a nitrocellulose membranes, is used to detect antigen-antibodies complexes in a sample. By adding streptavidin-HRP and chemiluminescent detection reagents sequentially, a light signal is produced at each spot in proportion to the amount of cytokine bound.

Table 2: Cytokine array targets (adapted from Mouse Cytokine Array Panel A product insert; R&D Systems, MN, USA).

Nr.	Symbol	Nomenclature
1	CXCL13, BLC	C-X-C motif chemokine 13, B lymphocyte chemoattractant
2	C5/C5a	Complement component 5
3	G-CSF	Granulocyte colony-stimulating factor
4	GM-CSF	Granulocyte macrophage colony-stimulating factor
5	CCL1, I-309	Chemokine (C-C motif) ligand 1
6	CCL11, ICAM-1	C-C motif chemokine 11, Eotaxin
7	CD54	Cluster of Differentiation 54, Intercellular Adhesion Molecule 1
8	IFN-γ	Interferon gamma
9	IL-1α	Interleukin-1 alpha
10	IL-1β	Interleukin-1 beta
11	IL-1ra	Interleukin-1 receptor antagonist
12	IL-2	Interleukin-2
13	IL-3	Interleukin-3
14	IL-4	Interleukin-4
15	IL-5	Interleukin-5
16	IL-6	Interleukin-6
17	IL-7	Interleukin-7
18	IL-10	Interleukin-10
19	IL-13	Interleukin-13
20	IL-12p70	Interleukin-12
21	IL-16	Interleukin-16
22	IL-17	Interleukin-17
23	IL-23	Interleukin-23
24	IL-27	Interleukin-27
25	CXCL10, IP-10	Chemokine (C-X-C motif) chemokine 10
26	CXCL11, I-TAC	Chemokine (C-X-C motif) chemokine 11
27	CXCL1, KC	Chemokine (C-X-C motif) ligand 1
28	M-CSF	Macrophage colony-stimulating factor
29	CCL2, MCP-1	Chemokine (C-C motif) ligand 2, Monocyte chemotactic protein 1
30	CCL12, MCP-5	Chemokine (C-C motif) ligand 12, Monocyte chemotactic protein 5
31	CXCL9, MIG	Chemokine (C-X-C motif) ligand 9, Monokine induced by gamma interferon
32	CCL3, MIP-1α	Chemokine (C-C motif) ligand 3, Macrophage inflammatory protein-1 alpha
33	CCL4, MIP-1β	Chemokine (C-C motif) ligand 4, Macrophage inflammatory protein-1 beta
34	CXCL2, MIP-2	Chemokine (C-X-C motif) ligand 2, Macrophage inflammatory protein 2
35	CCL5	Chemokine (C-C motif) ligand 5, RANTES
36	CXCL12, SDF-1	C-X-C motif chemokine 12, Stromal cell-derived factor 1
37	CCL17, TARC	Chemokine (C-C motif) ligand 17, Thymus and activation regulated chemokine
38	TIMP-1	TIMP metallopeptidase inhibitor 1
39	TNF-α	Tumor necrosis factor alpha
40	TREM-1	Triggering receptor expressed on myeloid cells 1

4.11 Cytokine beads assay

The concentration of inflammatory cytokines in serum was determined by a BD™ CBA Mouse Inflammation Kit (BD Pharmingen, NJ, USA) following the manufacturer's instructions. This assay quantitatively measures interleukins (IL) -6, -10, -12p70, monocyte chemoattractant protein-1 (MCP-1), Interferon-γ (IFN-γ), and tumor necrosis factor (TNF) protein levels in a single sample. Briefly, capture beads conjugated with a specific antibody and detector phycoerythrin (PE)-conjugated antibodies are incubated with an unknown sample. Then, sandwich complexes of capture bead, analyte and detection reagent are formed, and provide a fluorescent signal that is in proportion to the amount of bound analyte that can be measured by flow cytometry.

4.12 Measurement of serum immunoglobulins

The concentrations of the mouse immunoglobulin G (IgG) and immunoglobulin M (IgM) in serum were determined by the specific *in vitro* IgG Mouse Elisa Kit (ab151276, Abcam plc, Cambridge, UK) and IgM Mouse ELISA Kit (ab1330057, Abcam plc, Cambridge, UK), respectively, following the manufacturer's instructions.

4.13 Zebrafish breeding

Zebrafish (*Danio rerio*) embryos were obtained from the laboratory-breeding colony. Embryos were collected by natural spawning and raised at 28.5 °C in E3 medium (5 mM NaCl, 0.17 mM KCl, 0.33 mM $CaCl_2$, 0.3 mM MgSO4 equilibrated to pH 7.0); egg water was changed daily. Embryonic ages are expressed in hours post-fertilization (hpf) or days post-fertilization (dpf). Animals were anesthetized with MS-222 (Tricaine, A5040, Sigma-Aldrich, MO, USA) before each experiment. All procedures complied with guidelines of the Animal Ethics Committee of the University of Chile.

4.14 Zebrafish model of inflammatory response

Zebrafish (*Danio rerio*) embryos of the transgenic strain Tg(mpeg:EGFP) (Ellett *et al.*, 2011) expressing the enhanced green fluorescent protein (EGFP) in macrophages were collected and raised at 28.5 °C in E3 medium. *Escherichia coli*-RFP (*E. coli*-RFP) constitutively expressing the red fluorescent protein (RFP; Shetty, 2008) was grown in standard Luria Bertani (LB) medium supplemented with 50 $\mu g \cdot ml^{-1}$ kanamycin. Bacteria-cells used for the infection of zebrafish embryos were freshly grown overnight on LB, washed once by centrifugation (6000·g, 5 min) and suspended in TAPS-medium to a final concentration of 5×10^5 cells·μl^{-1}. *C. reinhardtii* cells were suspended to the same concentration in fresh TAPS-medium. Both bacterial and algae suspensions were loaded to glass capillary needles.

Using a microinjector (Microinjector MPPI-2 Pressure Injector, ASI), previously selected and dechorionated transgenic zebrafish embryos of 3 dpf were injected with 1 nl of the respective cell suspension into the otic vesicle. Control injections with TAPS were performed following the same protocol. About 20-30 zebrafish larvae were injected per group. Embryos were incubated for four hours in E3 medium at 28°C and imaged as described in section 4.16.

4.15 Zebrafish model of angiogenesis

Zebrafish (*Danio rerio*) embryos of the transgenic strain Tg(fli1a:EGFP)y1 (Lawson *et al.*, 2002) were collected and raised at 28.5 °C in E3 medium. *C. reinhardtii* cells were brought to a concentration of $5 \cdot 10^7$ cells·ml^{-1} in fresh TAPS-medium and loaded to glass capillary needles. Previously selected and dechorionated transgenic zebrafish embryos of 30 hpf were injected with approximately 10 nl of the respective cell suspension into the yolk sack. 20-30 zebrafish larvae were injected per group. Embryos were incubated for 24 hours in E3 medium and for further 48 hours in E3 with Phenylthiourea (PTU, N-Phenylthiourea, Sigma-Aldrich, MO, USA) at 28°C and imaged as described below in the next section.

4.16 Confocal microscopy and fluorescence microscopy of zebrafish

Living zebrafish embryos were chosen randomly, anesthetized and mounted in 0.75% low-melting point agarose containing 5% Tricaine in a 35 mm imaging dish, and fixed to a lateral position. The injected embryos were examined using an epifluorescence-inverted microscope (Olympus scan, Olympus Biosystems, Munich, Germany), equipped with a motorized stage. For quantification analysis, images in the bright field, green and red fluorescence channels were taken. Bright field and red fluorescence channels were used to locate and delineate the site of injection, whereas the number of recruited macrophages was obtained using only the images obtained in the green channel. Co-localization of red and green was the criterion used to determine phagocytosis. Z-stack images of the otic vesicles were taken at a distance of 10 μm between the planes in a confocal microscope (Zeiss LSM 510 Meta, Carl Zeiss AG, Oberkochen, Germany). Z-stack images of the whole fish and the yolk sack were taken at a fixed distance of 15 μm between the planes, using the same microscope. Merged projections of the frames were then used to generate a mosaic image of the whole fish using the software Image J (Schneider *et al.*, 2012) and the plugin MosaicJ (Thévenaz *et al.*, 2007).

4.17 Construction of transformation vector

The sequences coding for the human vascular endothelial growth factor A isoform l (accession number NP_001165097) and human full platelet-derived growth factor subunit B (accession number P01127) were adapted to the codon bias of *C. reinhardtii* (App. 9.1 and 9.2).

The synthetic genes pBC1-VEGF165 and pBC1-PDGF-B were assembled from synthetic oligonucleotides and polymerase chain reaction (PCR)-products (Gene Art AG, Life Technologies, Regensburg, Germany). The sequence was inserted into an expression cassette derived from the endogenous PsaD gene 5' and 3' UTRs regulatory elements and behind the export sequence encoding the leader peptide of the *C. reinhardtii* extracellular enzyme arylsulfatase (ARS2), in order to target the transgenic proteins for secretion into the culture medium (Fig. 7A).

The pBC1-CrGFP_J131 basis vector (Neupert *et al.*, 2009) contained the APHVIII resistance gene for selection on paromomycin, whose expression is controlled by the constitutively active HSP70/RBCS2 promoter regions and the first intron of the RBCS2 gene. The transgene fragments were cloned into the vector backbone pBC1-CrGFP_J131 using NdeI and EcoRI cloning sites (Fig. 7B). The final constructs were verified by sequencing. The plasmid DNA was replicated and purified from transformed *E. coli* K12 (dam+ dcm+ tonA rec-) bacteria and the plasmid concentration determined by UV spectroscopy.

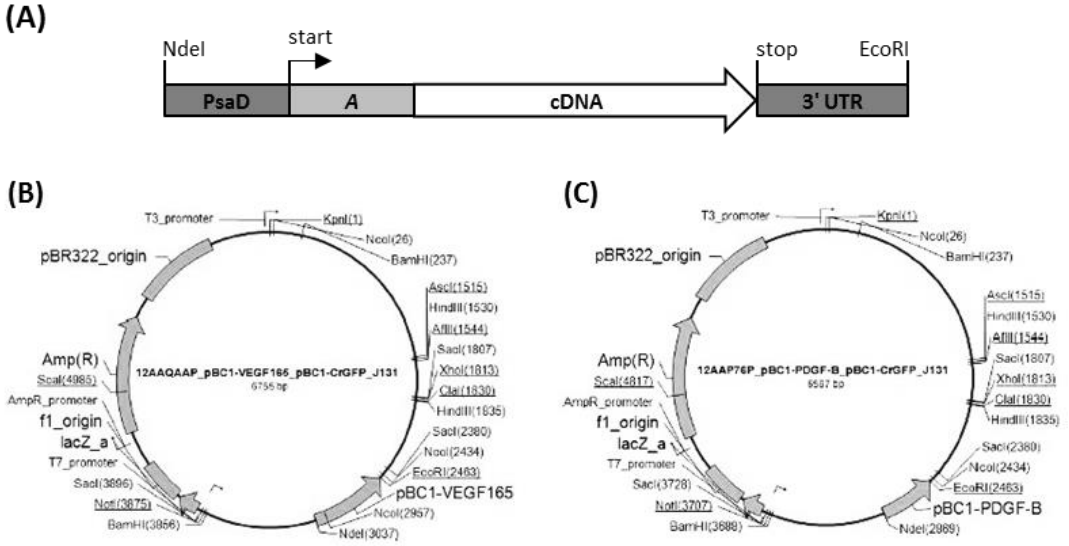

Figure 7: Schematic drawing of the transgene constructs and map of the plasmids. The export sequence for secretion of the ARS2 gene was attached to the codon adapted transgenes (cDNA). The exogeneous cDNA was inserted between the *C. reinhardtii* nuclear gene PsaD-promotor and the 3' untranslated regulatory sequences required for the high-level expression of PsaD. The positions of open reading frames (start, stop) and important restrictions sites are marked (A). The expression cassette was cloned into the vector pBC1-CrGFP using the NdeI and EcoRI cloning sites. The plasmid contained a selection gene for the antibiotic paramomyocin (B).

4.18 Transformation of *C. reinhardtii*

Nuclear transformation of *C. reinhardtii* was achieved by temporal cell membrane permeabilization. $1 \cdot 10^7$ UVM4 *C. reinhardtii* cells were suspended to a volume of 300 µl and vortexed with ø 0.5 mm glass beads for 20 seconds in the presence of 5 µg of the respective plasmid DNA. Then, the transformants were seeded in TAPS-liquid medium and incubated overnight protected from light under continuous shaking. Next, the algae were seeded over TAP-Agar plates containing 10 $\mu g \cdot ml^{-1}$ paromomycin and incubated for the first three days under

weak illumination. Upon successful transformation, the new created strains integrated an antibiotic-resistance gene and were therefore able to grow selectively in the presence of paromomycin. The plates were then moved to conditions with standard light exposition (2500 lux), until the colonies were large enough to be picked and platted into a fresh plate. Clones were subsequently maintained in solid TAP-medium under selective conditions.

4.19 Polymerase chain reaction

Genomic DNA from *C. reinhardtii* algae was extracted using the DNeasy Plant Mini Kit (Qiagen N.V., Lumburg, Netherlands) according to the manufacturer's instructions. The integration of the recombinant gene was confirmed by polymerase chain reaction (PCR) using gene specific primer pairs (Metabion GmbH, Planegg, Germany). The primer sequences 5'-GAAGTTCATGGACGTGTACC-3' and 5'-TTGTTGTGCTGCAGGAAG-3' were used to amplify the hVEGF-165 coding sequence (258 bp product), primers 5'-AACGCCAACTTCCTGGTG-3' and 5'-GTGGCCTTCTTGAAGATGGG-3' were used to amplify the hPDGF-B coding sequence (164 bp product). Primer sequences for the amplification of the psbD sequence were 5'-GCCGTAGGGTTGAATG-3' and 5'-GTTGGTGTCAACTTGGTGG-3' (413 bp product).

4.20 Southern blot

For southern blot, 10 µg DNA of each strain were digested using the restriction enzymes HindIII, BamHI and SalI (Conventional restriction enzymes; Fermentas, Thermo Fischer Scientific, Waltham, MA, USA), at 37°C for 48 h. Samples were separated by 0.8% agarose-TPE gel electrophoresis for 16 h at 25 V. The gel was afterwards stained with ethidium bromide (0.5 $\mu g \cdot ml^{-1}$) for 20 min and documented. Following depurination (15 min, 0.25 M HCl), denaturation (30 min, 0.4 M NaOH, 0.6 M NaCl) and neutralization (30 min, 1M Tris-HCl pH 8.0, 1.5 M NaCl) genomic DNA was transferred to a nylon membrane (Roti-Nylon plus, Porengröße 0,45 µm; Carl-Roth, Karlsruhe, Germany) in 20x SCC (3 M NaCl, 0.3 M Trisodiumcitrate) overnight. Digoxigenin-nucleotide labeled DNA-probes (Digoxigenin-11-dUTP alkali-labile, Roche, Basel, Switzerland) were obtained using the same primer pairs and

conditions as for the PCR. After blocking unspecific binding sites, immobilized genomic DNA was incubated with the labelled probes for 14h at 68°C for hybridization. Signals were detected using an alkaline phosphatase conjugated anti-DIG antibody (Roche, Basel, Switzerland) and CDP* (Roche, Basel, Switzerland) as reaction substrate.

4.21 Enzyme-linked immunosorbent assay

$5 \cdot 10^7$ *C. reinhardtii* cells were seeded in triplicate in 10 ml volume and incubated at room temperature for four days under constant agitation (150 rpm) and illumination (2500 lux). Culture supernatants were collected and then stored at -80°C until their analysis. Cell lysates were obtained by mechanical disruption of $1 \cdot 10^7$ *C. reinhardtii* cells in lysis buffer (100 mM Tris-HCl, 10 mM EDTA, 0.5% Triton X-100, 25 $\mu g \cdot ml^{-1}$ pepstatin, 25 $\mu g \cdot ml^{-1}$ leupeptin). To assess the secretion of the recombinant proteins from the encapsulated algae, scaffolds were seeded as described in section 4.2 with both *C.r.*-VEGF and *C.r.*-PDGF in a 1:5 ratio to a final concentration of $2.5 \cdot 10^6$ cells per scaffold and placed in 12 well-plates with 2 ml TAPS-medium. Medium was changed every day and collected every two days. Protein lysates from the explanted scaffolds after seven and fourteen days post-implantation were obtained by mechanical disruption using radio-immunoprecipitation assay-buffer (RIPA-buffer) with proteinase inhibitors (PIC; BD Pharmingen, NJ, USA), Pefabloc SC-Protease Inhibitor (Carl-Roth, Karlsruhe, Germany), cOmplete (Roche, Basel, Switzerland), phenylmethylsulfonyl fluoride (PMSF; Sigma-Aldrich, MO, USA).

For quantification of the secreted recombinant proteins in the supernatant samples and lysates enzyme-linked immunosorbent assay (ELISA) kits were used according to the manufacturer's instructions (human VEGF Quantikine ELISA kit; human PDGF-BB Quantikine ELISA Kit; R&D Systems, MN, USA). In the VEGF-detection assay, a monoclonal antibody raised against the Sf 21-expressed recombinant protein hVEGF-165 was used as a capture antibody and a specific polyclonal antibody as the detection antibody. In the PDGF-BB immunoassay, a PDGF-Rβ/Fc chimera served as the immobilized antibody and a polyclonal antibody against *E. coli*-expressed hPDGF-B was employed for its detection.

4.22 Recovery of the recombinant protein from the culture supernatant

The supernatants from confluent *C. reinhardtii* cultures were passed first through a 0.22 um filter. Then using a filtration tube capable of retaining peptides above 3000 dalton (Vivaspin 15R Hydrosart, Sarstedt, Göttingen, Germany) hVEGF-165 and hPDGF-B were recovered by centrifugation (3000 g, 47 min). In a final ultrafiltration step, the diluent medium was changed to cell starvation medium (RPMI 1640, 2.0 $g \cdot L^{-1}$ $NaHCO_3$, with stable glutamine; Biochrom, Berlin, Germany) supplemented with 1% fetal calf serum (FCS-Gold, PAA, Pasching, Austria) and 1% antibiotic/antimycotic (100x ab/am; Capricorn Scientific, Ebsdorfergrund, Germany).

4.23 Human primary cultures

Human umbilical vein endothelial cells (HUVECs) were either purchased (Promocell, Heidelberg, Germany) or obtained from umbilical cord donors following the protocol instructions of Davis *et al.* Cells were maintained in supplemented Endothelial Cell Growth Medium 2 (Promocell, Heidelberg, Germany).

Human mesenchymal stem cells (MSCs) were obtained from lipoaspirates from donors who underwent adipose tissue removal for medical or aesthetic reasons and had given informed consent to participate in the study. 25 ml volumes of the aspirated fraction were first rinsed with phosphate buffered saline (PBS; Biochrom, Berlin, Germany) and centrifuged (10 min, 260 g). An equal volume of 0.3 $U \cdot ml^{-1}$ collagenase A (Roche, Basel, Switzerland) was added and incubated for 30 min at 37°C. After centrifugation, the resulting cell pellet was plated under standard conditions in Dulbecco's modified eagle's medium with 4.0 mg $glucose \cdot L^{-1}$, stable glutamine, phenol red (DMEM; Biochrom, Germany), supplemented with 10% fetal bovine serum (FBS-Gold, PAA, Pasching, Austria), and 1% penicillin/streptomycin (Biochrom, Berlin, Germany) under standard cell culture conditions (37°C, 5% CO_2). In all experimental settings, cells from passages 2-4 were used.

4.24 Receptor phosphorylation assay

$1 \cdot 10^5$ cells per well were seeded on a 12 well-plate and starved for 16 h in starvation medium before activation. Cells were then stimulated for 2 min, with either 50 $ng \cdot ml^{-1}$ recombinant VEGF-165 (Preprotech, NJ, USA), 10 $ng \cdot ml^{-1}$ recombinant PDGF-B (Preprotech, NJ, USA) or the concentrated protein supernatants of 30 ml confluent cultures of the genetic modified and non-transformed control strains. Cells were then freeze-shocked in liquid nitrogen and lysed in RIPA-buffer with proteinase inhibitors as in section 4.21, and phosphatase inhibitors (Phosphatase Inhibitor Mini Tablets; Pierce-Thermo Fisher Scientific Inc, IL, USA). Cells were scratched from the well-floor and lysates were homogenized by pipetting up and down through a 1 ml syringe, centrifuged for 5 min at 9300·g and stored at -80°C for further analysis.

Equal protein amounts were separated by gel-electrophoresis under reducing conditions and then blotted to PVDF-membranes (Bio-Rad Laboratories, Hercules, California, USA). The following mononuclear antibodies (mAb) were used for the detection of the phosphorylated and non-phosphorylated receptor epitope with overnight incubation periods: rabbit mAb anti-VEGFR-2, rabbit mAb anti-phospho-VEGFR-2 (Tyr1175), rabbit mAb anti-PDGFR-β, rabbit mAb anti-phospho-PDGFR-β (Tyr751) (CellSignalling, MA, USA), and a goat anti-rabbit HRP secondary antibody (1:5000, Dianova GmbH, Hamburg, Germany). The SuperSignal West Pico detection system (Pierce-Thermo Fisher Scientific Inc, IL, USA) was used to trigger the chemilluminescence reaction. Pixel intensity quantification was performed with the software Fusion (Peqlab, Erlangen, Germany).

4.25 Histological analysis

Five days post-implantation, scaffolds were removed from the animals and fixed in 3.7% paraformaldehyde (PFA) for 24 hours at 4°C. Afterwards samples were shock frozen in Tissue-Tek® O.C.T.™ compound (Sakura, Alphen an den Rijn, Netherlands) and sections of 20 µm thickness were prepared, stained, and mounted in 4',6-diamidino-2-phenylindole (DAPI; DAPI-Prolong-Gold; Invitrogen, Carlsbad, CA).

Pictures were taken with a fluorescence microscope (Axio Observer, Carl Zeiss AG, Oberkochen, Germany) or an inverted phase contrast microscope (Axiovert 25, Carl Zeiss AG, Oberkochen, Germany) and analyzed with the Axiovision software (Carl Zeiss AG, Oberkochen, Germany).

Seven and fourteen days-post-implantation scaffolds including the surrounding skin-tissue were harvested, fixed in Bouin-solution for 24 hours at 4°C and then kept in 70% Ethanol up to their analysis. Tissues were dehydrated and embedded in paraffin. Transversal sections of 5 µm thickness were cut in a microtome and then stained following a masson's trichrome protocol. Pictures were taken with an inverted bright-field microscope (Leica DM IL LED; Leica Microsystems, Germany)

4.26 Statistical analysis

All assays were repeated in at least three independent experiments. Data was expressed as mean ± SD. Two-tailed student's t-test was used to compare differences between two groups. SigmaPlot software (Systat Software, San Jose, CA) was used for statistical analyses. Differences among means were considered significant when $p \leq 0.05$.

V. Results

5.1 Photosynthetic tissue engineering *in vitro*

In contrast to the published work by Hopfner *et al.*, an improved strategy to incorporate the algae to the collagen was used for this study. Since the principal aim was to assess the practicability of the implantation of photosynthetic materials *in vivo*, a biocompatible fibrin-hydrogel was used as a carrier to encapsulate the algae inside the material and increase their confinement within the scaffolds volume. The fibrin-algae suspension was homogeneously distributed throughout the entire scaffold (Fig.8A) and scanning electron microscopy showed that algae grew as encapsulated clusters (Fig. 8B).

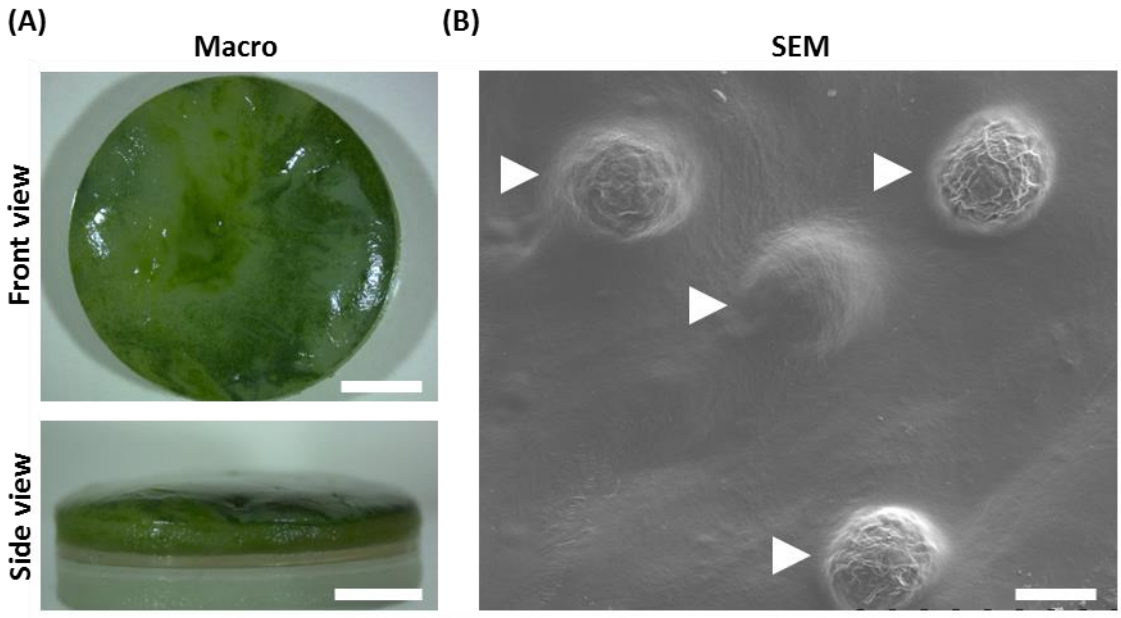

Figure 8: Seeding of encapsulated microalgae in the scaffold. Fibrin containing *C. reinhardtii* was incorporated in a collagen scaffold to a final cell density of $2.5 \cdot 10^7$ cells per scaffold and incubated in TAPS medium for three days at room temperature under continuous white light exposure (2500 lux). The overall green color shows that the fibrin-algae solution was homogeneously distributed in the scaffold (A, upper) and through all the depth layers of the scaffold (A, lower). SEM analysis showed the collagen covered by fibrin and how the microalgae grew forming fibrin embedded photosynthetic clusters (B, white arrow heads). Scale bar represents 25 mm in A upper, 25 mm in A lower and 25 µm in B.

Their proliferative capacity was quantified by measuring the chlorophyll content of the scaffolds. The signal given by chlorophyll's light absorbance was significantly higher after seven days of cultivation under continuous light exposure compared to one day-scaffolds (Fig. 9A). Also, as a consequence of the proliferation of the algae, the rate of oxygen release from the photosynthetic scaffolds upon light-stimulation increased. Following seven days of cultivation, scaffolds placed under hypoxic conditions (1% pO_2) reduced the time to reach saturation of the sensor ($pO_2 \geq$ 50%) by over seventy times (Fig. 9B).

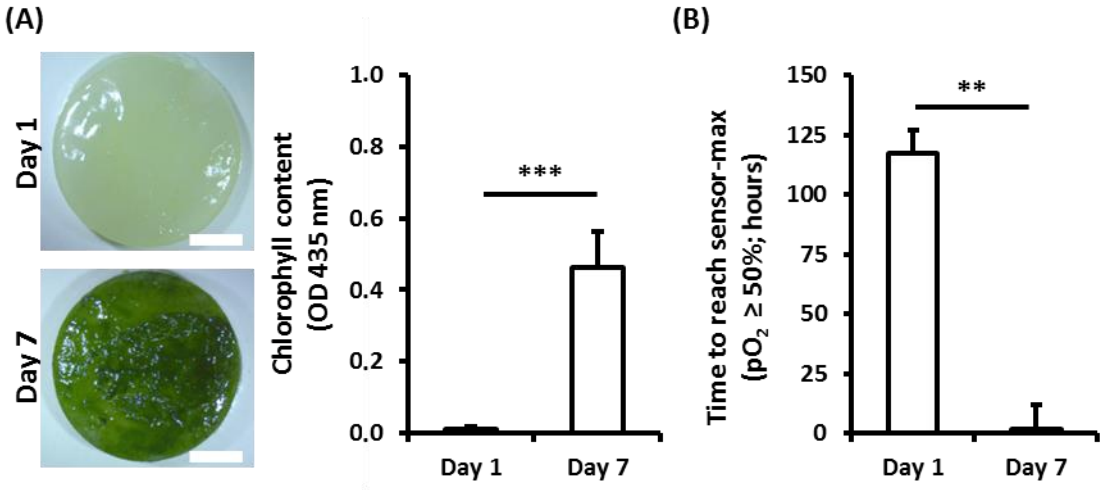

Figure 9: Proliferative and photosynthetic capacity of microalgae in the scaffold. Seven days after seeding the algae at a low density, a significant increase of the total chlorophyll content was observed in the scaffolds (A). Following one and seven days of cultivation, scaffolds were placed under hypoxic conditions (1% pO2) and the time to reach saturation of the oxygen sensor ($pO_2 \geq 50\%$) was recorded. While measurements from the control scaffolds without algae remained at about 1% pO_2 over the course of the experiment (data not shown), an increment of the oxygen release from the photosynthetic scaffolds was observed. The time to reach saturation was significantly reduced as a consequence of the proliferation of the algae (B). Scale bar represents 25 mm in A. ** $p \leq 0.005$; *** $p \leq 0.001$; $N \geq 3$. Results are shown as mean ± S.D.

Oxygen solubility in water is temperature and salinity dependent. Increasing temperature or salt concentration leads to a decrease in oxygen solubility, even though the pO_2 stays the same. Under the conditions the measurement was done (30°C, 1013 hPa, assuming a similar salinity to fresh water), 50 % pO_2 are equivalent to a dissolved oxygen concentration of 18.0 mg/L (563.0 µmol/L) and an oxygen pressure of 362 mmHg.

5.2 Photosynthetic tissue engineering *in vivo*

The first attempt to evaluate the tolerance of *C. reinhardtii* to the implantation in a mouse host, was made in an *in vivo* full-skin defect model (Schenck *et al.*, 2014), using athymic immunodeficient nude mice. Control fibrin-collagen scaffolds and scaffolds seeded with algae were engrafted in a bilateral full skin defect as described in section 4.6 (Fig. 10).

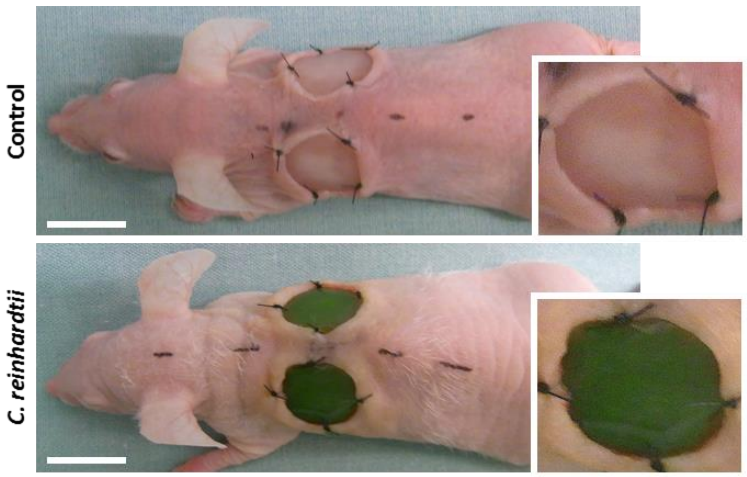

Figure 10: *In vivo* full-skin defect model. Control collagen scaffolds and scaffolds seeded with algae were engrafted in a bilateral full skin defect to substitute a skin-area of two times 78.5 mm² of the skin from the back of a nude mouse. Scaffolds were sutured leaving the wound edges above the scaffold, and covered with a transparent dressing. Scale bar represents 1 cm.

Following the operation wounds were covered with a transparent dressing and mice were kept individually in cages equipped with flexible LED modules, to stimulate the oxygen production in the implanted photosynthetic tissues (Fig. 11).

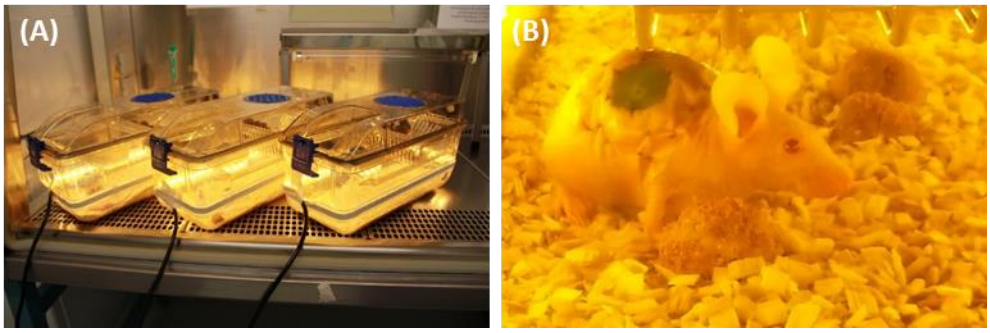

Figure 11: Light-stimulation of the photosynthetic scaffolds during *in vivo* studies. Cages were surrounded with flexible LED modules (A) to trigger photosynthesis in the implanted microalgae with additional 3500 Lux during daytime (B).

There were no complications during or after the procedure of implantation of photosynthetic materials into the defects and no abnormal behavior of the animals was witnessed during the experimental time.

Five days post-implantation no signs of infection or inflammation at the wound area were observed (Fig. 12A). Following the protocol described in section 4.7., the skin of the back of the mice including the scaffolds, was excised and set for tissue transillumination. An ingrowth of the skin vascularization towards the wound bed and below the implanted photosynthetic scaffolds was observed (Fig. 12, B-C), showing that the presence of the algae did not hinder vascularization of the scaffold *in vivo*.

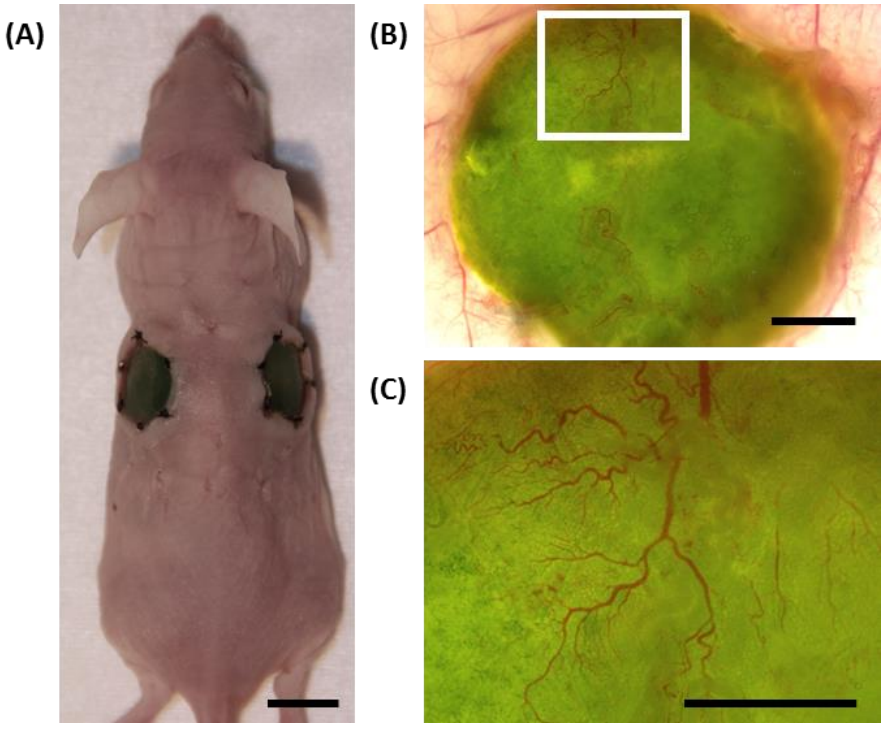

Figure 12: Engraftment of photosynthetic scaffolds *in vivo*. Five days post transplantation no macroscopic signs of infection or inflammation at the wound area were observed (A). Transillumination analysis of the implanted biomaterial showed normal ingrowth of the vascularization towards the wound bed in the presence of microalgae (B, C). Scale bar represents 1 cm in A, 4 mm in B and 1 mm in C. Results were obtained for at least six independent experiments.

Histological analysis of the explanted scaffolds after five days, showed the formation of chimeric tissues composed of photosynthetic algae and mouse cells. Both were evenly spread over the collagen and often in proximity to each other (Fig. 13A). The algae kept their normal shape and integrity, which suggested their viability within the regenerating tissue.

In order to further prove the survival of the microalgae and their sustained metabolic-activity after transplantation, RT-PCR analysis was performed to determine the presence of the algal-specific psbD mRNA. The results showed that algae mRNA could be detected in the wound area for at least five days post-transplantation (Fig. 13B). Then, viability of the algae was confirmed by their ability to grow from all six wound biopsies taken. Upon a short incubation period in liquid culture medium, *C. reinhardtii* living in the explanted tissue samples, formed colonies over an agar plate (Fig. 13C).

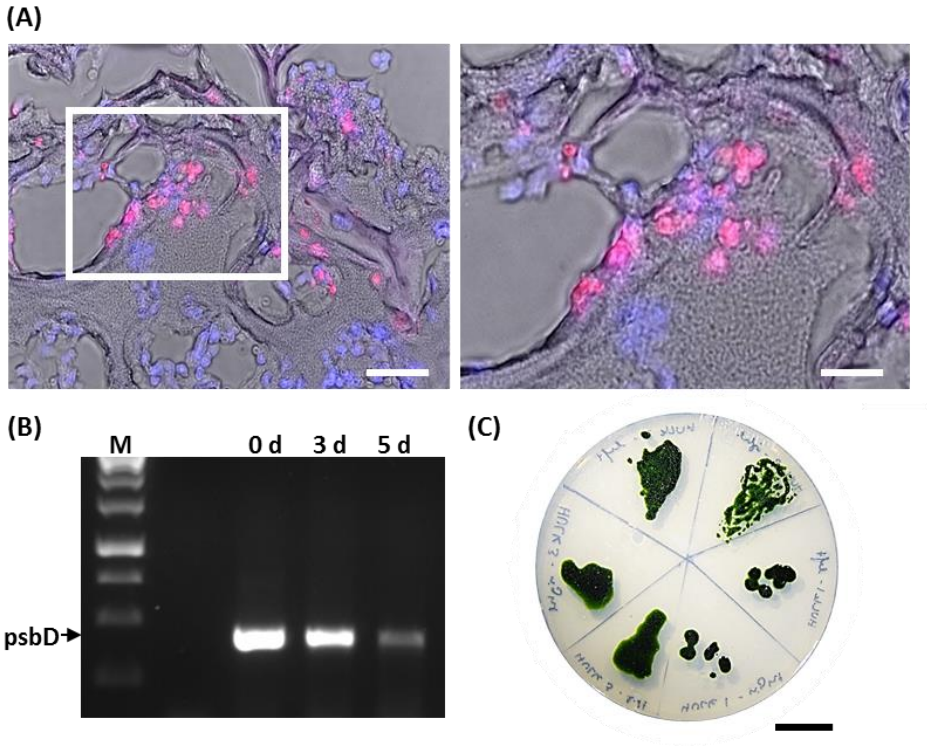

Figure 13: *Ex vivo* analysis of photosynthetic biomaterials. Histological sections showed the formation of chimeric tissues composed of photosynthetic (red/ chlorophyll autofluorescence) and mouse cells (blue/ DAPI) five days after implantation. The white rectangle outlines the area zoomed in the left picture. Microalgae had an intact appearance and remained equally distributed over the scaffold (A). RT-PCR analysis was performed to determine the presence of the microalgae specific psbD mRNA before (0), and at days three and five after implantation (B). Viability of the algae *in vivo* was confirmed by their capability to be re-grown out of six different wound biopsies taken (C). Scale bar represents 50 µm in A left, 20 µm in A right and 2 cm in C. N ≥ 6.

5.3 Immune response against *C. reinhardtii*

5.3.1 Inflammatory response against *C. reinhardtii* in immunodeficient mice

Five days post-implantation, tissues were explanted and analyzed by an inflammatory cytokine assay. Here, a protein array of antibodies against forty inflammation-related cytokines (Section 4.10, Tab. 2) was used for the semi-quantitative analysis of cytokines in a sample. Twenty-one different cytokines were found in the protein samples of all harvested tissues, but only the levels of two molecules, C5a and CCL12, were found significantly increased by the presence of the algae compared to the control group (Fig. 14A).

To evaluate the systemic effects of implanting photosynthetic biomaterials, the sizes and weights of spleen and the lymph nodes (Fig. 14B), and the weight loss of each animal (Fig. 14C) were compared at the end of the experimental time. No significant differences between the weights of the spleen and the lymphs between groups were found and the weight loss at the end of the experimental time was similar for both groups.

Quantification of IgG and IgM in the mice serum did not show any variation between the experimental and control group (Fig. 14D). Moreover, using the same cytokine assay mentioned above, the cytokines C5a, CCL1, CCL12, CD54, M-CSF and TIMP-1 were found equally present in the serum of animals regardless of their treatment (Fig. 14E).

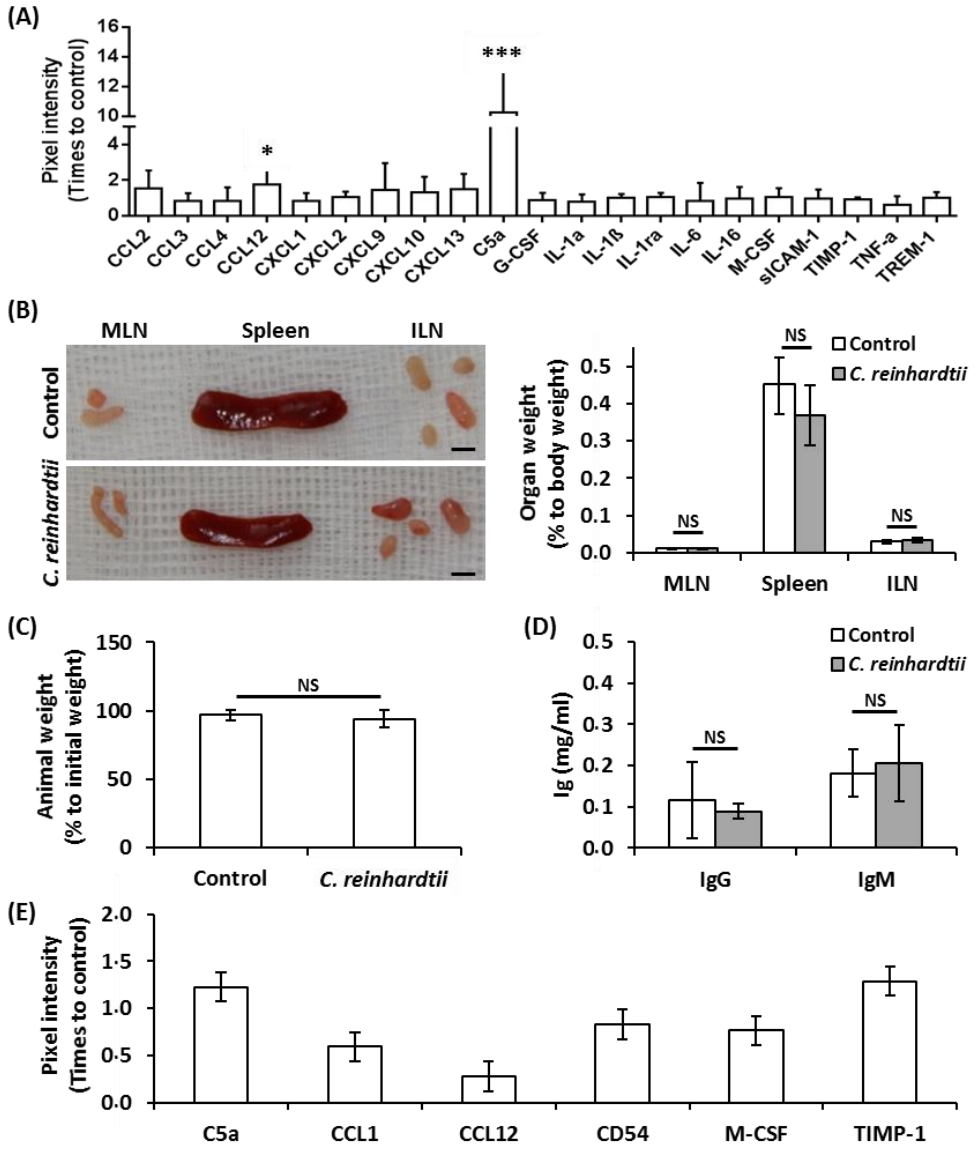

Figure 14: Local and systemic inflammatory response towards photosynthetic biomaterials. After five days post-implantation an inflammatory cytokine protein array was performed with the protein extracts obtained from the explanted tissues. Among 40 analyzed cytokines, the levels of only two molecules, C5a and CCL12, were significantly increased by the presence of the algae compared to the control group (A). No significant differences were detected among the groups in the size of the immune organs (spleen, MLN and ILN; B). The weight loss of the animals did not differ between the two groups (C). Quantification of IgG and IgM did not show variation between groups (D). Cytokines C5a, CCL1, CCL12, CD54, M-CSF and TIMP-1 were equally present in the serum of animals regardless the presence of the algae (E). Results are shown as mean ± S.D. NS non-significant, * $p \leq 0.05$, *** $p \leq 0.001$, $N \geq 3$.

5.3.2 Innate immune response against *C. reinhardtii* in a zebrafish model

The interaction of the microalgae with the cells of the innate immune system was also studied using a model of inflammatory response in zebrafish. *C. reinhardtii* was microinjected into the otic cavity of transgenic zebra fish larvae expressing EGFP in all macrophages (Fig. 15A, upper). The response against *C. reinhardtii* was quantified and compared to an injection of *E. coli* bacteria and a control injection of the algae culture medium (Fig. 15A, lower). In the injected area, the recruitment of macrophage did not vary between the control group and *C. reinhardtii*, however it was significantly increased with *E. coli* (Fig.15B). Furthermore, the number of phagocytic macrophages removing the injected cells was significantly lower for the algae as compared to *E. coli* (Fig. 15C).

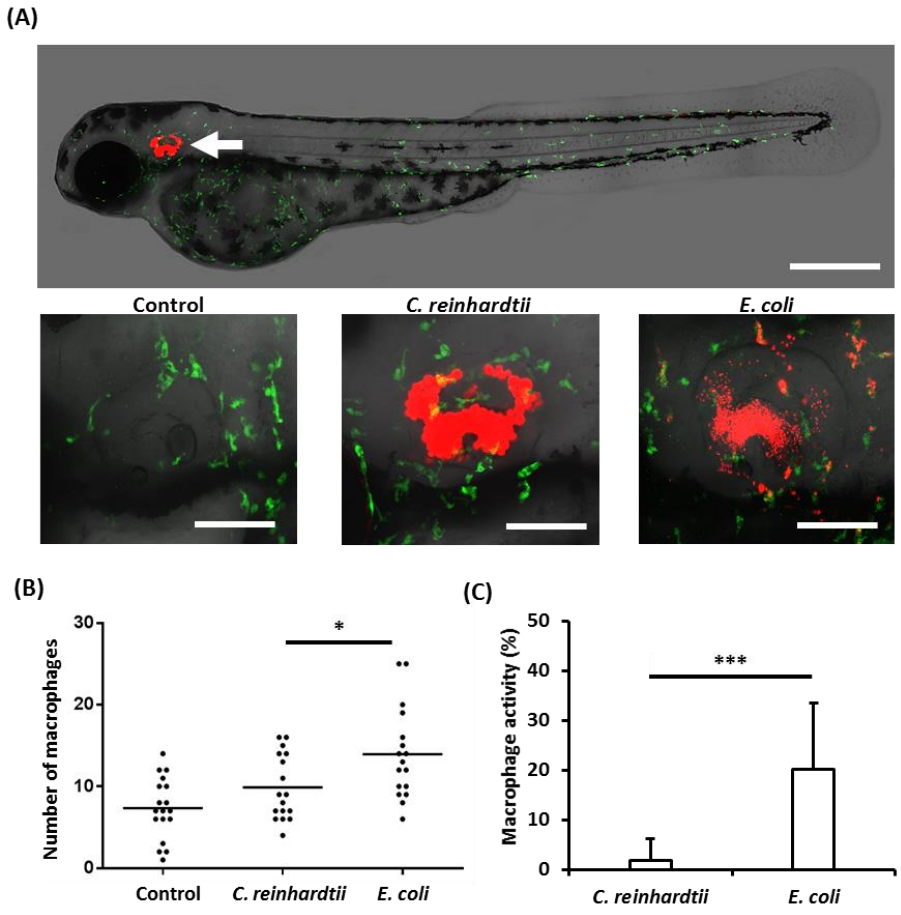

Figure 15: Inflammatory response towards *C. reinhardtii* in a zebrafish model. *C. reinhardtii* was microinjected in the otic-cavity of a zebrafish larvae expressing EGFP in macrophages (A, upper), and the response against the algae (red; chlorophyll autofluorescence) was quantified and compared to *E. coli*-RFP (A, lower). In the injected area, the total number of macrophages (B) and the number of phagocytic macrophages (C) were significantly lower for injections of algae compared to the bacteria. Scale bar represents 500 µm in A-upper and 100 µm in A-lower. * $p \leq 0.05$, *** $p \leq 0.001$. Results are shown as mean ± S.D. and were obtained for at least three independent experiments.

5.3.3 Inflammatory response of against *C. reinhardtii* in wild-type mice

After showing that *C. reinhardtii*, did not trigger a significant immune response in two different *in vivo* models, the local and systemic inflammatory response towards the photosynthetic scaffolds was further evaluated in fully immunocompetent Skh1-hairless mice (Benavides *et al.*, 2008). Scaffolds were prepared and implanted as described before and left for three weeks in the host.

Again, no significant loss of weight (Fig. 16B) was measured in either group. Furthermore, no signs of inflammation in the mice's spleen, thymus or lymph nodes were observed and no significant differences in the sizes of the harvested organs were measured (Fig. 16A). Same as observed with the nude mice, there was no overexpression of immunoglobulins caused by the implantation of scaffolds containing the algae (Fig. 16C).

Inflammatory cytokines in this case were evaluated using a bead-based assay, which quantitatively measures IL-6, IL-10, IL-12p70, MCP-1, IFN-γ, and TNF protein levels in a sample. Only three of these cytokines were present in relevant amounts in the serum samples of all mice, namely, IL-6, MCP-1 and IFN-γ. Although there were no increased amounts of cytokines in the group treated with the photosynthetic scaffolds, there was a significantly higher amount of IL-6 and IgG present in the serum of the animals of both experimental groups compared to the mice that were not operated (Fig. 16C, D).

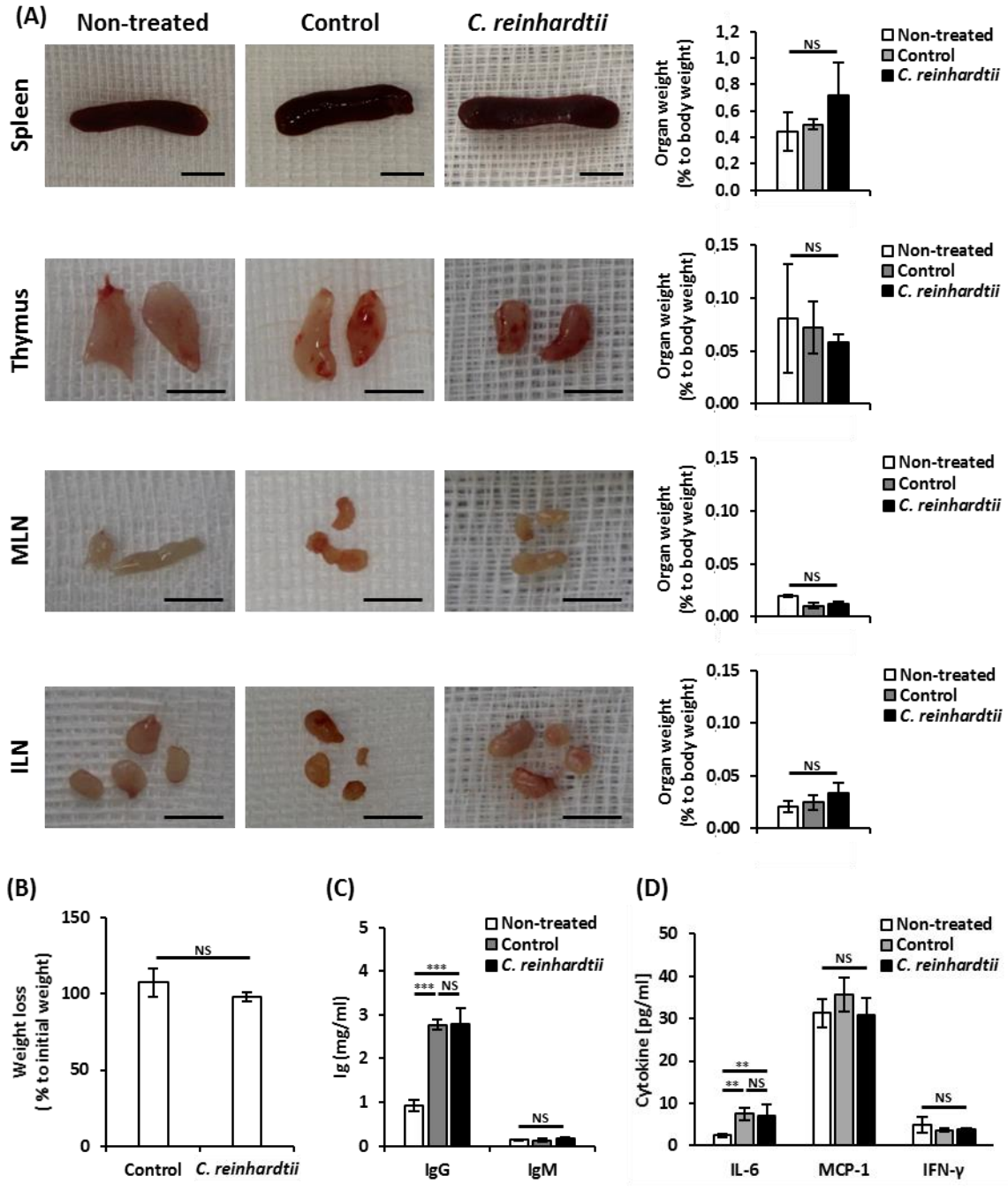

Figure 16: Inflammatory response in wild-type mice after three weeks. Photosynthetic scaffolds did not induce any local or systemic inflammatory response when implanted into wild-type mice. No signs of infection, significant weight loss or inflammation of the lymphatic organs (spleen, thymus, MLN and ILN) were observed between the mice transplanted with control scaffolds (Control) and with scaffolds containing algae (*C. reinhardtii*). (A, B). Compared to mice that were not operated (Non-treated), a significant increase in the levels of IgG and IL-6 was observed as a consequence of the procedure. However, there was no overexpression of immunoglobulins (IgG, IgM) or cytokines in the serum of the mice as a consequence to the exposure to the algae (C, D). Scale bar represents 1cm in A. NS non-significant, * $p \leq 0.05$, ** $p \leq 0.005$, *** $p \leq 0.001$. $N \geq 3$. Results are shown as mean ± S.D.

5.4 Genetic modification of *C. reinhardtii*

All the gathered evidence showing that the use of photosynthetic scaffolds is a feasible approach in dermal tissue engineering, and proving that *C. reinhardtii* microalgae do not generate significant innate and adaptive inflammatory responses, encouraged the idea of engineering a scaffold that in addition to oxygen, could locally release other therapeutic molecules into the wound area. As a proof of concept, the use of scaffolds seeded with genetically modified algae releasing human recombinant angiogenic growth factors was evaluated.

For this, hVEGF-165 and hPDGF-B were selected as target genes for their expression in *C. reinhardtii*. Upon successful transformation with the human transgenes, the new created *C. reinhardtii* strains co-integrated an antibiotic-resistance gene, which allowed their selective grow in the presence of paromomycin. Four clone-derived colonies of the new strain *C.r.*-VEGF and five of the strain *C.r.*-PDGF were created by nuclear transformation. No alteration on the size or morphology of the cells of the new generated strains in comparison to the non-transformed strain was noted, with all clones showing a normal oval shape of 5-8 μm in diameter (data not shown).

Following a quantitative ELISA protocol, the concentration of the recombinant growth factors released into the medium in each clone-derived culture was determined. Three out of the four *C.r.*-VEGF clones synthesized and secreted the recombinant protein successfully and in similar amounts (Fig.17A), while two of the five *C.r.*-PDGF respectively did so (Fig.17B). Interestingly, the results showed a proportionally higher intracellular concentration of hPDGF-B in *C.r.*-PDGF, than hVEGF-165 in *C.r.*-VEGF. From each created strain, the clone with the highest rate of recombinant protein secretion to synthesis was chosen (clone nr. 1, respectively) and used for all subsequent experiments.

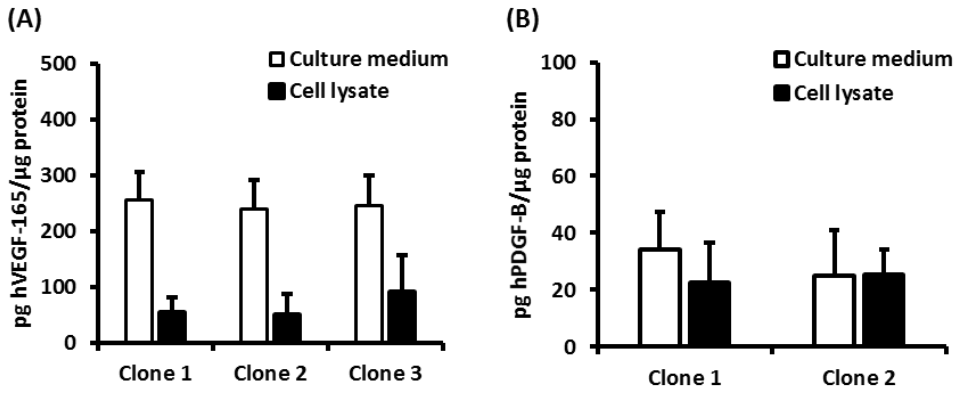

Figure 17: Quantification of recombinant protein expression in *C. reinhardtii*. The concentration of the recombinant hVEGF-165 and hPDGF-B synthesized by nuclear transformed *C. reinhardtii* clones was measured by ELISA, in both, cell culture medium and cell lysate samples. Results are normalized to the total protein amount in the sample. No significant differences in the expression rates were found between clones. N≥ 3.

Although *C.r.*-VEGF and *C.r.*-PDGF showed similar rates of population growth and reached comparable cell density numbers at the stationary phase ($2.094 \pm 0.394 \cdot 10^7$ cells·ml^{-1} and $2.385 \pm 0.412 \cdot 10^7$ cells·ml^{-1}, respectively), the amounts of recombinant protein expressed by each strain diverged considerably. Table 3 shows the results on the quantification of the synthesis and secretion of the recombinant growth factors by the selected *C.r.*-VEGF and *C.r.*-PDGF strains. The concentrations of the recombinant proteins found in the culture medium (ng·ml^{-1}), were normalized to the cell density achieved by the time the sample was taken (fg·cell^{-1}). While the concentration of hVEGF-165 reached almost 30 ng·ml^{-1} in the culture supernatant, hPDGF-B could not be even found in the ng·ml^{-1} range. Also the amount of human protein secreted per cell was 58.3 times lower for *C.r.*-PDGF.

Table 3: Quantification of synthesis and secretion of the recombinant growth factors by *C.r.*-VEGF and *C.r.*-PDGF.

	c (ng·ml^{-1})	c (fg·cell^{-1})
hVEGF-165	27.950 ± 4.379	1.4 ± 0.2
hPDGF-B	0.556 ± 0.114	0.024 ± 0.006

The correct insertion of the transgenes into the genome of the new created strains was evaluated first by PCR using transgene targeted primer-pairs (Fig. 18A) and then by detection of the human genes in the *C.r.*-VEGF and *C.r.*-PDGF DNA using hybridization probes (Fig. 18B). In both cases, signals were specific for the genetically modified strains. The southern blot method showed the integration of a single copy of hVEGF-165 in the *C.r.*-VEGF genome. However, hPDGF-B gene was found in two copies in *C.r.*-PDGF, in one of the three restriction products.

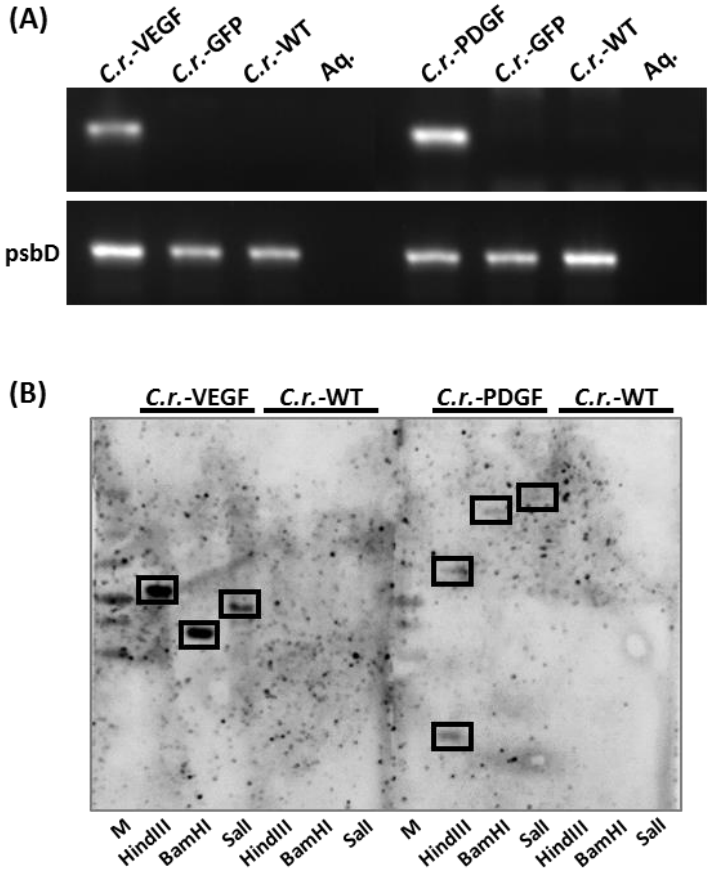

Figure 18: Transformation of *C. reinhardtii* with human transgenes. The DNA sequences coding for hVEGF-165 and hPDGF-B were inserted into the genome of *C. reinhardtii* to create the strains *C.r.*-VEGF and *C.r.*-PDGF. The insertion was verified by PCR using primers specific for the transgenes. A non-transformed strain (*C.r.*-WT) and a strain, which was genetically modified to express GFP using the same vector (*C.r.*-GFP), were used as negative controls (A). Southern blot showed a single inserted copy of the hVEGF-165-gene within the genome of *C.r.*-VEGF, whereas there were two copies of the hPDGF-B gene in *C.r.*-PDGF, as shown in the sample treated with the restriction enzyme HindIII (B).

5.5 Bioactivity of the recombinant growth factors *in vitro*

To test the biological functionality of the recombinant proteins, human primary cells were stimulated with the recovered recombinant growth factors from the *C.r.*-VEGF and *C.r.*-PDGF culture's medium. To prepare the growth factors suspensions, algae culture supernatants were passed through a sample concentrator by ultrafiltration and then re-suspended in human cell culture medium.

Although this recovery strategy was fairly straightforward, there was a significant variability in the final concentration of protein obtained. Debris-particles that remained in the supernatants even after its clarification through a 0.22 μm filter, clogged the concentrator tube. This restricted the use of a tube to a couple of cycles and affected the final volume of the diluent. As a result, the averaged final growth factor suspensions, which were obtained from a starting volume of 30 ml culture supernatant and used to stimulate the cells, had a concentration of 35.8 ± 10.1 $ng{\cdot}ml^{-1}$ and 3.1 ± 1.3 $ng{\cdot}ml^{-1}$ of hVEGF-165 and hPDGF-B, respectively.

Following the stimulation of human endothelial (Fig. 19A) and mesenchymal stem cells (Fig. 19B) with the different media, the rate of receptor auto-phosphorylation upon ligand-dependent dimerization was calculated. In both cases, the hVEGF-165 and hPDGF-B synthesized by the algae were able to bind to their correspondent VEGFR-2 and PDGFR-ß receptors, respectively, and induce their phosphorylation, which shows the capability of the recombinant growth factors expressed in *C. reinhardtii* to activate human cells. As a positive control, commercially available recombinant human growth factors were used, while culture supernatant of the non-transformed wild-type algae (*C.r.*-WT) was used as a negative control.

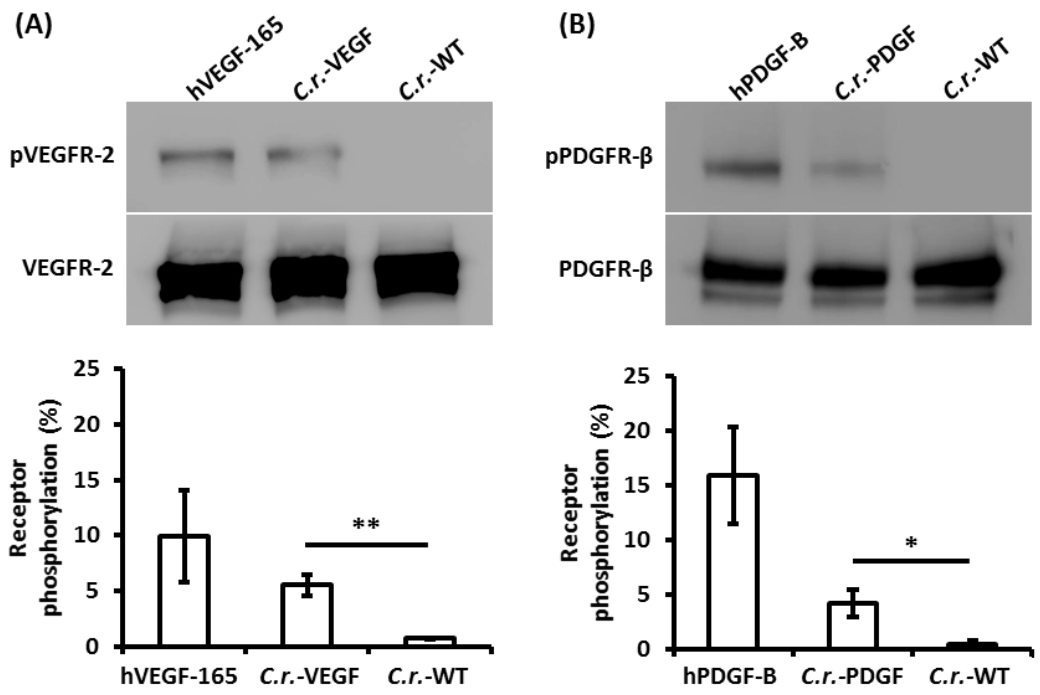

Figure 19: Bioactivity of the recombinant factors *in vitro*. hVEGF-165 and hPDGF-B were secreted into the culture medium by *C.r.*-VEGF and *C.r.*-PDGF, respectively. Binding of the growth factors to the correspondent receptors VEGFR-2 and PDGFR-ß induced their phosphorylation in HUVECs (A; pVEGFR-2) and MSCs (B; pPDGFR-ß). As a positive control, cells were stimulated with hVEGF-165 (50 ng·ml-1) and hPDGF-B (10 ng·ml-1). The phosphorylation rate of the receptor was quantified by analysis of the signal pixel density measured on the western blot. ** $p<0.005$. Results are shown as mean ± S.D. and were obtained for at least three independent experiments.

5.6 Bioactivity of the genetically modified algae *in vivo*

The bioactivity of the recombinant proteins *in vivo* was tested in transgenic zebrafish embryos expressing EGFP in endothelial cells. For this, microalgae were injected into the yolk sack of the embryos at one day post-fertilization. Three days after the injection, the anatomical arrangement of the vasculature in this area was observed. Representative results of each experimental group are shown (Fig. 20). No alteration of the larvae phenotype was observed in fish injected with wild-type algae. However, an ingrowth of blood vessels in the direction of the algae expressing the recombinant hVEGF-165 was evident in about 30% of the fish injected. Such vascular ingrowth was only observed, when the majority of the algae remained in a ventro-central position within the yolk sack. In contrast to *C.r.*-VEGF, the injection of *C.r.*-PDGF did not induce any notorious changes in the vasculature. Yet, it appeared to be an increased presence of EGFP-marked endothelial cells within the yolk.

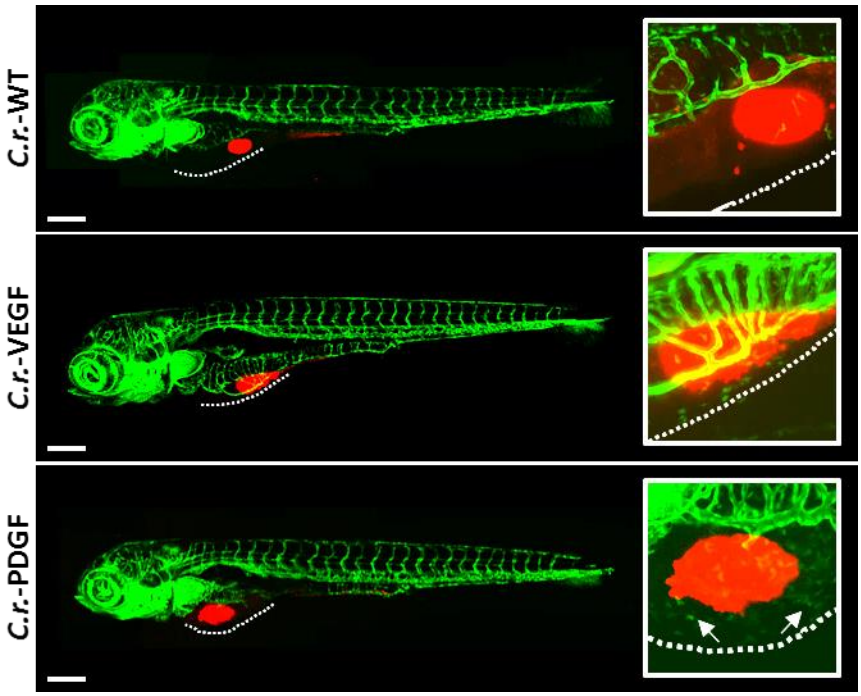

Figure 20: Bioactivity of GM-algae *in vivo*. Microalgae (red; chlorophyll autofluorescence) were injected at 30 hpf into the yolk sack of transgenic zebrafish embryos expressing EGFP in endothelial cells. Three days after injection, vessels appear to be growing into the injected algae expressing hVEGF-165 (*C.r.*-VEGF). Although the effect caused by the bioactivity of *C.r.*-PDGF was not as evident, more endothelial cells were seen in the yolk-sack area (white arrows). The phenotype was not observed in fish injected with wild-type algae (*C.r.*-WT). Projections of the yolk area front and side view are shown. Results were obtained for at least three independent experiments, using approximately 30 fish per group. Scale bar represents 250 µm.

Following the same protocol as before, by injecting a combination *C.r.*-VEGF and *C.r.*-PDGF microalgae in different ratios going from 1:10 to 10:1, the effect of combined GM-algae *in vivo* was evaluated. Three days after injection, only embryos injected with *C.r.*-VEGF and *C.r.*-PDGF algae at a ratio of 1:5, respectively, showed what seems to be an extended branch of the vasculature growing into the injected algae (Fig. 21). This phenomenon was observed in 25% of the embryos injected.

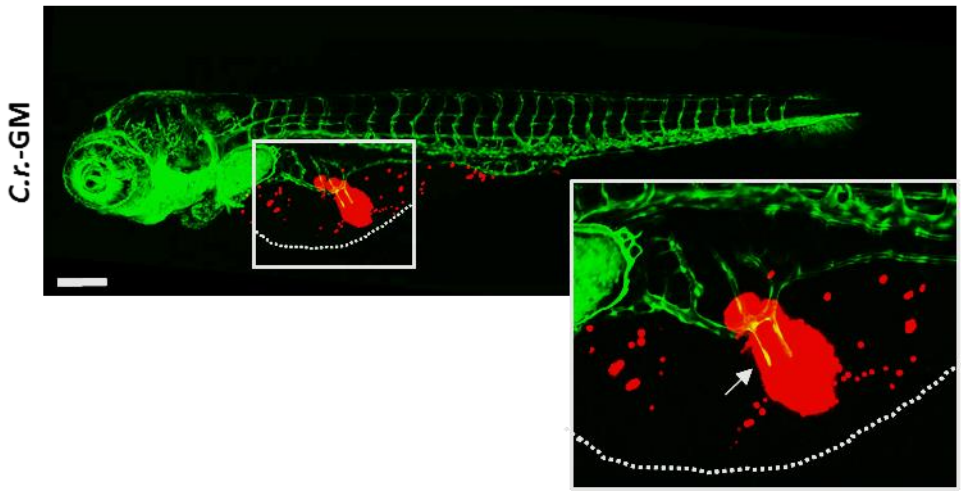

Figure 21: Bioactivity of combined GM-algae *in vivo*. *C.r.*-VEGF and *C.r.*-PDGF microalgae were injected at different ratios into the yolk sack of 30 hpf zebrafish embryos. Three days after injection, embryos injected with the GM-algae at a ratio of 1:5 (*C.r.*-GM), respectively, showed an apparent extension of the vasculature towards the algae (white arrow). Results were obtained in at least three independent experiments, using approximately 30 fish per group. Scale bar represents 250 µm.

5.7 Gene modified algae and photosynthetic biomaterials *in vitro*

The following experiments were designed to evaluate whether dermal scaffolds seeded with genetically modified algae could release both, oxygen and pro-angiogenic recombinant growth factors *in vitro*.

C.r.-VEGF and *C.r.*-PDGF algae were seeded at a 1:5 ratio in a dermal scaffold, as described in section 4.21. While the oxygen concentration in the control setting (scaffolds without algae) dropped under hypoxic conditions (1% pO_2), the encapsulated GM-algae showed an equal photosynthetic capacity upon light-stimulation compared to their wild-type and reached the saturation of the system (≥ 50% pO_2) in less than 24 hours (Fig. 22A). Further, the quantification of the non-cumulative supernatant concentrations of hVEGF-165 and hPDGF-B showed a constant secretion of both growth factors by the algae seeded in the scaffolds in physiological amounts for at least fourteen days (Fig. 22B).

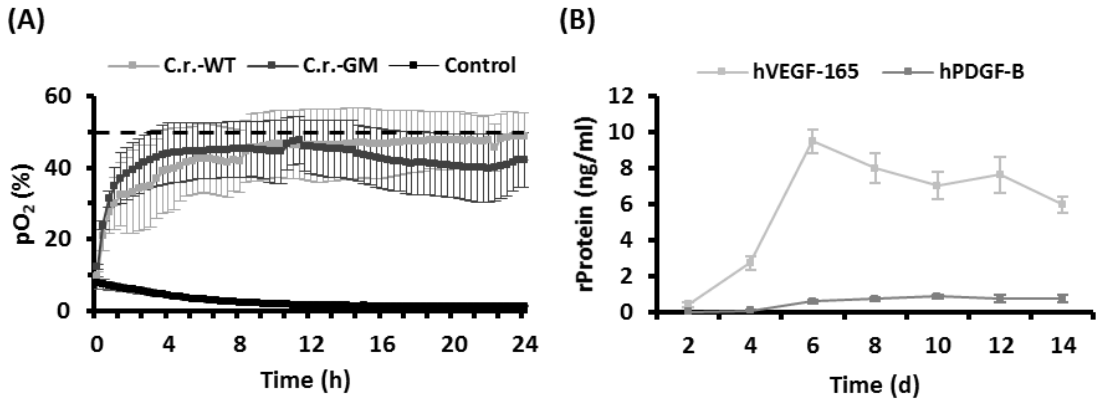

Figure 22: Bioactivity of the gene modified microalgae in a collagen scaffold. The transgenic strains *C.r.*-VEGF and *C.r.*-PDGF were encapsulated with a fibrin hydrogel inside a collagen matrix at a 1:5 ratio to a total cell density of $2.5 \cdot 10^6$ cells per scaffold. The genetically modified algae (*C.r.*-GM) had the same photosynthetic capacity (A) as the wild-type algae (*C.r.*-WT). In addition, they released the recombinant growth factors constantly into the culture medium for at least two weeks as measured by ELISA (B). Results are shown as mean ± S.D. and were obtained for at least three independent experiments.

5.8 Photosynthetic gene therapy *in vivo*

Scaffolds were prepared as described in section 4.6, and cultivated for five days under continuous light exposure. *C.r.*-VEGF and *C.r.*-PDGF algae were seeded at the same ratio as in the previous section. Then, scaffolds were implanted in the back of hairless Skh1 mice, following the same procedure as with the nude mice.

After seven (Fig. 23A) and fourteen (Fig. 23B) days, the general outcome of the implants was evaluated. Both control mice and mice treated with photosynthetic scaffolds seemed healthy, and showed no change in the behavior at any time during the experiment. Macroscopically, no signs of local infection or necrosis were observed in the surrounding wound area or within the engrafted tissues. No significant wound contraction was observed in either group. The algae-specific green color of the scaffold remained over time, although two weeks after implantation it seemed less bright.

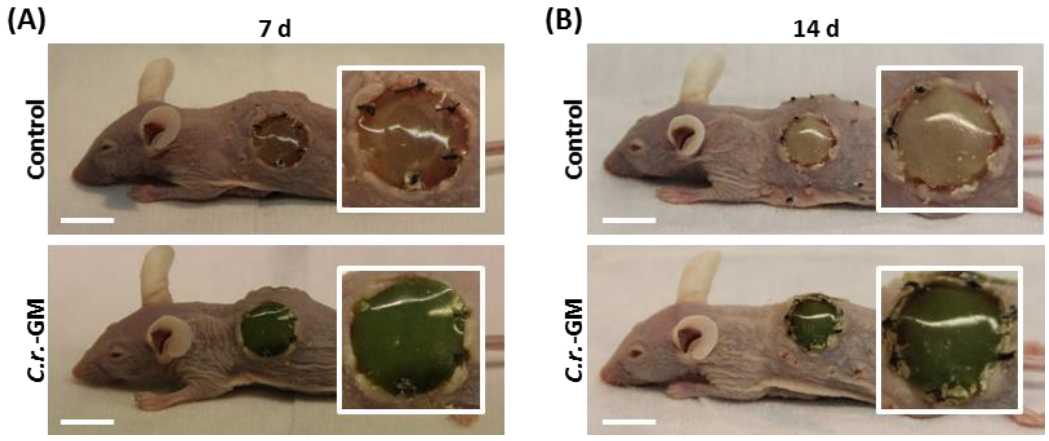

Figure 23: GM-algae seeded scaffolds in a dermal regeneration model. Collagen scaffolds were seeded with encapsulated *C.r.*-VEGF and *C.r.*-PDGF at a 1:5 ratio, respectively, and implanted in the back of hairless Skh1 mice. Seven (A) and fourteen days (B) after implantation tissues seemed intact and no signs of local inflammation were observed. Scale bar represents 1 cm. $N \geq 3$.

By the end of the experimental times, tissues were harvested and transillumination pictures were taken (Fig. 24A). The vascularization of the area underneath the scaffold was quantified as described in section 4.7.

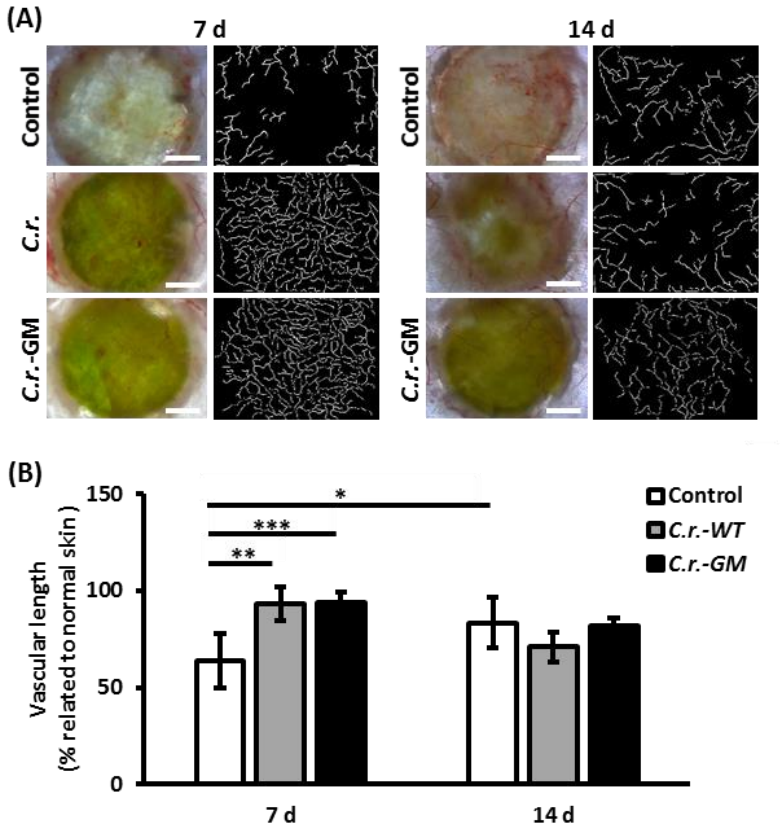

Figure 24: Quantification of the vascularization length over the wound area. Transillumination pictures of the harvested tissues after seven and fourteen days post-transplantation were taken using a stereomicroscope. Representative pictures are shown (A). The growing vascularization of the wound area was quantified by digital segmentation and related to normal skin tissue (B). Scale bar represents 25 mm. * $p \leq 0.05$, * * $p \leq 0.005$, * * * $p \leq 0.001$. Results are shown as mean ± S.D. $N \geq 6$.

While the pictures did not show an evident increase in the vascularization of the wound area, the quantification of the growing vascular network showed a significant increase in the vascular length with the photosynthetic scaffolds after seven days, suggesting an increased number of small blood vessels. However, the quantification of the vascularization of the regenerating tissues showed similar results for all groups after two weeks post-implantation. Further, it showed a decrease in the vascularization underneath the photosynthetic scaffolds over time (Fig. 24B).

Interestingly, the rate of vascularization of the normal skin tissue was significantly higher in the mice that had photosynthetic scaffolds implanted for two weeks (*C.r.*-WT: $p = 0.008$, *C.r.*-GM: $p = 0.0006$; $N \geq 3$) and in the mice that received scaffolds with GM-algae after seven days (*C.r.*-GM: $p = 0.002$; $N \geq 3$).

Both recombinant human growth factors were found in the protein lysates obtained from the explanted scaffolds after one (Fig. 25A) and two weeks (Fig. 25B) post-transplantation. The seeded algae inside the scaffold, raised the concentration of the therapeutic molecules significantly inside the implant. Interestingly, hPDGF-B was found in three-time higher amounts than hVEGF-165, which was contrary to the results obtained *in vitro*.

However, the concentration of the recombinant proteins was significantly decreased after two weeks compared to the earlier time-point. In a parallel experiment, the *ex vivo* outgrowth of the algae from biopsies taken, proved the viability of the algae inside the scaffold after seven, but not after two weeks post implantation (data not shown).

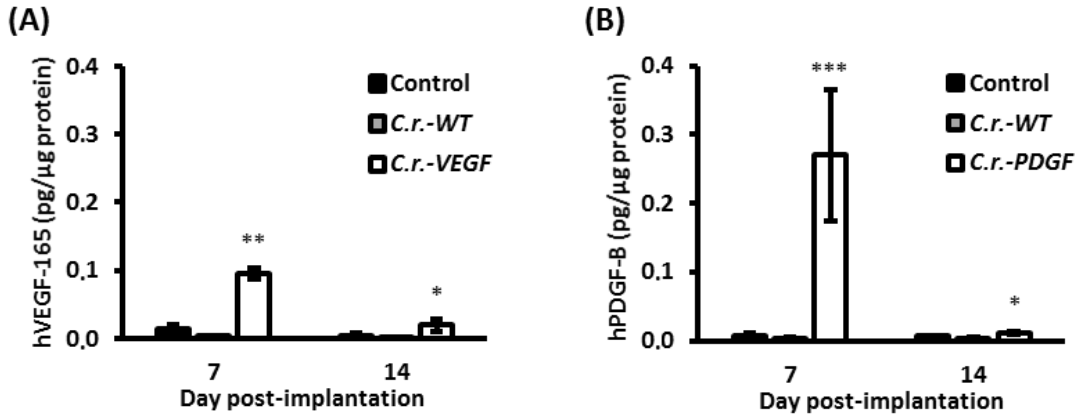

Figure 25: Expression of the recombinant proteins *in vivo*. The growth factors hVEGF-165 and hPDGF-B were found in the protein lysates obtained from the explanted scaffolds after both seven and fourteen days post-transplantation. * $p \leq 0.05$, ** $p \leq 0.005$, *** $p \leq 0.001$. Results are shown as mean ± S.D. $N \geq 6$.

A remarkable observation, was the formation of a tissue underneath the photosynthetic scaffolds, which covered the entire wound bed area and assembled a stable linkage with the wound edge, entirely closing the defect (Fig. 26).

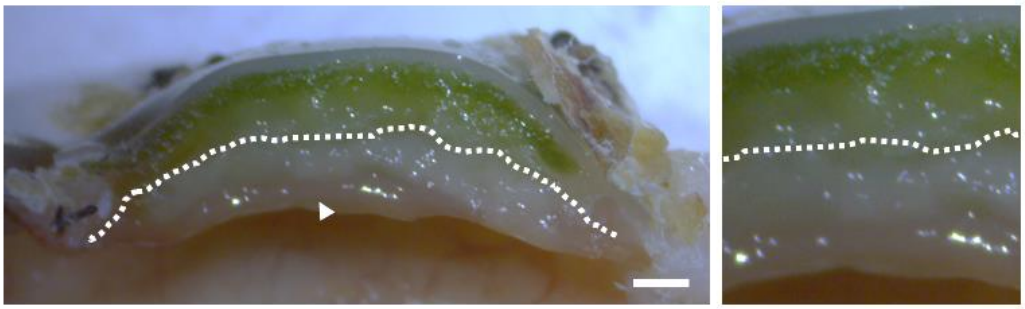

Figure 26: Explanted photosynthetic scaffold after two weeks post-implantation. A non-characterizing tissue (white arrowhead) covering the wound area (white dotted line) was observed underneath the algae-seeded scaffolds. The left picture shows a zoom-in of the area above the white arrowhead. Scale bar represents 1 mm.

Histological analysis of the harvested tissues showed an increased amount of granulation tissue below the photosynthetic scaffolds seeded with WT and GM-algae, respectively (Fig. 27, A-F). Although the thickness of the tissue was not statistically different after one week (Control: 152 ± 67 µm, *C.r.*-WT: 332 ± 133 µm, *C.r.*-GM: 226 ± 113 µm), it was indeed after two weeks (Control: 187 ± 102 µm, *C.r.*-WT: 534 ± 137 µm, *C.r.*-GM: 493 ± 230 µm, $p \leq 0.01$). Furthermore, blood capillaries were found at all depths within this tissue, although the number of them was not increased in the presence of the recombinant growth factors (Fig. 27, G-H).

Some signs of inflammation, such as an increased invasion of polymorphonuclear cells were found within the algae-seeded scaffolds. Also, a higher rate of matrix degradation in the photosynthetic scaffolds was noticed from the loss of the original scaffold-appearance over time. This was more obvious after two weeks, when some of the scaffolds appeared to be detached from the wound bed (Fig. 27I).

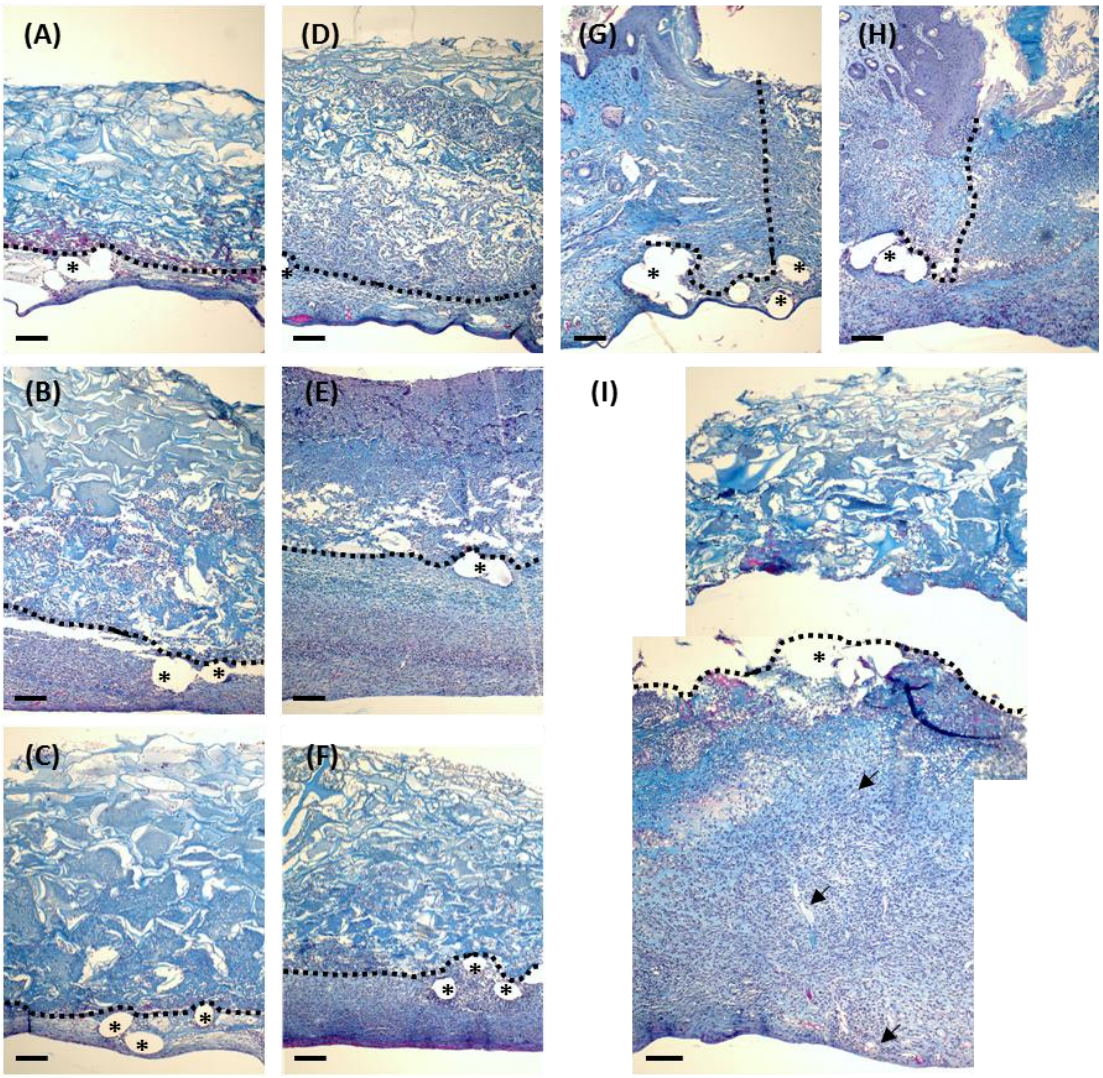

Figure 27: Histological analysis of photosynthetic dermal scaffolds. Masson's trichrome staining of transversal sections of the scaffold and wound-bed after one (A-C) and two (D-F) weeks post-implantation. The granulation tissue growing underneath the titan mesh (*), which was placed over the wound bed (dotted line), is thinner and less dense with cells in the defects filled with control scaffolds (A, D), than with wild-type *C. reinhardtii* (B, E) or gene-modified *C. reinhardtii* (C, F) seeded scaffolds. The connective tissue at the wound edge (dotted line) between the implant and the skin was further developed in the photosynthetic scaffolds (H) than in the control scaffolds (G). In some cases scaffold degradation lead to the detachment of the implant from the wound bed (I). Nevertheless, blood vessels (arrows) were to be found within the granulation tissue. Scale bar represents 100 µm. $N \geq 6$.

VI. Discussion

6.1 Photosynthetic biomaterials

One of the major limitations in tissue engineering is that artificial tissues cannot be implanted in clinically relevant sizes as nutrition, gas exchange, and elimination of waste products are limited by a maximum diffusion distance (Lalan *et al.*, 2001). In particular, one of the main challenges in the field is to find a strategy that achieves the gradual and sustained release of oxygen, in order to avoid post-implantation ischemia and prolong cell survival in the engineered tissue until host neovascularization is achieved (Dimmeler *et al.*, 2014).

The approaches developed so far, offer a limited burst of oxygen when embedded into a biomaterial (Oh *et al.*, 2009; Harrison *et al.*, 2007). Other advanced bioengineered strategies suggest the development of a pre-formed vascular network inside engineered tissues, which could inosculate with the host vasculature and hence be perfused. However, vast difficulties concerning immunogenicity, availability, and transport will have to be faced in order to achieve clinical success (Wu *et al.*, 2010, White *et al.*, 2013).

Following the approach presented by Hopfner *et al.*, this study proposes the development of a photosynthetic biomaterial that is able of oxygen self-production and hence could offer an unlimited source of oxygen for the regenerating tissue, which will merely depend on light stimulation (Hopfner *et al.*, 2014). For this, the green unicellular algae *C. reinhardtii* were incorporated into scaffolds and exposed to illumination to trigger photosynthesis and achieve oxygen production *in situ*. Although any photosynthetic cell could be a candidate for similar approaches, the use of *C. reinhardtii* is particularly attractive, because it is easy to handle, shows a fast growth rate compared to other photosynthetic organisms, reaches cell densities of over twenty million cells per milliliter in few days, and since it does not harbor any known pathogenic viruses or other harmful molecules, it is recognized as a GRAS organism by the FDA (Almaraz *et al.*, 2014).

As proof of concept, Integra® dermal regeneration template (IDRT) was chosen as an example of a scaffold for dermal regeneration. IDRT is a porous biodegradable matrix formed by bovine collagen I fibers and cross-linked glycosaminoglycans. On top, the collagen structure is covered with a removable silicon layer, which acts as a temporal epidermis, to decrease the risk of infection and dehydration. IDRT is the most successful and best characterized scaffold commercially available. It has been extensively studied in clinical and preclinical settings, and is considered the gold standard for the development of new products. It is used to cover partial and full thickness wounds, chronic and vascular ulcers and major trauma wounds (Moiemen *et al.*, 2006). However, as many other dermal scaffolds, many days are required before the vascular network grows into the 2 mm thick collagen structure (Shaterian *et al.*, 2009). During this time the injured tissue and the graft are subjected to ischemic conditions and become prone to tissue necrosis and anaerobic bacteria infections. This endangers the success of the treatment, especially in cases of impaired wound healing, where re-vascularization takes even longer (Machens *et al.*, 2000).

6.1.1 Biocompatibility in photosynthetic dermal scaffolds

In order to generate photosynthetic scaffolds, *C. reinhardtii* algae were incorporated into the collagen-matrices within a fibrin-encapsulation (Fig. 8). This granted a better confinement of the algae than in the previous published approach, where algae were seeded by letting the cell-suspension be absorbed by the matrix (Hopfner *et al.*, 2014).

Fibrin, an insoluble protein, which is formed by the proteolytic cleavage of its precursor protein fibrinogen through the action of thrombin, was chosen among the natural occurring molecules, partially because it is already an autologous component of the wound healing and remodeling mechanism. It acts as an essential clotting element during the final stages of the hemostatic coagulation cascade impeding the blood flow and scaffolding the injured site. Fibrin is also a very appealing biopolymer since it is currently used in the clinics as it is fully resorbable and has multiple interaction sites for cells and other proteins (Park *et al.*, 2007), but above all, because it allows oxygen diffusion (Colom *et al.*, 2013) and reaches oxygen tension values of over

125 mmHg, that actually exceeded the typical partial pressures of oxygen in soft tissues (25 mmHg; Demol, *et al.*, 2011). This would therefore allow the diffusion of oxygen produced by the algae through the scaffold.

Once within the biomaterials, the encapsulated *C. reinhardtii* formed evenly distributed clusters that maintained a high viability and proliferation activity, when cultivated under continuous illumination, conclusively proving their biocompatibility with the setting (Fig. 9A). The uniformity of the algae, can avoid the formation of regions with low oxygen concentrations within the scaffold, an obstacle that limits the thickness of engineered tissue substitutes to 1 mm^3 to date (Kim *et al.*, 2014).

6.1.2 Oxygen release sustainment *in vitro*

Photosynthetic activity was sustained for at least seven days and oxygen was released into the medium immediately upon light exposure. The rate of photosynthesis correlated with the algae density inside the scaffold, which in turn was a consequence of the proliferation of the photosynthetic cells (Fig. 9B). Although the concentration of dissolved oxygen reached higher values than it was possible to measure accurately ($pO_2 \geq 50\%$), photosynthetic scaffolds showed an increase in the pO_2 of at least 50 times compared to control scaffolds, which is far above the increase observed in other approaches presented in the past, where barely 0.2 times more oxygen were achieved (Oh, *et al.*, 2009; Seifu *et al.*, 2011).

As mentioned before, the oxygen production is primarily dependent on the number of algae and the light intensity that they are exposed to. A feasible approach to modulate the oxygen production of the scaffolds would be to optimize either the number of seeded algae inside the implant, or the intensity of light applied to the construct and assign them to meet the oxygen tension demanded by the tissue. Also, it will have to be considered that, *C. reinhardtii*, like many other photosynthetic organisms is sensitive to phototoxic effects when exposed to high light intensities (Eberhard *et al.*, 2008). A more detailed profile of the photosynthetic performance of the constructs and its constraints is therefore required.

The concentration of oxygen released by the photosynthetic scaffolds greatly exceed the solubility of oxygen in blood at arterial pO_2, which is approximately 130 µM (95 mmHg; Sen, 2009); and exceeded the usually found 54-70 mmHg partial pressure in dermal tissue (Bland *et al.*, 2013). Although, this could be considered potentially toxic due to the risk of oxidative damage, it is expected that the metabolic consumption of oxygen during wound healing will be higher (Hopf *et al.*, 2007). Therefore, photosynthetic oxygen will be required to sustain the hypermetabolic state of regenerating tissue and restore the decreased oxygen concentration in wounds (Bland *et al.*, 2013). In the future, it will be necessary to monitor the oxygen tension, to balance oxygen synthesis and requirements on the wound.

6.1.3 Photosynthetic scaffolds *in vivo*

The photosynthetic dermal scaffolds were engrafted in the back of mice without further complications (Fig. 10). Inside the graft, a chimeric tissue of algae and murine cells was formed already after five days and no signs of rejection were observed macroscopically (Fig. 12A).

Because of ethical concerns, mice could not be exposed to more than twelve hours to the extra illumination installed around the cages. *C. reinhardtii* is not able to maintain a high photosynthetic capacity in light-dark cycles. Furthermore, growth rate as well as light utilization efficiency decreases in comparison to continuous illumination (Janssen *et al.*, 2000). Despite this, the algae remained metabolically active for up to five days (Fig. 13B) and algal cultures could be re-grown from biopsies of the scaffold up to seven days post-implantation (Fig. 13C). It can therefore be concluded that they were photosynthetically active and oxygen was being synthesized and released for at least one week.

However, the viability of the algae seemed to terminate soon after this period of time. Many factors may be contributing to the late morbidity of the algae, considering that while being in the host, the algae were exposed to conditions far off from their optimal. For instance, the mouse body temperature is about 18°C higher to the one at which algae are usually cultivated. During the dark periods, algae survived solely on the remaining acetate inside the scaffold and could

have therefore undergone nutrient starvation. Moreover, even though the microalgae were inside of a hydrogel, it is difficult to say, if their aqueous environment was sufficiently maintained once implanted.

Interestingly, *C. reinhardtii* can be habituated to extreme conditions such as higher temperatures (Tanaka *et al.*, 2000) and their cell-cycle synchronized to light-dark cycles (Rochaix *et al.*, 2011). A pre-conditioning adaptation time might increment the viability of the algae *in vivo*. On the other hand, the approach benefits from its transiency, meaning that, if photosynthesis could sustain the oxygen needs of the tissue until it is sufficient vascularized, then there will be no need for the algae to remain alive. Further experiments will have to study if other strategies, such as a different encapsulation technique, could be developed to extend the viability of the algae *in vivo*.

Photosynthetic oxygen did not impair angiogenesis in the wound area, although it is known that the primary angiogenesis-related gene activation mechanisms occur via activation of the hypoxia-sensor molecule HIF-1α (Tandara *et al.*, 2004). On the one side, algae respiration might be taking place during the dark periods to which the scaffolds are exposed, consuming therefore oxygen just as the animal cells. On the other hand, it has been written, that it is not the actual partial oxygen pressure, but the changes of it registered by the cells, what triggers the hypoxic pro-angiogenic transcriptional function of HIF-1α (Sen, 2009). Further measurements to estimate the effect of the succession of photosynthetic and respiratory activity over the wound bed oxygen tension are needed.

As long as oxygenation is sufficient to sustain life, HIF-dependent survival responses may benefit wound healing (Krock *et al.*, 2011). Photosynthetic scaffolds could help to maintain an adequate tissue oxygenation, to prevent the risk of stalled wound healing or tissue loss due to chronic hypoxia, but without impairing the hypoxia-dependent processes involved in wound re-vascularization. Also, in a wound with hypoxic zones ranging in magnitude, the applied therapy should re-establish normoxia in the worst affected hypoxic areas without exposing other parts of the wound tissue to levels of pO_2 that would antagonize healing by hyperoxia (Sen, 2009). The local induction of photosynthesis could solve this predicament.

6.2 Inflammatory response

The exposure of two different vertebrate species to *C. reinhardtii* algae, did not induce any significant inflammatory response. Although athymic nude mice present a low T-cell mediated response, the innate immune system in this model is fully functional (Belizário, 2009). In fact, several inflammatory related molecules were detected inside the scaffolds regardless of the scaffold implanted (Fig. 14A). From these, only two cytokines appeared to be overexpressed in the presence of *C. reinhardtii*, C5a and CCL12.

C5a is a component of the complement system, it has both chemotactic and anaphylatoxic properties and plays a key role in increasing migration and adherence of neutrophils and monocytes (Manthey, *et al.*, 2009). CCL12, sometimes referred as MCP-1-related chemokine, is a small cytokine that attracts eosinophils, monocytes and lymphocytes (Sarafi *et al.*, 1997). The expression of these molecules can be induced in macrophages as an immune mechanism to speed up the phagocytosis of pathogens. This suggests that even though the inflammatory response is not severe, the eradication of the *C. reinhardtii* algae by the innate immune system cannot be ruled out.

On the other hand, the assay only measures the amount of cytokines semi-quantitatively, and thus gives no estimation of the physiological relevance of the results. Therefore, the calculated numerical statistical difference, might not correlate with a considerable negative response from the immune system of the host against the algae. Also, it is important to point out that, the full-skin defect is intrinsically inflammatory, and all the gathered results in this work sustain the relevance of the immune system as a key mediator in tissue repair. Therefore, a specific response towards the algae might not be discernible within such high inflammatory background. Tests to determine the antigenicity of the algae can help to address this issue further.

Nevertheless, no evidence of a systemic inflammatory reaction towards the photosynthetic implants was found (Fig. 14, B-E). A possible explanation could be, that the encapsulation of the algae may have served an immune-isolation function and contributed to the hampering of their

recognition by the cells of the immune system of the mice. Fibrin has shown before to be effective in minimizing the host immune response (Hunt *et al.*, 2010) and to enhance transplanted cell survival and their regenerative potential (Murphy *et al.*, 2014).

This proved to be further valid, when photosynthetic scaffolds were implanted in immunocompetent mice (Fig. 16). Again, no signs of inflammation were to be seen or measurable in any of the immune system organs examined after three weeks and the serum of the mice that received the algae-containing scaffold, showed comparable parameters to the control mice.

The zebrafish model allowed a better evaluation of the cell-pathogen interactions orchestrated by the innate immune system (Fig. 15). Given the advantages of optical transparency of fully developed larvae and the availability of transgenic lines, that permit tracking particular cell types, this model has become popular in other research areas such as inflammation (Novoa *et al.*, 2012; Fang *et al.*, 2012), and wound repair (Poss *et al.*, 2003). The zebrafish otic cavity provided a confining site for injection and facilitated the study of local inflammation induced by the microorganisms (Benard *et al.*, 2012). The results obtained after the quantification of the recruitment and the phagocytic activity of macrophages, proved the low pathogenicity of the microalgae and suggest that the algae could co-exist as a "symbiotic" organism.

Altogether these results show that the presence of *C. reinhardtii* microalgae does not trigger a significant immune response inside a host and that photosynthetic scaffolds can be implanted in full-skin defects without causing a major inflammation.

6.3 Recombinant growth factors expression in *C. reinhardtii*

6.3.1 Potential of *C. reinhardtii* as platform of recombinant protein expression

Showing that it is possible to engineer scaffolds that could provide both, an architecture to guide the growth of migrating cells, and oxygen to enable their survival, without causing a major inflammatory response upon implantation in a host, encouraged the idea of incorporating a complementary strategy to supply the cells with the necessary growth factors to promote the regeneration of the tissue. Therefore, taking the approach one further step towards autotrophic tissue engineering, *C. reinhardtii* algae were genetically modified so that, in addition to oxygen, they could release other pro-regenerative bioactive molecules. In this study, hVEGF-165 and hPDGF-B were selected as an example to introduce the concept of photosynthetic gene therapy.

hVEGF-165 is a potent mitogen for endothelial cells and induces endothelial cell migration, sprouting, and survival. It is a well described pro-angiogenic growth factor involved in tissue repair that has been used to improve vascularization in tissue engineering before. hPDGF-B is also a mitogen, whose signaling is associated to tissue remodeling and cellular differentiation. It has shown to improve wound healing by enhancing granulation tissue formation and increasing angiogenesis as well as epithelialization (Barrientos *et al.*, 2008).

In the past fifteen years, *C. reinhardtii* has become an increasingly attractive organism for the expression of therapeutic proteins. In fact, Rasala *et al.* reported over thirty recombinant proteins that are now being expressed in the microalgae (Section 1.5.3, Tab. 1). However, these studies aimed to use the algae as a platform for industrial purposes, and in most of the approaches a protein purification process was required to isolate the chloroplast-synthetized proteins. Since, the objective in this work was to use the microalgae as carriers for the delivery of functional growth factors, the strategy of expression follow suit nuclear transformation of the algae to enable eukaryotic post-translational modifications, and the extracellular targeting of the recombinant proteins.

Transgenic *C. reinhardtii* microalgae could have many advantages in gene therapy compared to other eukaryotic cells, which would make them attractive for further applications other than tissue engineering approaches. For a start, they do not depend on external oxygen supply, and therefore will not die from hypoxia upon any form of implantation. Further, human transgenes are modified for the specific expression by the algae and their transformation means no risk of insertional mutagenesis, nor potential oncogenicity for the patient. Finally, if required, they could be eliminated from the recipient by simple methods such as light deprivation of the wound area or the local application of non-toxic herbicides.

Despite the disadvantages of the random integration of the transgenes, such as, the loss of parts of the genome, the integration of the selection gene only and the lack of control over the copies inserted, enough transformants that successfully integrated the human genes and exported the recombinant proteins into the medium were obtained (Fig. 17).

Both growth factors were detectable by primary antibodies in an ELISA-assay, probing their right conformation. The genetically modified strains *C.r.*-VEGF and *C.r.*-PDGF reached yields of 0.05% and 0.001% of total protein expression in the culture medium, respectively (Tab. 3). Yet, these are rather low yields, compared to other eukaryotic platforms of recombinant protein expression, like yeast or insect cells.

Moreover, the difference of the expression of both transgenes was intriguing, knowing that both genes had been codon optimized and inserted into the same expression cassette (Fig. 7A). One of the restriction enzyme digests showed two copies of the gene in the genome of *C.r.*-PDGF (Fig. 18B). Although high copy numbers are desired for improving recombinant protein yield, it can result in protein aggregation and deficient post-translational modification in other expression systems (Palomares *et al.*, 2004).

Other authors have also reported similar variations of the expression yields in *C. reinhardtii*. For instance, in a study that examined the expression of seven recombinant human proteins in the chloroplast of *C. reinhardtii*, only three of the proteins were accumulated to levels above 1% of total soluble protein, with VEGF-165 being the best expressed by reaching yields of 3%. The

authors concluded that the reason for poor expression was either protein instability or inefficient translation of the chimeric mRNAs (Rasala *et al.*, 2010). Coragliotti *et al.* agreed that the accumulation of heterologous proteins in the algae was defined by protein synthesis (Coragliotti *et al.*, 2011).

6.3.2 Biofunctionality of human growth factors expressed by *C. reinhardtii*

The stimulation of human cells with the recombinant growth factors expressed by transgene *C. reinhardtii* proved to be successful (Fig.19). The autophosphorylation detected in the respective receptors upon ligand binding, proved the biofunctionality of hVEGF-165 and hPDGF-B.

To generate the activation medium, algae were grown in TAPS-medium in order to reach proper cell-densities and hence high amounts of recombinant protein. Then, by filtration, the growth factors were recovered and suspended in animal cell-medium. The actually low concentrations[2] in the activation media suggest that a more refined method of growth factor recovery should be used in the future.

In vivo, injection of transgenic fish with recombinant algae, showed an angiogenic effect that modified the architecture of the developing vascular network (Fig. 20 and 21). While all injections were done inside the yolk sack and the volume of the cell-suspension was consistent for all the fish injected, it was not possible to know with precision the number of cells injected nor to control the distribution of the algae due the fluctuations in yolk. Therefore, the phenotype observed three days after injection could only be evaluated qualitatively. Nevertheless, similar phenotypes were observed upon injections of other angiogenic molecules or angiogenesis promoting cells (Habeck *et al.*, 2002; Nicoli *et al.*, 2009; Li *et al.*, 2012). All this evidence, indicates that transgenic *C. reinhardtii* microalgae are capable to synthesize and secrete functional pro-angiogenic growth factors in physiologically relevant amounts.

[2] 30 ml of a *C.r.*-VEGF culture with approx. 30 ng/ml hVEGF-165, should have a final concentration of 300 ng/ml if the final volume was 3 ml. However, the ELISA assay reported a ten times lower concentration.

6.4 Photosynthetic gene therapy for dermal regeneration

6.4.1 *In vitro* approach assessment

The genetically modified strains sustained a release of both oxygen and growth factors for fourteen days, when cultured under optimal conditions (Fig. 22). The proportion at which the algae were seeded inside the scaffold, directly affected the amount of each protein found in the supernatant. Since there was a fivefold lesser amount of *C.r.*-VEGF algae expressing fifty times more recombinant protein than *C.r.*-PDGF, a ratio of approximately ten between hVEGF-165 and hPDGF-B is possible to explain.

Compared to other approaches of controlled growth factor delivery, the released amount of by the pro-angiogenic photosynthetic scaffolds is equivalent (Richardson *et al.*, 2001, Reckhenrich *et al.*, 2011). Yet, contrary to the release kinetics of some of these approaches, there is no peak of expression or a secretion burst at the beginning (Li *et al.*, 2009; Xie *et al.*, 2013). The expression curves rather follow the growth curve of the algae inside the scaffold, therefore sustaining a constant recombinant protein secretion as long as the algae are able to proliferate within the scaffold.

6.4.2 *In vivo* approach assessment

In vivo, the recombinant factors were found in the protein extracts obtained from the explanted scaffolds for up to two weeks post-implantation (Fig. 25). Although, the growth factor concentration is shown in proportion to the total protein amount in the lysate, which increased with the time the scaffold remain implanted, there was already a significant net decrease on the measured concentrations of both factors (data not shown). Together with the results obtained from the *ex vivo* growth of the algae, one could conclude that after seven days, the protein expression in the algae begins to cease. Again, the cycling light-dark periods and the under-optimal environmental conditions impeding the survival of the algae, might also have an effect on the protein expression rates.

Dual delivery of hVEGF-165 and hPDGF-B in the context of therapeutic angiogenesis has been studied before and found critical for both the initial formation of blood vessels and their maturation. By developing a system that allowed controlled dose and rate of delivery, Richardson *et al.* showed a rapid formation of a mature vascular network inside subcutaneously implanted scaffolds by the daily release of 1.7 pmol VEGF-165 and 0.1 pmol PDGF-B (Richardson *et al.*, 2001). Although, the ratio achieved *in vitro* by the photosynthetic scaffolds laid close to this results (Fig. 22B), *in vivo* there was almost 3 times more hPDGF-B after one week, and only 1.7 times more hVEGF-165 after two weeks post-implantation (Fig. 25).

Moreover, by implanting retrovirally transduced myoblasts that constitutively express VEGF-165 into muscles of adult mice, Osawa *et al.* reported that a range of 5 ng VEGF·10^{-6} cells/day to at least 70 ng VEGF·10^{-6} cells/day in culture, induces normal neovascularization without signs of aberrant growth (Osawa *et al.*, 2004). The expression of hVEGF-165 by the encapsulated algae lay near this range after six days of cultivation *in vitro* (Fig. 22B), although is difficult to estimate the algae density at this time (~10 ng·ml^{-1}, 2.5 ·10^{6} cell initially seeded).

However, the presence of the recombinant pro-angiogenic growth factors, did not significantly increase the rate of vascularization over the wound bed (Fig. 24). It should be noted that, the visualization of the growing vasculature depends greatly on the transparency of the tissue. In addition to the hindrance from the green color of the photosynthetic scaffolds, the underlying wound bed tissue is far thicker and developed after two weeks. Therefore, it is not possible quantify the entire developing microvasculature accurately at later times with this method.

The efficient release of the growth factors from the scaffold to the wound was shown by the results obtained from the *in vitro* experiments (Fig. 22) and the presence of the factors in the lysates (Fig. 25). Yet, the stability of the growth factors *in vivo* remains to be assessed. It is known that both factors are susceptible to proteolysis in an inflammatory environment (Barrientos *et al.*, 2008). Therefore, some attempts have been made to rescue the recombinant molecules from degradation by modifying sensitive cleavage sites in the polypeptide (Eming *et al.*, 2007). This could be an alternative to increase the levels of active molecules expressed by the algae *in vivo*.

Even though recombinant human growth factors have been shown to effectively induce angiogenesis in other species, there have been reports on differences in the relative activation of their receptors (Mujagic *et al.*, 2013). Therefore, the doses at which the human recombinant growth factors are being released by the algae in the implanted scaffolds, might not be high enough to induce the formation of new vessels in mice. Indeed, the bioactivity of the growth factors expressed by the algae was demonstrated *in vitro* using human primary cells (Fig. 19). It would be interesting to examine the potential of the recombinant human growth factors to activate murine cells, and compare it with the already obtained results, in order to assess the biological activity of the angiogenic proteins across species.

There are other strategies to improve transgene expression rates that could correct the low recombinant protein yield, which is key for the success of the approach. For instance, the Hsp70A promoter fragment has been reported to enhance activity of neighboring promoters and decrease the probability of transcriptional silencing (Fischer and Rochaix, 2001). Moreover, a new expression system has been recently reported to allow the production of up to 10 mg recombinant protein per liter culture, which is approximately thousand times more than the ones achieved in this work (Lauersen *et al.*, 2013). Also, stronger targets to promote angiogenesis might be chosen. HIF-1α, which is pointed out above VEGF-165 and PDGF, as the master regulator of angiogenesis, could provide a therapeutic benefit (Krock *et al.*, 2011). For instance, Trentin *et al.* engineered a HIF-1α molecule which acts insensitive to oxygen and by delivering it on a fibrin carrier, it showed to produce more mature, functional blood vessels than the delivery of VEGF (Trentin *et al.*, 2006).

Interestingly, there seemed to be a convoluted effect of oxygen and the growth factors over the whole skin vasculature, which suggested a more systemic effect of both oxygen and recombinant growth factors of the proposed photosynthetic gene therapy. In this regard, HBO-therapy has shown to increase angiogenesis in hypoxic and injured tissues suggestively via oxidant-mediated mechanisms and the up-regulation of angiogenesis-related molecules (Hopf *et al.*, 2007). The possibility that the photosynthetic oxygen released by the scaffolds could be neutralizing the angiogenic effect of the growth factors may be viewed as thought-provoking.

6.4.3 Evaluation of the improvement on dermal regeneration

Although both, matrix degradation and the degree of inflammatory cell infiltration seemed to be increased with the photosynthetic scaffolds, the formation of an extended granulation tissue underneath them and practically covering the defect was remarkable (Fig. 26 and 27).

It is known that epithelialization depends on the presence of a bed of healthy granulation tissue, which is oxygen dependent (Hopf *et al.*, 2007). Furthermore, a typical feature of chronic non-healing wounds is the reduced granulation tissue formation (Eming *et al.*, 2007). If the health of this tissue and its degree of vascularization were sufficient, the photosynthetic approach could be re-defined as a wound dressing, and promote tissue restoration and wound closure, instead of becoming part of it.

Furthermore, the angiogenic effect of photosynthetic scaffolds was more evident at the earlier stages of wound healing (Fig. 24), which correlates with the viability of the algae *in vivo*. This has also been reported using stem cell-based wound therapy approaches (Edwards *et al.*, 2014). Photosynthetic tissues could have a major impact on avoiding infections and promoting wound closure during the first stages of the wound healing or the immediate treatment of stalled wounds. Otherwise, they could be applied on a later stages and sustain the processes of inflammation and proliferation, which correlate with peaking hypoxia (Haroon *et al.*, 200) and angiogenesis (Shaterian *et al.*, 2009).

At this point, it should be mentioned that maintaining the implanted tissues under the transparent dressing for more than one week, required considerable manipulation of the scaffold to be able to change and suture the bandages back on. This was performed as often as it was necessary and, therefore not regularly or equally among the mice. This might have interfered with the architecture of the developed tissues and increased the variability in the results. Also, because of these handling difficulties and the increasing risk of losing the implant during the experimental time, the model does not allow the study of the regeneration progress for periods of time much longer than two weeks.

In this work, it was demonstrated that *C. reinhardtii* microalgae can be engineered to express and deliver human growth factors into disrupted tissues. Most of the problems associated with foreign gene expression in the microalgae, such as inefficient DNA delivery, failing on the integration into the chromosome, inadequate recognition of the promoter region and epigenetic silencing mechanisms were successfully overcome due to the implemented strategy for recombinant protein expression that considered the biased codon usage, the necessary regulatory sequences and the required targeting signals for protein secretion. Following this system, other therapeutic proteins such as antibiotics, enzymes involved in the regulation of tissue remodeling, or immune-modulatory molecules, could be incorporated into the approach to generate a full pro-regenerative environment for wound treatment. In addition, control of the gene expression by the microalgae could be effected by exploring the use of inducible promoters, and so be able to couple recombinant protein synthesis with the progress of the healing of the wound and the consequent requirements.

Because working with healthy young animals gives an elusive reference of the approach performance, it is not possible to estimate the therapeutic success based on the results of this work at this current stage. Other preclinical model-animals, with more similar regeneration mechanisms to the ones involved in humans, such as the pig, should be used to optimize the approach in matters of algal-cell density in the scaffolds and the effects of light intensity and exposure. Then, once the safety and feasibility have been demonstrated, further research using model organisms of compromised wound healing or critical size defects should be implemented to better evaluate the limitations and capacities of the method and give important insights of the potential application of photosynthetic gene therapy in regenerative medicine and wound healing.

VII. Conclusions

To overcome hypoxia, the main drawback of tissue engineering, it had been previously suggested that photosynthesis might be used as an alternative source of oxygen supply to blood vessel-perfusion. In this work, it was demonstrated that *C. reinhardtii* algae can be biocompatibly encapsulated into artificial dermal scaffolds to create photosynthetic scaffolds that are capable of producing and releasing oxygen for more than a week. Additionally, they can be applied as skin substitutes in fully immunocompetent mice without causing a severe inflammatory response. The gene modification of the nuclear genome of *C. reinhardtii* allowed the expression of human genes encoding pro-angiogenic growth factors. The microalgae were capable of synthesizing and secreting the recombinant proteins from the implanted photosynthetic scaffolds into a wounded tissue for at least seven days *in vivo*. If the recombinant protein yield and the timing of expression were to be optimized, the use of engineered microalgae could have a tremendous impact as an alternative method for recombinant growth factor administration. The results of this work represent a step forward in the development of autotrophic tissues and suggest the use of photosynthetic microalgae cells to treat a broad spectrum of hypoxic conditions as well as a gene therapy option to supply functional biomolecules to improve regeneration and wound healing in human tissues.

VIII. Literature

Almaraz, A., Flores, J., Pérez, V., Salgado, E., Badillo, J. (2014). Production of therapeutic proteins in the chloroplast of *Chlamydomonas reinhardtii. AMB Express, 4*, 57.

Asahara T, Murohara T, Sullivan A, Silver M, van der Zee R, Li T, Witzenbichler B, Schatteman G, Isner JM. (1997). Isolation of putative progenitor endothelial cells for angiogenesis. *Science, 275*, 964 –967

Baltzis D, Elheriadou I, Veves A. (2014). Pathogenesis and treatment of impaired wound healing in *diabetes mellitus*: new insights. *Advances in Therapy, 31*(8), 817-36.

Banfi, A., Degenfeld, G., Gianni-Barrera, R., Reginato, S., Merchant, M., Mcdonald, D., Blau, H. (2012). Therapeutic angiogenesis due to balanced single-vector delivery of VEGF and PDGF-BB. *The FASEB Journal, 26*, 2486-2497.

Barrientos, S., Stojadinovic, O., Golinko, M., Brem, H., Tomic-Canic, M. (2008). Growth factors and cytokines in wound healing. *Wound Repair and Regeneration, 16*, 585-601.

Belizário, J. (2009). Immunodeficient Mouse Models: An Overview. *The Open Immunology Journal, 2,* 79-85.

Benard, E., Benard, E., van der Sar, A., Ellett, F., Lieschke, G., Spaink, H., Meijer, A. (2012). Infection of zebrafish embryos with intracellular bacterialpathogens. *Journal of Visualized Experiments, 61*(e3781).

Benavides, F., Oberyszyn, T., Vanbuskirk, A., Reeve, V., Kusewitt, D. (2008). The hairless mouse in skin research. *Journal of Dermatological Science, 53*(1), 10-18.

Bland, E., Dréau, D., Burg, K. (2013). Overcoming hypoxia to improve tissue-engineering approaches to regenerative medicine. *Journal of Tissue Engineering and Regenerative Medicine, 7,* 505-514.

Carter, S., Tate, R. (2006). The relationship of the transcutaneous oxygen tension, pulse waves and systolic pressures to the risk for limb amputation in patients with peripheral arterial disease and skin ulcers or gangrene. *International Angiology, 25*(1), 67-72.

Castellon, R., Hamdi, H., Sacerio, I., Aoki, A., Kenney, M., Ljubimov, A. (2001). Effects of angiogenic growth factor combinations on retinal endothelial cells. *Experimental Eye Research, 74*, 523-535.

Centis, V., Vermette, P. (2009). Enhancing oxygen solubility using hemoglobin- and perfluorocarbon-based carriers. *Frontiers in Bioscience, 14*, 665–88.

Ceradini, D., Kulkarni, A., Callaghan, M., Tepper, O., Bastidas, N., Kleinman, M., Capla, J., Galiano, R., Levine, J., Gurtner, G. (2004). Progenitor cell trafficking is regulated by hypoxic gradients through HIF-1 induction of SDF-1. *Nature Medicine, 10*(8), 858-864.

Chang, T. (2004). Hemoglobin-based red blood cell substitutes. *Artificial Organs, 28*(9), 789-794.

Colom, A., Galgoczy, R., Almendros, I., Xaubet, A., Farré, R., Alcaraz, J. (2013). Oxygen diffusion and consumption in extracellular matrix gels: Implications for designing three-dimensional cultures. *Journal of Biomedical Materials Research Part A, 102*(8), 2776-84.

Coragliotti, A., Beligni, M., Franklin, S., Mayfield, S. (2011). Molecular factors affecting the accumulation of recombinant proteins in the *Chlamydomonas reinhardtii* chloroplast. *Molecular Biotechnology, 48*, 60-75.

Dauvillée, D., Delhaye, S., Gruyer, S., Slomianny, C., Moretz, S., D'hulst, C., Lonf, C., Ball, S., Tomavo, S. (2010). Engineering the chloroplast targeted malarial vaccine antigens in *Chlamydomona*s starch granules. *PLoS ONE*, *5*(12), E15424-E15424.

Davis, J., Crampton, S., Hughes, C. (2007). Isolation of Human Umbilical Vein Endothelial Cells (HUVEC). *Journal of Visualized Experiments, 3*(183).

Debels H, Hamdi M, Abberton K, Morrison W. (2015). Dermal matrices and bioengineered skin substitutes: a critical review of current options. *Plastic and Reconstructive Surgery Global Open*, *3*(1):e284.

Demol, J., Lambrechts, D., Geris, L., Schrooten, J., Van Oosterwyck, H. (2011). Towards a quantitative understanding of oxygen tension and cell density evolution in fibrin hydrogels. *Biomaterials, 32*, 107-118.

Demurtas, O., Massa, S., Ferrante, P., Venuti, A., Franconi, R., Giuliano, G., Chen, W. (2013). A *Chlamydomonas*-derived human papillomavirus 16 E7 vaccine induces specific tumor protection. PLoS ONE, *8*(4), E61473-E61473.

Dent, R., Han, M., Niyogi, K. (2001). Functional genomics of plant photosynthesis in the fast lane using *Chlamydomonas reinhardtii. Trends in Plant Science, 6*(8), 364-371.

Dimmeler, S., Ding, S., Rando, T., Trounson, A. (2014). Translational strategies and challenges in regenerative medicine. *Nature Medicine, 20*(8), 814-21.

Dreesen, I., Hamri, G., Fussenegger, M. (2010). Heat-stable oral alga-based vaccine protects mice from Staphylococcus aureus infection. *Journal of Biotechnology*, *145*(3), 273-280.

Dunn, K. (1987). Growth of endosymbiotic algae in the green hydra, *Hydra viridissima. Journal of Cell Science, 88*, 571-578.

Eberhard, S., Finazzi, G., Wollman, F. (2008). The dynamics of photosynthesis. *Annual Review of Genetics, 42,* 463-515.

Edwards, S., Zavala, G., Prieto, C., Elliott, M., Martínez, S., Egaña, J., Bono, M., Palma, V. (2014). Functional analysis reveals angiogenic potential of human mesenchymal stem cells from Wharton's jelly in dermal regeneration. *Angiogenesis, 17*(4), 851-66.

Egaña, J., Condurache, A., Lohmeyer, J., Kremer, M., Stöckelhuber, B., Lavandero, S., Machens, H. (2009). *Ex vivo* method to visualize and quantify vascular networks in native and tissue engineered skin. *Langenbeck's Archives of Surgery, 394,* 349-356.

Egaña, JT. (2009). Stem cells and collagen scaffold in dermal tissue regeneration. Chile, Univ., Diss.

Eichler-Stahlberg, A., Weisheit, W., Ruecker, O., Heitzer, M. (2009). Strategies to facilitate transgene expression in *Chlamydomonas reinhardtii. Planta, 229*, 873-883.

Ellett, F., Pase, L., Hayman, J., Andrianopoulos, A., Lieschke, G. (2011). Mpeg1 promoter transgenes direct macrophage-lineage expression in zebrafish. *Blood, 117*(4), E49-E56.

Eming, S., Brachvogel, B., Odorisio, T., Koch, M. (2007). Regulation of angiogenesis: Wound healing as a model. *Progress in Histochemistry and Cytochemistry, 42*, 115-170.

Eming, S., Martin, P., Tomic-Canic, M. (2014). Wound repair and regeneration: mechanisms, signaling, and translation. Science Translational Medicine, 6(265), 265sr6.

Enoch, S., Leaper, D. (2005). Basic science of wound healing. *Surgery, 23*(2), 31-37.

Fadini, G., Losordo, D., Dimmeler, S. (2012). Critical Reevaluation of Endothelial Progenitor Cell Phenotypes for Therapeutic and Diagnostic Use. *Circulation Research, 110*(4), 624-637

Fang, L., Miller, Y. (2012). Emerging applications for zebrafish as a model organism to study oxidative mechanisms and their roles in inflammation and vascular accumulation of oxidized lipids. *Free Radical Biology and Medicine, 53*(7), 1411–20.

Ferrara N. (2001). Role of vascular endothelial growth factor in regulation of physiological angiogenesis. *American Journal of Physiology, 280*(6), 1358-66.

Fischer, N., Rochaix, J. (2001). The flanking regions of PsaD drive efficient gene expression in the nucleus of the green alga *Chlamydomonas reinhardtii. Molecular Genetics and Genomics, 265*, 888-894.

Fong, G. (2009). Regulation of angiogenesis by oxygen sensing mechanisms. *Journal of Molecular Medicine, 87*(6), 549-560.

Freeman, I., Cohen, S. (2009). The influence of the sequential delivery of angiogenic factors from affinity-binding alginate scaffolds on vascularization. *Biomaterials, 30*, 2122–2131.

Fries, R., Wallace, W., Roy, S., Kuppusamy, P., Bergdall, V., Gordillo, G., Melvin, S., Sen, C. (2005). Dermal excisional wound healing in pigs following treatment with topically applied pure oxygen. *Mutation Research, 579*, 172-181.

Georgianna, D., Hannon, M., Marcuschi, M., Wu, S., Botsch, K., Lewis, A., Mendez, M., Mayfield, S. (2013). Production of recombinant enzymes in the marine alga *Dunaliella tertiolecta. Algal Research, 2*, 2-9.

Greaves, N., Ashcroft, K., Baguneid, M., Bayat, A. (2013). Current understanding of molecular and cellular mechanisms in fibroplasia and angiogenesis during acute wound healing. *Journal of Dermatological Science, 72*(3), 206-217.

Gregory, J., Li, F., Tomosada, L., Cox, C., Topol, A., Vinetz, J., Mayfield, S. (2012). Algae-produced Pfs25 elicits antibodies that inhibit malaria transmission. *PLoS ONE, 7*(5), E37179-E37179.
Gregory, J., Topol, A., Doerner, D., Mayfield, S. (2013). Alga-produced cholera toxin-Pfs25 fusion proteins as oral vaccines. *Applied and Environmental Microbiology, 79*(13), 3917-3925.

Habeck, H., Odenthal, J., Walderich, B., Maischein, H., Schulte-Merker, S. (2002). Analysis of a zebrafish VEGF receptor mutant reveals specific disruption of angiogenesis. *Current Biology, 12*, 1405-1412.

Haroon, Z., Raleigh, J., Greenberg, C., Dewhirst, M. (2000). Early wound healing exhibits cytokine surge without evidence of hypoxia. *Annals of Surgery, 231*(1), 137-137.

Harris, E. (2001). Chlamydomonas as a novel organism. *Annual Review of Plant Physiology and Plant Molecular Biology, 52*, 363-406.

Harris, E. (2008). The *Chlamydomonas* sourcebook introduction to *Chlamydomonas* and its laboratory use, 2nd ed. Burlington. Elsevier.

Harrison, B., Eberli, D., Lee, S., Atala, A., Yoo, J. (2007). Oxygen producing biomaterials for tissue regeneration. *Biomaterials, 28,* 4628-4634.

He, D., Qian, K., Shen, G., Zhang, Z., Li, Y., Su, Z., Shao, H. (2007). Recombination and expression of classical swine fever virus (CSFV) structural protein E2 gene in *Chlamydomonas reinhardtii* chroloplasts. *Colloids and Surfaces B: Biointerfaces, 55*(1), 26-30.

Hirsch, T., Spielmann, M., Yao, F., Eriksso, E. (2007). Gene therapy in cutaneous wound healing. Frontiers in *Bioscience, 12*, 2507-2518.

Hoeben, A., Landuyt, B., Highley, M., Wildiers, H., Van Oosterom, A., De Bruijn, E. (2004). Vascular endothelial growth factor and angiogenesis. *Pharmacological Reviews, 56*(4), 549-580.

Hopf, H., Rollins, M. (2007). Wounds: An overview of the role of oxygen. *Antioxidants and Redox Signaling, 9*(8), 1183-1192.

Hopfner, U., Schenck, T., Chávez, M., Machens, H., Bohne, A., Nickelsen, J., Giunta, R., Egaña, J. (2014). Development of photosynthetic biomaterials for *in vitro* tissue engineering. *Acta Biomaterialia, 10*(6), 2712-7.

Hou, Q., Qiu, S., Liu, Q., Tian, J., Hu, Z., Ni, J. (2013). Selenoprotein-transgenic *Chlamydomonas reinhardtii. Nutrients, 5*(3), 624-636.

Hunt, N., Grover, L. (2010). Cell encapsulation using biopolymer gels for regenerative medicine. *Biotechnology Letters, 32*, 733–42.

Janssen, M., de Winter, M., Tramper, J., Mur, L., Snel, J., Wijffels, R. (2000). Efficiency of light utilization of *Chlamydomonas reinhardtii* under medium-duration light/dark cycles. *Journal of Biotechnology, 78*(2), 123-37.

Jin, Q., Wei, G., Lin, Z., Sugai, J., Lynch, S., Ma, P., Isalan, M. (2008). Nanofibrous scaffolds incorporating PDGF-BB microspheres induce chemokine expression and tissue neogenesis *in vivo. PLoS ONE, 3*(3), e1729.

Jones, C., Luong, T., Hannon, M., Tran, M., Gregory, J., Shen, Z., Briggs, S., Mayfield, S. (2013). Heterologous expression of the C-terminal antigenic domain of the malaria vaccine candidate Pfs48/45 in the green algae *Chlamydomonas reinhardtii. Applied Microbiology and Biotechnology, 97*(5), 1987-1995.

Kano, M., Morishit, Y., Iwata, C., Iwasaka, S., Watabe, T., Ouchi, Y., Miyazono, K., Miyazawa, K. (2005). VEGF-A and FGF-2 synergistically promote neoangiogenesis through enhancement of endogenous PDGF-B-PDGFR-beta signaling. *Journal of Cell Science, 118*(16), 3759-68.

Kim, J., Andersson, K., Jackson, J., Lee, S., Atala, A., Yoo, J. (2014). Downregulation of metabolic activity increases cell survival under hypoxic conditions: potential applications for tissue engineering. *Tissue Engineering Part A, 20*(15-16), 2265-72.

Krock, B., Skuli, N., Simon, M. (2011). Hypoxia-induced angiogenesis: Good and evil. *Genes and Cancer, 2*(12), 1117-1133.

Lalan, B., Pomerantseva, M., Vacanti, M. (2001). Tissue engineering and its potential impact on surgery. *World Journal of Surgery, 25*, 1458-1466.

Langer R., Vacanti J. (1993). Tissue engineering. *Science, 14*, 920-6.

Lauersen, K., Berger, H., Mussgnug, J., Kruse, O. (2013). Efficient recombinant protein production and secretion from nuclear transgenes in *Chlamydomonas reinhardtii*. *Journal of Biotechnology, 167*, 101-110.

Lawson, N., Weinstein, B. (2002). *In vivo* imaging of embryonic vascular development using transgenic zebrafish. *Developmental Biology, 248,* 307-318.

Lee, K., Silva, E., Mooney, D. (2011). Growth factor delivery-based tissue engineering: General approaches and a review of recent developments. *Journal of The Royal Society Interface, 8,* 153-170.

Leon, R., Galván, A., Fernández, E. (2008). Transgenic microalgae as green cell factories. New York, N.Y. Springer Science.

León-Bañares, R., Gonzalez, D., Galvan, A., Fernandez, E. (2004). Transgenic microalgae as green cell-factories. *Trends in Biotechnology, 22*(1), 45-52.

Li, B., Davidson, J., Guelcher, S. (2009). The effect of the local delivery of platelet-derived growth factor from reactive two-component polyurethane scaffolds on the healing in rat skin excisional wounds. *Biomaterials, 30*(20), 3486-3494.

Li, D., Li, X., Wang, H., Shen, Q., Li, X., Wen, L., Qin, X., Jia, Q., Kung, H., Peng, Y. (2012). VEGF induces angiogenesis in a zebrafish embryo glioma model established by transplantation of human glioma cells. *Oncology Reports, 28*, 937-42.

Liu, P., Liu, K., Wang, X., Badiavas, E., Rieger-Christ, K., Tang, J., Summerhayes, I. (2005). Efficacy of combination gene therapy with multiple growth factor cDNAs to enhance skin flap survival in a rat model. *DNA and Cell Biology, 24*(11), 751-757.

Machens, H., Berger, A., Mailaender, P. (2000). Bioartificial Skin. Cells Tissues Organs, 167(2-3), 88-94.

Madison, K. (2003). Barrier function of the skin: "La raison d'être" of the epidermis. Journal of Investigative *Dermatology, 121*, 231-241.

Manthey, H., Woodruff, T., Taylor, S., Monk, P. (2009). Complement component 5a (C5a). *The International Journal of Biochemistry and Cell Biology, 41*(11), 2114-7.

Manuell A., Beligni M., Elder J., Siefker D., Tran M., Weber A., McDonald T., Mayfield S. (2007) Robust expression of a bioactive mammalian protein in *Chlamydomonas* chloroplast. *Journal of Plant Biotechnology*, 5, 402–412.

Mayfield S., Franklin S., Lerner R. (2003). Expression and assembly of a fully active antibody in algae. *Proceedings of the National Academy of Sciences*, 100:438–442.

McFadden, G. (2001). Primary and secondary endosymbiosis and the origin of plastids. *Journal of Phycology, 37*, 951-959.

Merchant, S. *et al.* (2007). The *Chlamydomonas* genome reveals the evolution of key Animal and plant functions. *Science, 318*(5848), 245-50.

Moiemen, N., Vlachou, E, Staiano, J., Thawy, Y., Frame, J. (2006). Reconstructive surgery with Integra dermal regeneration template: histologic study, clinical evaluation, and current practice. *Plastic and Reconstructive Surgery, 117*, 160.

Mokos, Z., Mosler, E. (2014). Advances in a rapidly emerging field of hair follicle stem cell research. *Collegium Antropologicum, 38*(1), 373-8.

Mujagic, E., Gianni-Barrera, R., Trani, M., Patel, A., Gürke, L., Heberer, M., Wolff, T., Banfi, A. (n.d.). Induction of aberrant vascular growth, but not of normal angiogenesis, by cell-based expression of different doses of human and mouse VEGF is species-dependent. *Human Gene Therapy Methods, 24*, 28-37.

Murphy, K., Fang, S., Leach, J. (2014). Human mesenchymal stem cell spheroids in fibrin hydrogels exhibit improved cell survival and potential for bone healing. *Cell and Tissue Research, 357*(1), 91-9.

Mutsaers, S., Bishop, J., Mcgrouther, G., Laurent, G. (1997). Mechanisms of tissue repair: From wound healing to fibrosis. *The International Journal of Biochemistry and Cell Biology, 29*(1), 5-17.

Neupert, J., Karcher, D., Bock, R. (2009). Generation of *Chlamydomonas* strains that efficiently express nuclear transgenes. *The Plant Journal, 57*(6), 1140-50.

Nickelsen, J., Kück, U. (2000). The unicellular green alga *Chlamydomonas reinhardtii* as an experimental system to study chloroplast RNA metabolism. *Naturwissenschaften, 87*(3), 97-107.

Nicoli, S., Sena, G., Presta, M. (2009). Fibroblast growth factor 2-induced angiogenesis in zebrafish: The zebrafish yolk membrane (ZFYM) angiogenesis assay. *Journal of Cellular and Molecular Medicine, 13*(8B), 2061-2068.

Novoa, B., Figueras, A. (2012). Zebrafish: model for the study of inflammation and theinnate immune response to infectious diseases. *Advances in Experimental Medicine and Biology, 946*, 253–75.

Oh, S., Ward, C., Atala, A., Yoo, J., Harrison, B. (2009). Oxygen generating scaffolds for enhancing engineered tissue survival. *Biomaterials, 30*, 757-762.

Ozawa, C., Banfi, A., Glazer, N., Thurston, G., Springer, M., Kraft, P., McDonald, D., Blau, H. (2004). Microenvironmental VEGF concentration, not total dose, determines a threshold between normal and aberrant angiogenesis. *Journal of Clinical Investigation, 113*, 516-527.

Palomares, L., Estrada, S., Ramírez, O. (2004). Production of recombinant proteins. *Recombinant Gene Expression Methods in Molecular Biology*, *267*, 15-51.

Park, J., Lakes, R. (2007). Biomaterials - An Introduction, Chapter 11.1.3. Tissue Adhesives, 3rd ed., p. 299. Springer, NY.

Poss, K., Keating, M., Nechiporuk A. (2003). Tales of regeneration in zebrafish. *Developmental Dynamics, 226*(2), 202–10.

Priestley, J. (1772). Observations on different kinds of air. *Philosophical Transactions, 62*,147–264.

Priestley, J. (1781). Experiments and observations on different kinds of air, 3th ed., pp 86. London. J Johnson.

Raica, M., Cimpean, A. (2010). Platelet-derived growth factor/ PDGF-receptors axis as target for antitumor and antiangiogenic therapy. *Pharmaceuticals, 3*, 572-599.

Rasala, B., Lee, P., Shen, Z., Briggs, S., Mendez, M., Mayfield, S., Stiller, J. (2012). Robust expression and secretion of xylanase1 in *Chlamydomonas reinhardtii* by fusion to a selection gene and processing with the FMDV 2A peptide. *PLoS ONE, 7*(8), E43349-E43349.

Rasala, B., Mayfield, S. (2014). Photosynthetic biomanufacturing in green algae; production of recombinant proteins for industrial, nutritional, and medical uses. *Photosynthesis Research.* [Epub ahead of print].

Rasala, B., Muto, M., Lee, P., Jager, M., Cardoso, R., Behnke, C., Kirk, P., Hokanson, C., Crea, R., Mendez, M., Mayfield, S. (2010). Production of therapeutic proteins in algae, analysis of expression of seven human proteins in the chloroplast of *Chlamydomonas reinhardtii. Plant Biotechnology Journal*, 719-733.

Reckhenrich, A., Hopfner, U., Krötz, F., Zhang, Z., Koch, C., Kremer, M., Machens, H., Plank, C., Egaña, J. (2011). Bioactivation of dermal scaffolds with a non-viral copolymer-protected gene vector. *Biomaterials, 32*, 1996-2003.

Reed S., Wu B. (2014). Sustained growth factor delivery in tissue engineering applications. *Annals of Biomedical Engineering, 42*(7), 1528-36.

Richardson, T., Peters, M., Ennett, A., Mooney, D. (2001). Polymeric system for dual growth factor delivery. Nature *Biotechnology 19*, 1029 - 1034.

Riedel, K., Riedel, F., Goessler, U., Holle, G., Germann, G., Sauerbier, M. (2006). Current status of genetic modulation of growth factors in wound repair. *International Journal of Molecular Medicine, 17*, 183-193.

Rochaix, J. (2001). Assembly, function, and dynamics of the photosynthetic machinery in *Chlamydomonas reinhardtii. Plant Physiology, 127*, 1394-1398.

Rochaix, J. (2011). Regulation of photosynthetic electron transport. *Biochimica et Biophysica Acta. Bioenergetics, 1807*(3), 375-383.

Rosales-Mendoza, S., Paz-Maldonado, L., Soria-Guerra, R. (2012). *Chlamydomonas reinhardtii* as a viable platform for the production of recombinant proteins: Current status and perspectives. *Plant Cell Reports, 31*, 479-494.

Ruangsetakit, C., Chinsakchai, K., Mahawongkajit, P., Wongwanit, C., Mutirangura, P. (2010). Transcutaneous oxygen tension: A useful predictor of ulcer healing in critical limb ischaemia. *Journal of Wound Care, 19*(5), 202-6.

Rumpho, M., Pelletreau, K., Moustafa, A., Bhattacharya, D. (2011). The making of a photosynthetic animal. *Journal of Experimental Biology, 214*, 303-311.

Sarafi, M., Garcia, E., MacLean, J., Charo, I., Luster, A. (1997). Murine monocyte chemoattractant protein (MCP)-5: A novel CC-chemokine that is a structural and functional homologue of human MCP-1. *Journal of Experimental Medicine, 185*(1), 99–110.

Schenck, T., Chávez, M., Condurache, A., Hopfner, U., Rezaeian, F., Machens, H., Egaña, J. (2014). A full skin defect model to evaluate vascularization of biomaterials *in vivo*. *Journal of Visualized Experiments, 90*, e51428.

Seifu, D., Isimjan, T., Mequanint, K. (2011). Tissue engineering scaffolds containing embedded fluorinated-zeolite oxygen vectors. *Acta Biomaterialia, 7*, 3670–8.

Sen, C. (2009). Wound healing essentials: let there be oxygen. *Wound Repair and Regeneration, 17(*1), 1-18.

Shahrokhi, S., Arno, A., Jeschke, M. (2014). The use of dermal substitutes in burn surgery: Acute phase. *Wound Repair and Regeneration, 22*, 14-22.

Shaterian, A., Borboa, A., Sawada, R., Costantini, T., Potenza, B., Coimbra, R., Baird, A., Eliceiri, B. (2009). Real-time analysis of the kinetics of angiogenesis and vascular permeability in an animal model of wound healing. *Burns, 35*(6), 811-817.

Singhal, G., Renger, G., Sopory, S., Irrgang K., and Govindjee. (1999). Concepts in photobiology: photosynthesis and photomorphogenesis, 1st ed., pp. 11-51. Narosa Publishers. New Delhi.

Sokolsky-Papkov, M., Agashi, K., Olaye, A., Shakesheff, K., Domb, A. (2007). Polymer carriers for drug delivery in tissue engineering. *Advanced Drug Delivery Reviews, 59*, 187-206.

Spahn, D. (2000). Current status of artificial oxygen carriers. *Advanced Drug Delivery Reviews, 40*, 143-151.

Stücker, M., Struk, A., Altmeyer, P., Herde, M., Baumgärtl, H., Lübbers, D. (2004). The cutaneous uptake of atmospheric oxygen contributes significantly to the oxygen supply of human dermis and epidermis. *The Journal of Physiology, 538*(3), 985-994.

Su, Z., Qian, K., Tan, C., Meng, C., Qin, S. (2005). Recombination and Heterologous Expression of Allophycocyanin Gene in the Chloroplast of *Chlamydomonas reinhardtii*. *Acta Biochimica Et Biophysica Sinica*, *37*(10), 709-712.

Sun M., Qian K., Su N., Chang H., Liu J., Shen G. (2003). Foot-and-mouth disease virus VP1 protein fused with cholera toxin B subunit expressed in *Chlamydomonas reinhardtii* chloroplast. *Biotechnology Letters*, *25*(13):1087-92.

Surzycki, R., Greenham, K., Kitayama, K., Dibal, F., Wagner, R., Rochaix, J., Ajam, T., Surzycki, S. (2009). Factors effecting expression of vaccines in microalgae. *Biologicals*, 3, 133-138.

Tallquist, M., Kazlauskas, A. (2004). PDGF signaling in cells and mice. *Cytokine and Growth Factor Reviews, 15*, 205-213.

Tanaka, Y., Nishiyama, Y., Murata, N. (2000). Acclimation of the photosynthetic machinery to high temperature in *Chlamydomonas reinhardtii* requires synthesis de novo of proteins encoded by the nuclear and chloroplast genomes. *Plant Physiology, 124*(1), 441-9.

Tandara, A., Mustoe, T. (2004). Oxygen in wound healing - more than a nutrient. *World Journal of Surgery, 28*, 294-300.

Thévenaz, P., Unser, M. (2007). User-friendly semiautomated assembly of accurate image mosaics in microscopy. *Microscopy Research and Technique, 70*, 135-146.

Thom, S. (2011). Hyperbaric oxygen: its mechanisms and efficacy. *Plastic and Reconstructive Surgery, 127*(Suppl 1), 131S-141S.

Tonnesen MG, Feng X, Clark RA. (2000). Angiogenesis in wound healing. *Journal of Investigative Dermatology Symposium Proceedings, 5*(1), 40-6.

Tortora, G., Grabowski, S. (2012). Principles of anatomy and physiology, 13th ed., pp. 153-178. New York: Wiley.

Tran M., Henry R., Siefker D., Van C., Newkirk G., Kim J., Bui J., Mayfield S. (2013a). Production of anti-cancer immunotoxins in algae: ribosome inactivating proteins as fusion partners. *Biotechnology and Bioengineering, 110*(11):2826-35.

Tran M., Van C., Barrera D., Pettersson P., Peinado C., Bui J., Mayfield S. (2013b) Production of unique immunotoxin cancer therapeutics in algal chloroplasts. *Proceedings of the National Academy of Sciences, 110*(1):E15-22.

Tran M., Zhou B., Pettersson P., Gonzalez M., Mayfield S. (2009). Synthesis and assembly of a full-length human monoclonal antibody in algal chloroplasts. *Biotechnology and Bioengineering, 104*(4):663-73.

Trentin, D., Hall, H., Wechsler, S., Hubbell, J. (2006). Peptide-matrix-mediated gene transfer of an oxygen-insensitive hypoxia-inducible factor-1alpha variant for local induction of angiogenesis. *Proceedings of the National Academy of Sciences of the United States of America, 103*(8), 2506-11.

Wang, X., Brandsma, M., Tremblay, R., Maxwell, D., Jevnikar, A., Huner, N., Ma, S. (2008). A novel expression platform for the production of diabetes-associated autoantigen human glutamic acid decarboxylase (hGAD65). *BMC Biotechnology,* 8, 87-87.

Werner, S., Grose, R. (2003). Regulation of wound healing by growth factors and cytokines. *Physiological Reviews, 83*(3), 835-70.

White, S., Pittman, C., Hingorani, R., Arora, R., Esipova, T., Vinogradov, S., Hughes, C., Choi, B., George, S. (2014). Implanted cell-dense prevascularized tissues develop functional vasculature that supports reoxygenation after thrombosis. *Tissue Engineering Part A, 20*(17-18), 2316-28.

Wu S., Marston W., Armstrong D. (2010). Wound care: the role of advanced wound healing technologies. *Journal of Vascular Surgery, 52*(3 Suppl), 59S-66S.

Xie, Z., Paras, C., Weng, H., Punnakitikashem, P., Su, L., Vu, K., Tang, L, Yang, J., Nguyen, K. (2013). Dual growth factor releasing multi-functional nanofibers for wound healing. *Acta Biomaterialia, 9*(12), 9351-9359.

Yang, Z., Li, Y., Chen, F., Li, D., Zhang, Z., Liu, Y., Zheng, D., Wang, Y., Shen, G. (2006.). Expression of human soluble TRAIL in *Chlamydomonas reinhardtii* chloroplast. *Chinese Science Bulletin, 51*(14)1703-1709.

Yoon, S., Kim, S., Li, K., Yoon, B., Choe, S., Kuo, M. (2011). Transgenic microalgae expressing *Escherichia coli* AppA phytase as feed additive to reduce phytate excretion in the manure of young broiler chicks. *Applied Microbiology and Biotechnology, 91*(3), 553-563.

Zhang, M., Malik, A., Rehman, J. (2014). Endothelial progenitor cells and vascular repair. *Current Opinion in Hematology, 21*(3), 224-228.

Zhang, Y., Shen, G., Ru, B. (2006). Survival of human metallothionein-2 transplastomic *Chlamydomonas reinhardtii* to ultraviolet B exposure. *Acta Biochimica et Biophysica Sinica*, 38(3):187-93.

IX. Appendix

9.1 Transgene DNA-sequence of hVEGF-165

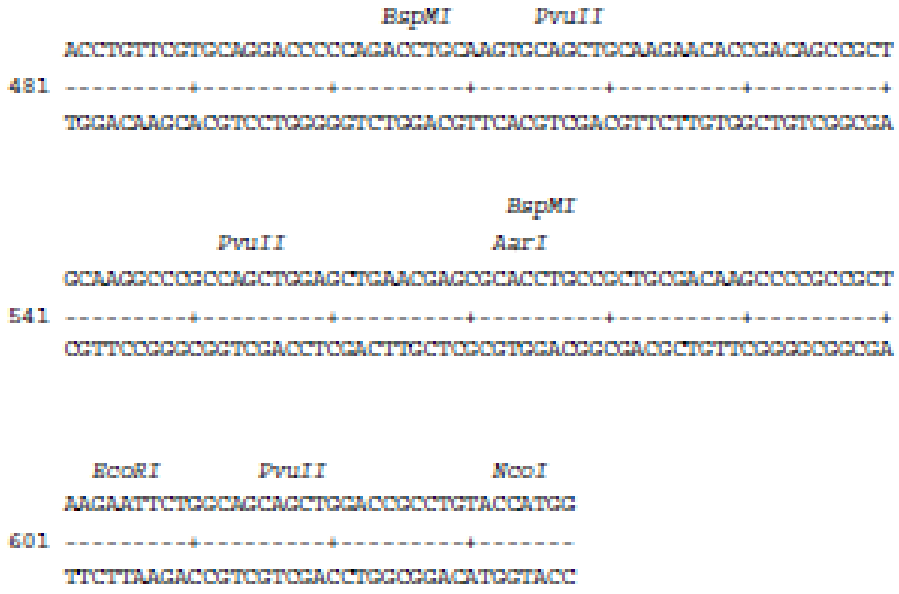
BspMI
PvuII
ACCTGTTCGTGCAGGACCCCCAGACCTGCAAGTGCAGCTGCAAGAACACCGACAGCCGCT
481
TGGACAAGCACGTCCTGGGGGTCTGGACGTTCACGTCGACGTTCTTGTGGCTGTCGGCGA
BspMI
PvuII
AarI
GCAAGGCCCGCCAGCTGGAGCTGAACGAGCGCACCTGCCGCTGCGACAAGCCCCGCCGCT
541
CGTTCCGGGCGGTCGACCTCGACTTGCTCGCGTGGACGGCGACGCTGTTCGGGGCGGCGA
EcoRI
PvuII
NcoI
AAGAATTCTGGCAGCAGCTGGACCGCCTGTACCATGG
601
TTCTTAAGACCGTCGTCGACCTGGCGGACATGGTACC

9.2 Transgene DNA-sequence of hPDGF-B

X. List of abbreviations

ADP	Adenosine diphosphate
ATP	Adenosine triphosphate
bFGF	Basic fibroblast growth factor
C. reinhardtii	*Chlamydomonas reinhardtii*
C5a	Complement component 5a
CCL	Chemokine (C-C motif) ligand
CD54	Cluster of Differentiation 54, also known as ICAM-1
CO_2	Carbon dioxide
CXC4	C-X-C chemokine receptor 4
Cyt b_6f	Cytochrome b_6f
DAPI	4', 6-diamidino-2-phenylindole
DMEM	Dulbecco's modified eagle medium
DMSO	Dimethyl sulfoxide
DNA	Deoxyribonucleic acid
dpf	days post-fertilization
E. coli	*Escherichia coli*
ECM	Extracellular matrix
EDTA	Ethylenediaminetetraacetic acid
EGF	Epidermal growth factor
EGFP	Enhanced green fluorescent protein
ELISA	Enzyme-Linked ImmunoSorbent Assay
FBS	Fetal bovine serum
Fd	Ferredoxin
Fig.	Figure
FNR	Ferredoxin-NADP oxidoreductase
g	Gravity of Earth; 1 g = 9.81 $m \cdot s^{-2}$
GFP	Green fluorescent protein
GM	Genetically modified
GM-CSF	Granulocyte-macrophage colony-stimulating factor
GRAS	Generally recognized as safe
H_2O	Water
HBO	Hyperbaric oxygen
HGF	Hepatocyte growth factor
HIF-1α	Hypoxia-inducible factor-1α
hPDGF-B	Human platelet-derived growth factor B
hpf	Hours post-fertilization
HUVECs	Human umbilical vein endothelial cells
hVEGF-165	Human vascular endothelial growth factor-165
IFN-γ	Interferon-γ
Ig	Immunoglobulin
IGF-1	Insulin-like growth factor-1
IL	Interleukin
ILN	Iliac lymph nodes

IM	Integra matrix
KGF	Keratinocyte growth factor
LHCII	Light-harvesting complex
mAb	Mononuclear antibody
MCP-1	Monocyte Chemoattractant Protein-1, also known as CCL-2
M-CSF	Macrophage colony-stimulating factor
MLN	Mesenteric lymph nodes
mRNA	Messenger RNA
MSC	Mesenchymal stem cells
MW	Molecular weight
NADPH	Nicotinamide adenine dinucleotide phosphate
NO	Nitric oxide
NRP-1	Neuropilin-1
O_2	Oxygen
PBS	Phosphate buffered saline
PC	Plastocyanin
PCR	Polymerase chain reaction
PDGF	Platelet-derived growth factor
PDGFR-α	Platelet-derived growth factor receptor-α
PDGFR-αβ	Platelet-derived growth factor receptor-αβ
PDGFR-β	Platelet-derived growth factor receptor-β
PF4	Platelet factor-IV
PFA	Paraformaldehyde
pH	from the latin pondus Hydrogenii
PlGF	Placenta growth factor
pO_2	Oxygen partial pressure
PQ	Plastoquinone
PSI	Photosystem I
PSII	Photosystem II
RIPA	Radio-Immunoprecipitation Assay
RNA	Ribonucleic acid
rpm	Rounds per minute
RT-PCR	Reverse transcription polymerase chain reaction
SDF-1	Stromal cell-derived factor-1
SEM	Scanning electron microscopy
TAPS	Tris Acetate Phosphate Sorbitol
$TcPO_2$	Transcutaneous oxygen tension
TGF-β	Transforming growth factor-β
TIMP-1	Tissue inhibitor of metalloproteinase-1
TNF	Tumor Necrosis Factor
tRNA	Transfer RNA
VEGF	Vascular endothelial growth factor
VEGFR-1	Vascular endothelial growth factor receptor-1, Fms-like tyrosine kinase-1, Flt-1
VEGFR-3	Vascular endothelial growth factor receptor-3, Fms-like tyrosine kinase-4, Flt-4
VEGRF-2	Vascular endothelial growth factor receptor-2, Kinase domain region, Flk-1/ KDR
WT	Wild-type

XI. List of figures

XII. List of publications

- Development of photosynthetic biomaterials for *in vitro* tissue engineering.
  Hopfner U, Schenck TL, **Chávez MN**, Machens HG, Bohne AV, Nickelsen J, Giunta RE, Egaña JT.
  Acta Biomaterialia, 2014; 10(6):2712-7. doi: 10.1016/j.actbio.2013.12.055.

- A full skin defect model to evaluate vascularization of biomaterials *in vivo*.
  Schenck TL, **Chávez MN**, Hopfner U, Rezaeian F, Machens HG, Condurache AP, Egaña JT.
  Journal of Visualized Experiments, 2014; (90). doi: 10.3791/51428.

- Photosynthetic biomaterials: A pathway towards autotrophic tissue engineering.
  Schenck TL*, Hopfner U*, **Chávez MN***, Giunta RE, Machens HG, Bohne AV, Nickelsen J, Allende ML, Egaña JT.
  Acta Biomaterialia, 2015; 15:39–47. doi: 10.1016/j.actbio.2014.12.012.
  *Equal contribution.

XIII. Acknowledgements

I would like to acknowledge the people whose help and advice got me through these years as a PhD-student. First, I wish to thank Prof. Dr. Machens, Prof. Dr. Harder and Prof. Dr. Nickelsen, for following my progress, for their feedback and encouragement, and their interest in the project. I would like to also thank Dr. Allende of the University of Chile and Dr. Brown of the University of Valparaiso, for making their laboratories available to perform part of this work and placing their resources and their assistance readily at my disposal.

Many thanks go to Frau Hopfner, for keeping the lab running in spite of all and in many occasions against all odds. You are our lab's pacemaker and I am happy to have met a person like you, with everlasting enthusiasm for both life and work. Also, thanks to Dr. Schenck for his friendship and tutoring on rodents-associated bureaucracy and handling, and to Dr. Schwarz for introducing me into the world of algae.

To Dr. Egaña: as the famous Stan Lee once said, "When you work with people whom you like and you admire because they're so good at what they do, it doesn't feel like work, …it's like you're playing". We both know it wasn't playing, but under your supervision I have learned to experience research as it should be: thrilling and ambitious, reliant on a certain level of skill, perseverance and patience, lots of endurance, a bit of performance, and of course, always accompanied with the right background music. Thank you very much for the excellent supervision, for the infallible reassurance, for answering each and every email, and above all for your trust in my work and me.

Thanks to my family for their love, encouragement and support, always imminently present despite the long distances between us, the different time zones, sometimes broken internet connection and unusual working hours. Special thanks go to Anuja Sathe and Michelle McLuckie for proofreading. And finally, to all the "crazy scientists", who acted both as a support group and the best fellowship companions one could ever wish in this dark path of pursuing a PhD-degree. May you all be blessed by all seven old Gods and the new ones too. May the powers of the Arda shape your projects and rule your results. And always, may the Force be with you.